NOTICE

AVIS

The quality of this microform is heavily dependent upon the quality of the original thesis submitted for microfilming. Every effort has been made to ensure the highest quality of reproduction possible.

La qualité de cette microforme dépend grandement de la qualité de la thèse soumise au microfilmage. Nous avons tout fait pour assurer une qualité supérieure de reproduction.

If pages are missing, contact the university which granted the degree.

S'il manque des pages, veuillez communiquer avec l'université qui a conféré le grade.

Some pages may have indistinct print especially if the original pages were typed with a poor typewriter ribbon or if the university sent us an inferior photocopy.

La qualité d'impression de certaines pages peut laisser à désirer, surtout si les pages originales ont été dactylographiées à l'aide d'un ruban usé ou si l'université nous a fait parvenir une photocopie de qualité inférieure.

Canada

UNIVERSITY OF ALBERTA

ACOUSTIC EMISSION MONITORING OF DELAYED HYDRIDE CRACKING IN

ZIRCONIUM 2.5% NIOBIUM

BY

SUSAN MCFARLAND

A THESIS SUBMITTED TO THE FACULTY OF GRADUATE STUDIES AND
RESEARCH

IN PARTIAL FULFILMENT OF THE REQUIREMENTS FOR THE DEGREE OF

MASTER OF SCIENCE

in

METALLURGICAL ENGINEERING

DEPARTMENT OF MINING, METALLURGICAL AND PETROLEUM
ENGINEERING

EDMONTON, ALBERTA

SPRING 1995

UNIVERSITY OF ALBERTA

RELEASE FORM

NAME OF AUTHOR: SUSAN MCFARLAND

TITLE OF THESIS: ACOUSTIC EMISSION MONITORING OF DELAYED HYDRIDE CRACKING IN ZIRCONIUM 2.5% NIOBIUM

DEGREE: MASTER OF SCIENCE

YEAR THIS DEGREE WAS GRANTED: 1995

Box 12, Site 2, RR 4

Stony Plain, Alberta

Canada

T7Z 1X4
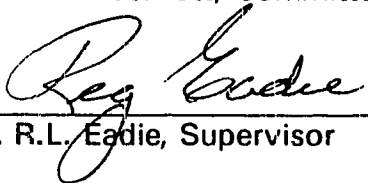
Date: April 20/95

UNIVERSITY OF ALBERTA

FACULTY OF GRADUATE STUDIES AND RESEARCH

The undersigned certify that they have read, and recommend to the Faculty of Graduate Studies and Research for acceptance, a thesis entitled **ACOUSTIC EMISSION MONITORING OF DELAYED HYDRIDE CRACKING IN ZIRCONIUM 2.5% NIOBIUM** submitted by **SUSAN MCFARLAND** in partial fulfilment of the requirements for the degree of **MASTER OF SCIENCE**

in Metallurgical Engineering.

_____
DR. B.M. Patchett, Committee Chairman

_____
DR. R.L. Eadie, Supervisor

_____
DR. M.L. Wayman, Committee Member

_____
DR. M.C. Williams, Committee Member

DATE: _April 12/95_

ABSTRACT

ABSTRACT

Delayed hydride cracking (DHC) in zirconium and zirconium alloys occurs when atomic hydrogen diffuses up a stress gradient and accumulates in a highly stressed region. Under specific temperature and pressure conditions, zirconium hydrides precipitate and subsequently fracture under the applied stresses. It is the fracture of these hydrides, which has caused premature failure of Zr-2.5 wt.% Nb pressure tubes in CANDU-type nuclear reactors.

In this study, a series of isothermal DHC tests was conducted on samples of as-manufactured and cold worked Zr - 2.5% Nb pressure tube material using acoustic emission (AE) monitoring. The objective of this study was an attempt to quantify AE as a function of area cracked, hydrogen content and material hardness. Following sample testing a *post mortem* fracture surface analysis was conducted to measure the crack surface area and to examine the crack morphology.

This study determined that there was a distinct increase in acoustic emissions (AE) per mm^2 of area cracked with increasing test temperatures. Detailed examination of the fracture surface also revealed an increase in striation spacings with temperature. The results of testing at varying amounts of hydrogen indicated a lower overall amount of AE per mm^2 with increasing hydrogen content and a corresponding decrease in striation spacings.

Additional work needs to be done to quantify further the relationship which appears to exist between striation spacing and AE per mm^2.

ACKNOWLEDGEMENT

TABLE OF CONTENTS

TABLE OF CONTENTS

PAGE

TABLE OF CONTENTS

LIST OF TABLES

LIST OF TABLES

LIST OF FIGURES

LIST OF FIGURES

LIST OF FIGURES

1.0 STATEMENT OF WORK

The deleterious effects of hydrogen in metals have been known for many years. Hydrogen blistering, hydrogen-induced cracking, hydrogen-assisted cracking, hydrogen embrittlement, hydrogen attack and delayed hydride cracking are several of the varying forms of hydrogen damage which have been described in the past [Bradford, 1993; Fontana, 1986].

Hydrogen damage has contributed significantly to operating costs in the form of equipment damage and down time particularly in the Canadian nuclear industry. Perryman, 1978 describes some of the failures which have occurred to pressure tubes in CANDU (Canada Deuterium Uranium) reactors owned and operated by Ontario Hydro (Provincial Crown Corporation). These pressure tubes, which are manufactured from Zr - 2.5% Nb, are used in the reactor core to contain the fuel bundles and heavy water coolant [Choubey and Puls, 1994].

Failure of the pressure tubes at Ontario Hydro was attributed to a phenomenon referred to as delayed hydride cracking (DHC). Over a period of time, the Zr - 2.5% Nb pressure tubes pick uphydrogen due to corrosion processes [Choubey and Puls, 1994]. DHC occurs when this atomic hydrogen diffuses up a stress gradient and accumulates as zirconium hydrides in a highly stressed region. These hydrides are more brittle than the zirconium alloy matrix, subsequently they fracture at lower applied stresses than the matrix material. This results in premature failure of the pressure tubes [Perovic, Weatherly and Simpson, 1983].

Transient elastic stress waves (acoustic emission) are released during DHC. These stress waves are detected with the use of a piezoelectric crystal which oscillates in a damped sinusoid at its resonant frequency [Coleman, 1987]. A transducer, containing the crystal, is fastened either directly to the sample or by a waveguide which is attached directly to the sample.

AE has been used significantly in the detection and monitoring of DHC in zirconium alloys [Perryman,1978; Arora and Tangri, 1979; Coleman, 1987]. In the past, it has primarily had a qualitative role, either to locate pressure tubes which have already been cracked or to confirm the onset/arrest of cracking such as in a testing situation.

A series of isothermal delayed hydride cracking tests were undertaken in this study. Samples of as-manufactured and cold worked Zr - 2.5% Nb pressure tube material were prepared for AE testing under constant stress conditions. Material of different hydrogen content was tested to simulate "in service" conditions. The cold worked material was tested in order to simulate material which had experienced hardening through irradiation. Following sample testing, a post mortem-type fracture surface analysis was conducted to measure surface area and the crack morphology.

The object of this study was to conduct a series of isothermal holds in order to quantify AE, as a function of area cracked, hydrogen contents and material hardness.

2.0 INTRODUCTION AND LITERATURE REVIEW

2.1 Zirconium and the Nuclear Industry

Natural uranium is used in the production of electricity from the Canada Deuterium Uranium (CANDU) pressurized heavy water reactor. In this process, a moderator of heavy water is used to slow down the high energy neutrons from the fission of uranium into thermal neutrons and continue the fission process [Ont. Hydro, 1978]. For this process to remain continuous, the moderator and the pressure vessel(s) used to contain the moderator must be able to slow down neutrons without absorbing them.

Early in the development of the nuclear industry it was discovered that zirconium metal allowed the passage of thermal neutrons without absorption. This characteristic, a very low thermal neutron capture cross section, has contributed to the significant usage of zirconium metal in pressure vessels and other containers in nuclear reactors. Other contributing factors have been zirconium's excellent corrosion resistance to high temperature water (343 degree Celsius) along with good mechanical properties [ASTM Manual, 1977].

In the United States, Zircaloy (trade name), an alloy of zirconium, tin, iron chromium and nickel is used extensively in reactors particularly for fuel cladding [ASTM Manual, 1977]. In CANDU-type reactors, zirconium - 2.5% niobium (Zr-2.5% Nb) is used in addition to zircaloy.

The alloy, Zr-2.5 Nb, was developed by Atomic Energy Canada Limited (AECL) for the production of pressure tubes in CANDU reactors. It has higher strength and superior creep resistance than zircaloy [ASTM Manual 1977].

2.2 Zirconium Metal

Zirconium metal is produced from the mineral zircon, which is mined as a beach sand. Hafnium occurs naturally with zirconium and the main problem of refining zirconium is getting the two separated. Hafnium is undesirable when occurring with zirconium because it absorbs thermal neutrons. Separation is achieved through a solvent extraction process with the resulting zirconium tetrachloride being reduced to zirconium metal using the Kroll process. This zirconium sponge is futher purified by the iodide decomposition process. The final reactor grade zirconium has less than 100 ppm Hf [ASTM Manual, 1977].

2.21 Zirconium - 2.5% Niobium Alloy

Zr - 2.5% Nb is produced by double-arc melting zirconium sponge with a master alloy of zirconium and niobium [Cheadle, Coleman and Licht, 1982]. Zr - 2.5% Nb is a two phase alloy consisting of alpha (α) zirconium (~.6 wt % Nb) and beta (β) zirconium (18-20 wt % Nb) Figure 2.1 shows the phase diagram for zirconium - niobium. Alpha phase zirconium is hexagonal close packed while beta phase is body centred cubic. The beta phase in Zr - 2.5% Nb is metastable at room temperature [Cheadle, Coleman and Licht, 1982].
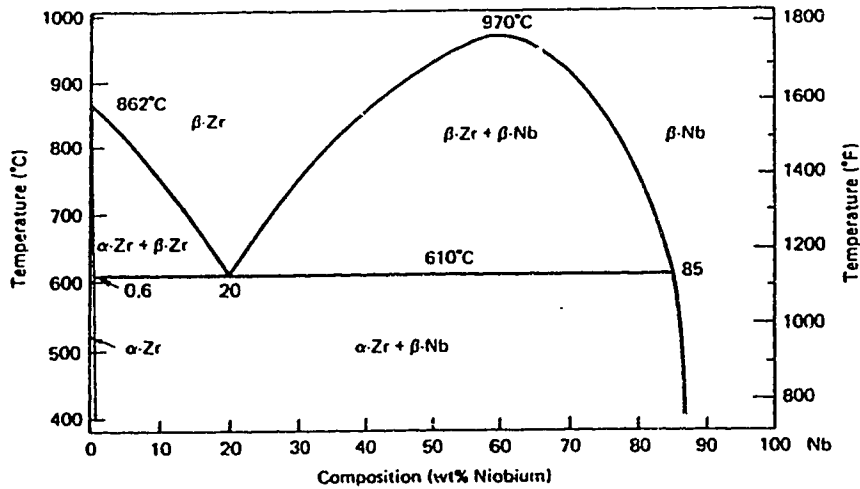
Figure 2.1: Phase diagram Zirconium - Niobium [Cheadle, Coleman and Licht, 1982].
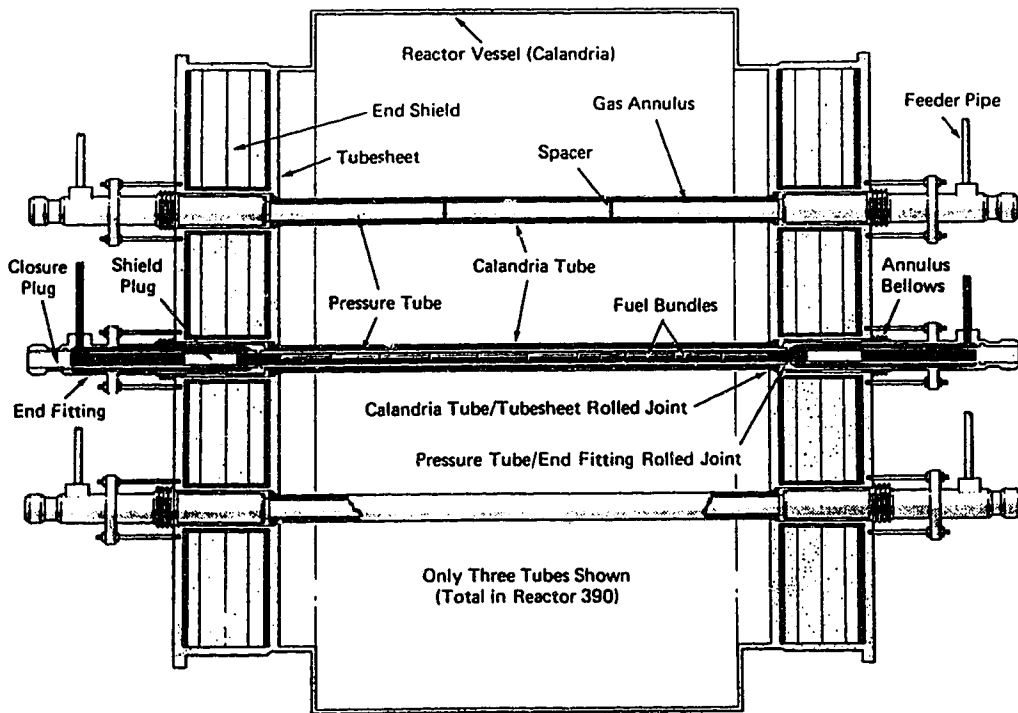
Figure 2.2: Simplified Diagram of a CANDU Reactor [Cheadle, Coleman and Licht, 1982].

2.3 CANDU Pressure Tubes - As-manufactured material

Zr - 2.5% Nb pressure tubes used in the CANDU reactor are manufactured on the basis of Section III of the American Society of Mechanical Engineers (ASME) Pressure Vessel Code. The tubes are formed based on a maximum design stress of one-third the ultimate tensile stress (UTS). They are extruded and cold drawn from billets of essentially inclusion-free Zr - 2.5% Nb in a process which introduces approximately 25 - 30 % cold work to the pressure tubes [Cheadle, Coleman and Licht, 1982].

At room temperature, following extrusion, the pressure tube has an elongated grain structure composed of approximately 10% retained beta (β) zirconium. This retained beta (β) phase is found as a network surrounding the remaining alpha (α) zirconium grains [Perovic, Weatherly and Simpson, 1983]. The alpha α zirconium grains are deformed such that their basal plane normals are oriented parallel to the hoop direction [Cheadle, Coleman and Licht, 1982].

When the pressure tubes are placed into service they contain approximately 10 to 15 ppm hydrogen. As a result of the cathode reaction during corrosion processes,

$$H^+ + 1e^- \rightarrow H^o \quad \text{and} \quad 2H^o \rightarrow H_2$$

atomic hydrogen is produced, some of which is absorbed into the pressure tubes. It is expected that these pressure tubes will absorb up to 50 ppm of hydrogen from the heavy water moderator over a period of 30 years [Cheadle, Coleman and Licht, 1982].

2.4 Delayed Hydride Cracking

Delayed hydride cracking (DHC) in zirconium and zirconium alloys occurs when atomic hydrogen diffuses up a stress gradient and accumulates in a highly stressed region. Under specific temperature and pressure conditions, zirconium hydrides precipitate and subsequently fracture under the applied stresses. It is the fracture of these re-oriented hydrides (Figure 2.3) which are substantially more brittle than the surrounding zirconium alloy, that has caused premature failure of Zr-2.5 wt% Nb pressure tubes [Perryman, 1978].

At the elevated temperatures of reactor service, 250° C to 315° C, most of this hydrogen remains in solution. When temperatures are allowed to drop below the solvus for the precipitation of zirconium hydrides, such as during periods of maintenance, delayed hydride cracking (DHC) may occur.

2.41 Zirconium Hydride Hysteresis

Slattery, 1967 discussed the presence of a hysteresis in the terminal solid solubility (TSS), precipitation and dissolution solvus curves, for Zirconium - Hydrogen. This hysteresis is demonstrated in figure 2.4 where Eadie, Metzger and Leger, 1993 show that a sample containing 60 ppm hydrogen (pt A), would precipitate hydrides on cooling at a temperature of 243°C. If the same sample were reheated, it would require a temperature of 306°C (pt B) to completely dissolve the hydrogen in the sample.
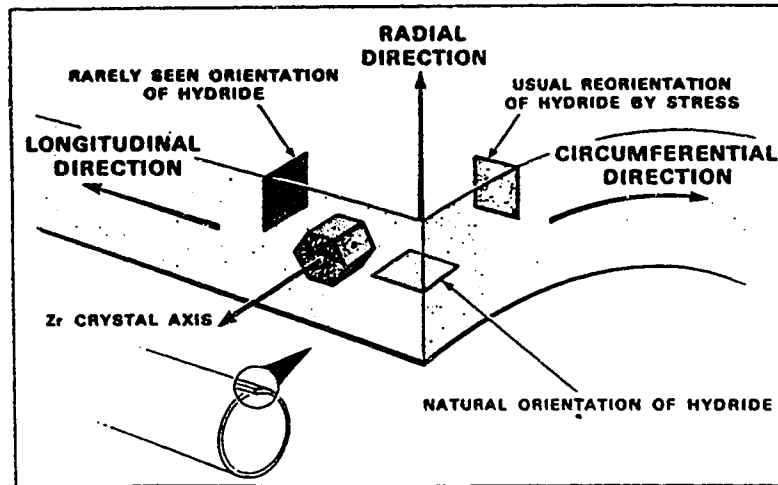
Figure 2.3:   Stress reorientation of zirconium hydrides [Coleman, Cheadle, Ainbler, Lichtenber and Eadie 1985].
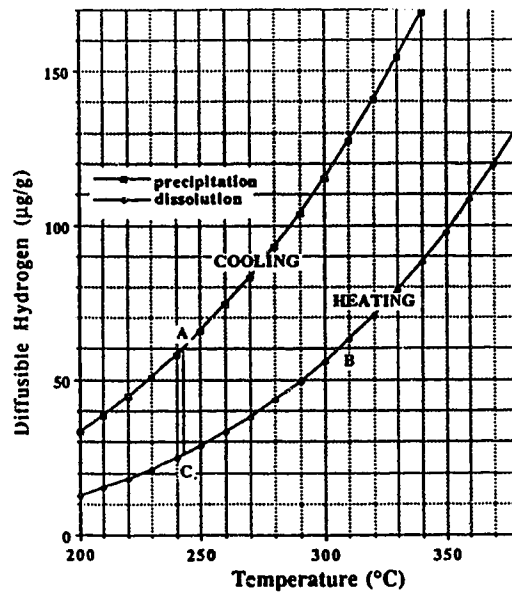
Figure 2.4:   Hydrogen solvi for zirconium-niobium [Eadie, Metzger and Leger, 1993].

Puls, 1994 has suggested various elastic and plastic accommodation effects as possible explanations for this phenomenon.

As a result of this hysteresis, an effect referred to as "direction of approach to temperature" (T_{DAT}) has been described by Ambler, 1984. For temperatures above T_{DAT}, the DHC rate is higher when the pressure tube material is cooled down to test temperature than if the material was cooled down significantly then heated back up to the holding temperature. This occurs because there is less diffusible hydrogen available, after cooling down, to cause DHC at the crack tip.

It is this effect, which has provided a means to control the DHC problem. During periods of maintenance, the temperature of the reactor is allowed to drop significantly then increased to the required holding temperature. The holding temperature is approached from below, causing the rate of DHC to be reduced significantly if not completely arrested [Coleman, Cheadle, Ambler, Lichtenberger and Eadie, 1985]. This type of approach has been referred to as the reactor shutdown manoeuvre.

2.42 Stress Effects

The effects of stressed cracks or notches in the presence of an elevated hydrostatic field has been studied by many [Eadie and Smith, 1988; Eadie and Coleman 1989; Eadie and Ellyin, 1989; Eadie, Mok, Scarth and Leger, 1991; Li, Oriani and Darken, 1966; Puls 1989; Eadie, Tashiro, Harrington and Leger, 1992]. Applied or residual stresses can act on pre-existing cracks to produce stress gradients which concentrate hydrogen in the area of the crack tip.

Eadie, Mok, Scarth and Leger, 1991 have described how the hydrostatic tensile stress at a crack tip lowers the chemical potential of hydrogen, μ_H, according to the expression,

$$\mu_{H,p} = \mu_{H,0} - pV_H \tag{1}$$

In this expression, the chemical potential depends on both the hydrostatic tension, p (p is positive if tensile) and the atomic fraction of hydrogen in zirconium, C_H (this solution is considered dilute, therefore, C_H approximately equals a_H, the activity of hydrogen),

$$\mu_{H,0} = \mu_0 + RTlnC_H \tag{2}$$

V_H is the partial molar volume of hydrogen dissolved in the zirconium lattice and μ_0 represents the chemical potential of hydrogen at zero stress. According to this expression it is expected that the chemical potential would be lower in highly stressed regions. This would account for the flow of hydrogen into the crack tip, an area of minimal free energy [Eadie, Mok, Scarth and Leger, 1991].

As hydrogen migrates, under the influence of an applied stress, to a notch or highly stressed region, its concentration builds up, until zirconium hydrides precipitate. These hydrides, which are building up at the crack tip, grow until a critical length is reached upon which fracture occurs. The crack subsequently arrests in the more ductile material (zirconium alloy) ahead of the hydride platelet(s). Following hydride fracture, an incubation period

occurs as sufficient hydrogen must accumulate at the crack tip allowing the hydrides to regrow to a critical cracking length. The presence of the stress field at crack tip allows the process to restart, producing a discontinuous-type of crack propagation [Dutton, Woo, Nuttall, Simpson and Puls, 1978; Perryman, 1978; Northwood and Kosasih, 1983].

The location of the region of peak stress within this stress field is thought to be a short distance ahead (<100 microns) from the actual crack tip. Hydrogen diffuses to this peak stress area allowing the growth of zirconium hydrides when the solubility limit is reached [Eadie, Mok, Scarth and Leger, 1991].

This stress reorientation of hydrides at the crack tip is assisted if the original texture in the host material consists of basal plane poles parallel to the applied stress (Figure 2.3) [Hardie and Shanahan, 1975].

Reorientation of hydrides due to a plastic flow process rather than precipitation by stress at temperatures greater than 100°C has also been suggested. These results have been reported by Choubey and Puls, 1994 during tensile testing of Zr - 2.5% Nb.

2.43 Hydride Morphology

According to Yuan and Tangri, 1982 stress re-oriented hydrides at the crack tip appear as narrow bands of adjacent platelets parallel to the crack growth plane. Yuan and Tangri found evidence of hydrides reorienting themselves up to 120 μm ahead of crack tip.

Recently, Eadie, Jovanovic and Ma, 1994 have described unfractured crack tip hydride plateletes growing in clusters and increasing in length and thickness at elevated temperatures (~250°C).

2.44 Striation Ridges

Resulting from this discontinuous cracking, a series of striations or ridges are present on the fracture surface. The distance between the individual striations is thought to increase with temperature [Dutton, Woo, Nuttall, Simpson and Puls, 1977; Eadie, Jovanovic and Ma, 1994 - unpublished, Anderson, 1994 - unpublished].

Recent results from the testing of Zr- 2.5% Nb material at different temperatures (200° C & 250°C), [Eadie, Jovanovic and Ma, 1994 - unpublished] suggest that this inter-striation distance corresponds to the length of a hydride cluster. While Yuan and Tangri, 1982, did not find striations on testing done at 140° C on as-manufactured material, they did find ductile tearing ridges perpendicular to the direction of crack growth. The distance between these ridges was also found to correspond approximately to the length of these clusters.

2.45 Secondary Cracking

Wilkins and Nuttall, 1978 discuss the appearance of secondary cracking by non-stress oriented hydrides during the DHC process (Figure 2.3 - "natural orientation of hydride" , basal plane normal oriented in the radial direction). This secondary cracking occurs near the area of fatigue without extending far into the DHC zone. Wilkins and Nuttall also state, that a continuous sheet of hydride presents a path of low fracture resistance and favours the

propagation of secondary cracks. These secondary cracks are thought to grow within
the plastic zone of the main DHC crack at a point where the transverse stress exceeds the
uniaxial yield stress.

Wilkins and Nuttall have suggested that the presence of these secondary cracks could
reduce the hydrostatic stress at the DHC crack tip, due to the relaxation of transverse
stress, and slow down the DHC crack growth.

2.46 Lengthwise Cracks

Eadie, Jovanovic, Ma and Shek, 1994 (unpublished) also found a type of secondary
cracking in several samples. These secondary cracks, although found on a much smaller
scale (5,000 - 10,000X) than that of Wilkins and Nuttall (200 to 300X), were oriented in
the same direction. Eadie, Jovanovic, Ma and Shek referred to these cracks as lengthwise
cracks. This lengthwise cracking was only found in samples which had been thermally
cycled following testing.

2.47 Beta Phase

Perovic and Weatherly, 1982 and Perovic, Weatherly and Simpson, 1983 discussed the
influence of the alpha (α) - beta (β) zirconium interface on hydride formation. Large hydride
platelets (actually composed of several smaller hydride platelets grouped together) were
examined using transmission electron microscope (TEM) techniques. This $\alpha - \beta$ interface
was found to influence the nucleation of zirconium hydrides.

Perovic and Weatherly, 1982 and Perovic, Weatherly and C.J Simpson, 1983 and Eadie,
Jovanovic, Ma and Shek, 1994 (unpublished) have produced results indicating the
breakdown of this $\alpha - \beta$ interface with prolonged heat treatment. Testing done by Eadie,
Jovanovic, Ma and Shek, 1994 (unpublished) shows the breakdown of beta (β) phase
zirconium at temperatures of $400°$ C and times extending from 24 hours to 1,000 hours.

2.5 Sample Testing - Available Techniques

Most commonly a sample of Zr - 2.5% Nb pressure tube material is prepared for testing by
the addition of hydrogen, either gaseously or by aqueous electrolytic techniques. This is
followed by a diffusion anneal to form hydrides within the material. This process produces
approximately the amount of hydrogen which would be acquired by the pressure tube during
normal reactor operation.

A compact toughness (CT) or tapered double cantilever beam (DCB) sample is machined
from the hydrided material (figure 2.5). This sample is then fatigued to produce a sharp
notch and ensure concentration of the hydrides. A DHC testing rig is designed to allow the
sample to be held at varying loads within the confines of a heated environment.

The study of DHC is requires an online detection technique, providing an instantaneous
method of detection of crack movement. Two of the more common methods used are
potential drop (PD) and acoustic emission (AE). Both methods are nondestructive and can
be used in elevated temperature environments (200 to $250°$ C).

applied stress
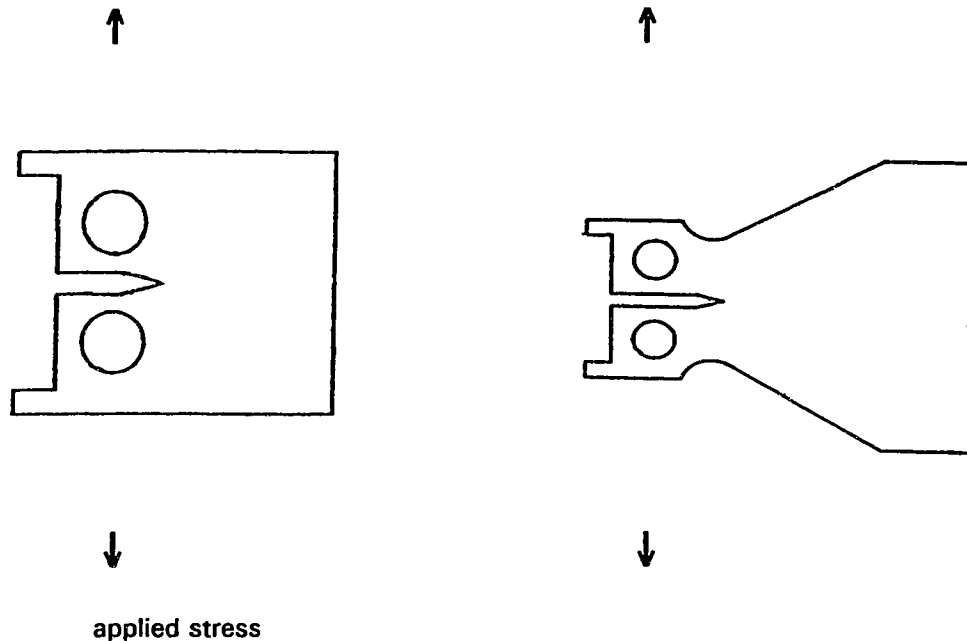
Figure 2.5:   Compact Toughness/Double Cantilever Beam Samples.

2.6 Potential Drop

Potential drop (PD) is a crack measuring technique which requires the use of a stable constant-current power supply. Equipment is required to measure microvolt changes in a signal of several millivolts across a crack opening. A comparison of fractographic features with potential drop data can be used to obtain crack velocity [Simpson and Clark, 1977].

2.7 Acoustic Emission

The abrupt relaxation of either localized or long range stresses within a solid material to produce strain waves is referred to as acoustic emission (AE) [Frederick and Felbec, 1972]. There are several sources of AE which can be considered when examining a solid material; dislocation slip, twinning, crack initiation and crack propagation [Frederick and Felbec, 1972].

AE can span a broad spectrum of frequencies [Fowler and Papadakis, 1972]. Some workers have reported AE in the frequency range of 200 kHz to MHz for brittle fracture events and in the range of 40 to 50 KHz for ductile fracture in the study of plastic deformation of steels [Ono, Stern, and Long, 1972]. The opposite of this result has also been reported; less than 200 kHz for brittle fracture and emissions in the 800 kHz region for ductile deformation, also

for a type of steel [Spanner, 1972].

If the propagation medium is non-dispersive, as with most engineering materials, the entire burst arrives at the receiver undistorted [Fowler and Papadakis, 1972]. Metals are usually of a dispersive nature only when operated at Curie temperatures, superconducting critical temperatures or martensitic phase transition temperatures [Fowler and Papadakis, 1972]. Some engineering structures can be of a dispersive nature due to their shape, in particular rods and plates [Fowler and Papadakis, 1972].

AE, when released during an cracking event such as DHC, can be detected by a piezoelectric crystal which oscillates in a damped sinusoid at its resonant frequency [Coleman, 1986].

2.8 AE Detection System

An AE detection system is composed of several parts; a transducer, preamplifier and threshold detector.

The AE transducer can be fastened either directly to the sample, or to a separate waveguide which has been attached to the sample (figure 2.6). The waveguide can consist of a metal rod or tube or a wire bundle [Anderson, Gavin, Karvinen, Price and Reimann, 1972]. From the literature, it is thought that the shape of a waveguide may influence the transmission of AE emission [Spanner, 1972;Anderson, Gavin, Karvinen, Price and Reimann, 1972]. A tube is thought to behave similar to a bandpass filter, limiting the passage of higher frequencies when compared to a wire bundle [Anderson, Gavin, Karvinen, Price and Reimann, 1972].

A variable, which is of importance in each individual AE system, is the amount and type of couplent connecting the transducer to the waveguide or sample [Hill and El-Dardiry, 1981; Higo and Inaba, 1991;Beatty, 1983; Beatty, Baron, Algera and Feng, 1983]. Most often a type of grease is used as the couplant. Beatty, Baron, Algera and Feng, 1983 felt that the type of couplant used was not important as long as the layer used was thin and uniformly spread out. It was also felt that no couplant at all was acceptable as long as sufficient pressure was used to maintain sensor/sample contact and that the contact area was smooth.

Contact pressures varied significantly among these studies, 70 kPa to 900 kPa, depending on the setup and the couplant used. In summary, most researchers stated that care should be taken in mounting the transducer to the sample whatever the couplant used and that this would influence the reproducibility of results.

The AE transducer contains the piezoelectric crystal which detects AE from a sample. Considerable variations exist between manufactures of AE transducers [Spanner, 1974]. Each transducer is designed to sense AE over a particular range of frequencies, making comparison of data between researchers difficult.

The transducer converts AE into a voltage reading which can be filtered, amplified (preamplifier/gain-depending on the equipment) and fed into a threshold detector. The signal from the transducer is usually measured between a specified range (eg. 0.1 to 0.3 MHz) to minimize external interference. Unfortunately, interference from outside sources can occur throughout this frequency range; hydraulic noise (500 kHz to 1 MHz), machinery noise (not usually above 100 kHz) and electrical interference, which can occur anywhere within the frequency range [Hart, 1976].

There are several ways to process AE signals once they reach the threshold detector. The most common method is measuring the number of AE counts; this is referred to as ringdown counting. When this signal exceeds a threshold voltage, often preset at one volt, it can be expressed in number of events, total counts or rate of counts [Coleman, 1986].

The energy of the signal may be measured or it may be analyzed by its amplitude or frequency distribution. Amplitude distribution analysis occurs when an amplitude sorter performs a per event sorting and storage of acoustic emission signals according to peak amplitude of the AE burst counts [Amouzouvi and Clegg, 1988] (figure 2.7). The peak amplitude of each event is measured and a plot is made of the amplitude distribution.

2.9 Acoustic Emission and DHC - Previous Work

AE methods have been used in DHC studies for developing a detailed understanding of the fracture mechanism and its kinetics.

Using a high temperature transducer attached directly to the sample, Tangri, 1977 counted the number of times an AE signal exceeded a fixed threshold. Tangri felt that the sharp bursts were the brittle hydrides cracking and that zirconium matrix was ductile and therefore quiet. Using this method of testing it was thought that crack growth was intermittant. Arora and Tangri, 1979 also discuss the use of AE techniques to study time dependent failure of components. AE burst counts were correlated with cracked area to estimate the extent of crack growth. They were able to conclude that cumulative burst counts were directly proportional to the area cracked (figure 2.8) (frequencies used were not reported).

Several researchers [Arora and Tangri, 1981; Tangri and Yuan, 1982] have produced results (figure 2.9) indicating three different regimes or areas shown in a plot of cumulative burst counts versus time. Arora and Tangri have suggested that the fast activity regime represents a zone of secondary cracking and does not contribute significantly to primary DHC cracking. Arising from these conclusions a linear relationship was developed in the stable activity regime between count rates (counts/sec) and crack velocities. These tests were done under conditions of differing stress, temperature (100 to 300° C) and hydrogen content.

Relative crack growth rates and the minimum load necessary for crack growth were studied by Sagat, Ambler and Coleman, 1986. The threshold K_{IH} (stress intensity for hydride cracking) was determined by reducing the load until the cracking stops. The total number of AE counts was linearly related to the cracked area and converted to crack length.
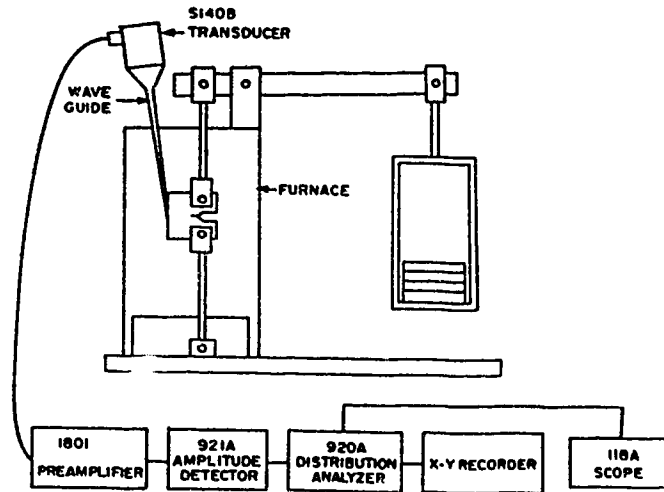
Figure 2.6:   Wave guide used with AE Transducer [Amouzouvi and Clegg, 1988].
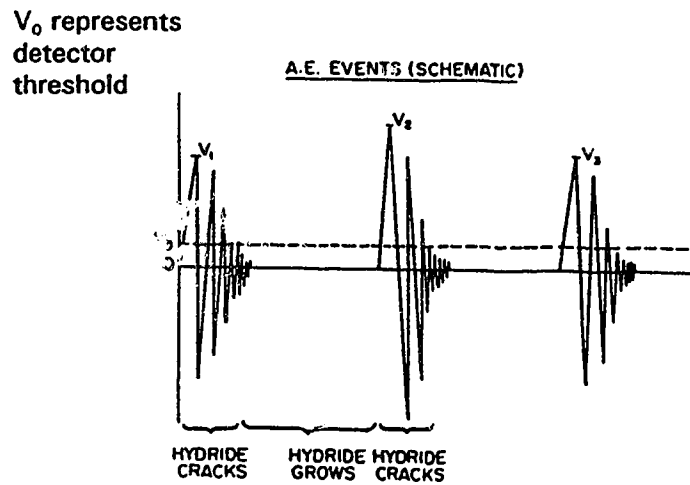

Figure 2.7:   AE Signal Amplitude [Amouzouvi and Clegg, 1988].
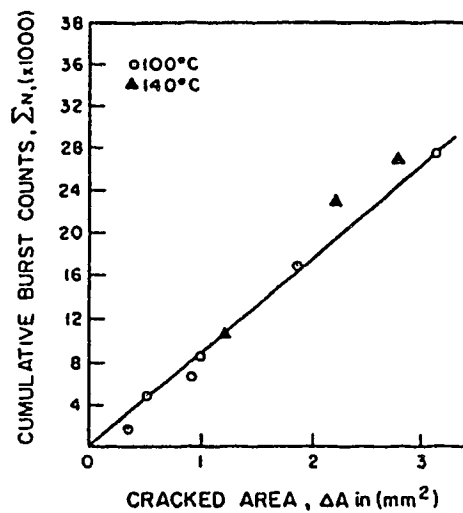
Figure 2.8: Cumulative burst counts vs. cracked area [Arora and Tangri, 1979].
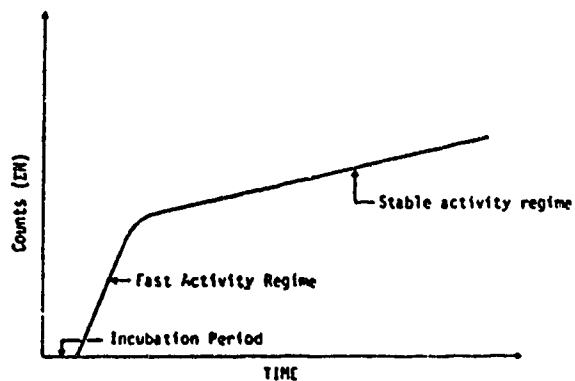
Figure 2.9: Cumulative burst counts vs. time [Arora and Tangri, 1981].

Crack growth was estimated by measuring the number of acoustic emission events produced by a unit area of cracking, at a constant temperature and load. After a specific amount of cracking, the sample was broken open and the crack area was measured to determine the calibration constants. The calibration constant varied between different AE equipment setups, different pressure tubes and different alloys but remained relatively constant for different temperatures [Sagat, Ambler and Coleman, 1986].

Coleman,1986 discusses his previous work which has used AE extensively to determine periods of cracking during DHC in Zr - 2.5% Nb. Coleman, 1982 has also used the relationship between AE counts and area of cracking to estimate crack lengths and velocities. The constant of proportionality, thus established, appeared to be independent of stress intensity (K) and temperature.

Amouzouvi and Clegg, 1988 discuss the amplitude distributions of AE counts and are able to approximate these counts with a power law; $N(Vi) = A\{Vi/Vo\}^{-b}$, where $N(Vi)$ is the cumulative number of events with amplitude greater than Vi, Vo is the detector threshold, and b is the amplitude distribution parameter. A log-log plot of $N(Vi)$ versus Vi showed that for plastic deformation events, which proceed in small steps, low amplitude events are dominant and b is large. For mechanisms involving brittle cracking where a large proportion of high amplitude emissions are produced, b values are low. Amouzouvi and Clegg, 1988 have suggested that it m.. be possible to characterize fracture events by the determination of this single parameter, .

Amouvzouvi and Clegg, 1988 performed DHC testing on samples of Zr - 2.5% Nb containing finely dispersed hydrides. During this testing, it was discovered that the amplitude of the AE signals decreased with an increase in stress intensity factor (K_I)(high amplitude signals were apparent with low K's). The amplitude of the AE signal was also found to increase with test temperature.

Simpson, 1979 discusses unpublished results which were obtained using combined AE and potential drop monitoring techniques. The AE equipment recorded a rapid series of AE bursts which were thought to be related to the fracturing of individual hydride platelets. Similar bursts were not recorded by potential drop which indicated only the tearing of large shear ridges in the more ductile zirconium matrix [Simpson, 1979].

Eadie, Li and Shek, 1993 have indicated that the relationship between AE count rates and area cracked may not be linear over a range of wide temperatures. If the results from Figure 2.10, (testing done on DCB samples of as-manufactured Zr - 2.5% Nb pressure tube material) were plotted as counts versus area cracked the resulting slopes would vary with temperature.

Tensile testing of Zr - 2.5% Nb material at elevated temperatures was done by Choubey and Puls, 1994. In their article, there is some discussion of the possible contributions to AE by the effects of twinning in zirconium at high temperatures.
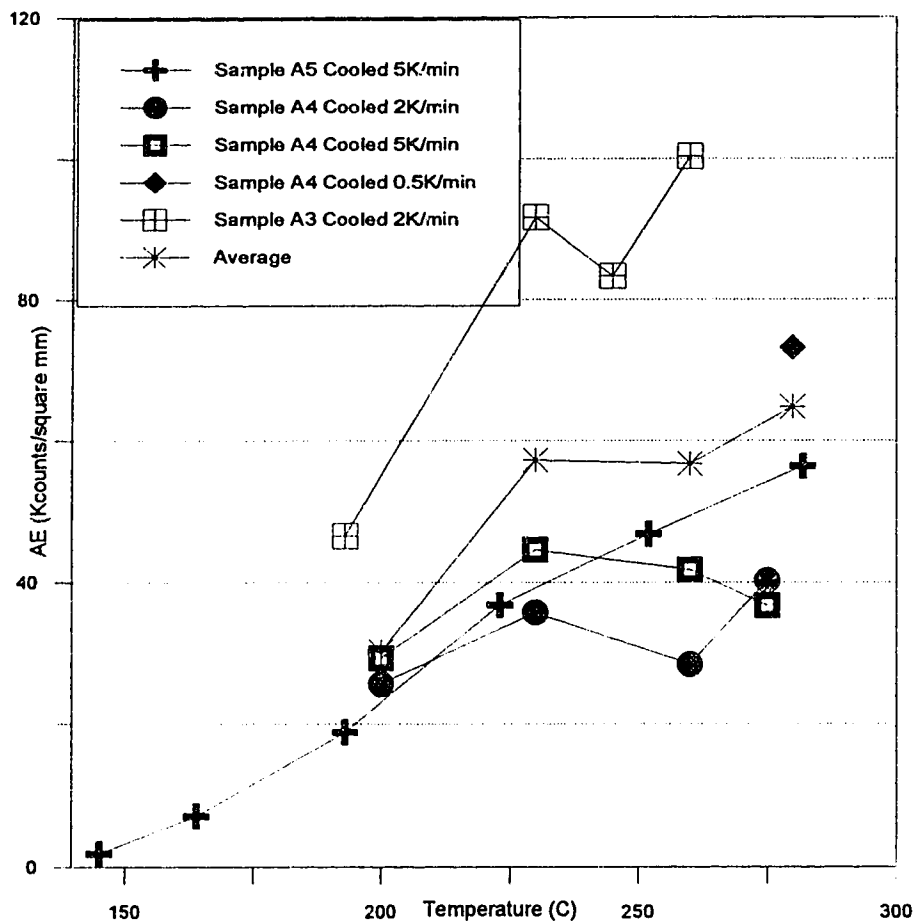
Figure 2.10: Kilocounts per mm^2 versus temperature [Eadie, Li, Shek and Sagat, 1993].

2.10 Summary

Prior to the work of Eadie, Li and Shek, 1993, most isothermal DHC testing indicated a nearly constant relationship between AE cumulative counts and area cracked over a range of temperatures [Arora and Tangri, 1981; Tangri and Yuan, 1982; Sagat, Ambler and Coleman, 1986]. The DHC testing done by Eadie, Li and Shek, 1993 has produced results that indicate AE has a strong dependence on temperature.

If AE is dependent on temperature, delayed hydride crack velocity (DHCV) can not be correlated directly with area cracked and AE. This point will be discussed further in Section 5.10.

3.0 EXPERIMENTAL

3.1 Material Preparation

Two different types of samples were prepared; eight were prepared from as-manufactured material, the other, a single sample, was cold worked an additional 40% in the axial direction to simulate the yield strength of irradiated material.

3.11 As-Manufactured Material

A sample of CANDU pressure tube material was first sectioned, then flattened by a continuous reverse bending technique. This method introduces very little additional cold work into the sample. These samples contained only the original amount of cold work necessary to form the pressure tubes, approximately 30%. The flattened sample was stress-relief annealed for 24 hours at 370 degrees Celsius (C). Blanks of approximately 45 by 45 mms were cut in preparation for introduction of hydrogen. A total of 8 specimens were prepared in this manner.

3.2 Introduction of Hydrogen

A thin layer of zirconium hydride was deposited on the sample surface by using electrolytic techniques. This was followed by a high temperature diffusion anneal to force hydrogen into the specimens.

3.21 Surface Preparation & Hydriding

Initially surface preparation consisted of an acid pickle composed of 25% sulphuric acid (H_2SO_4), 25% Nitric acid (HNO_3), 5% hydrofluoric acid (HF) and the balance being water. This was followed by a thorough scrubbing with a fine alumina powder.

The actual hydriding process consisted of placing an individual sample in a large beaker of 5% H_2SO_4 which was kept at a temperature of approximately $90^\circ C$ (figure 3.1). The zirconium sample (cathode) was connected to the negative side of a DC power supply which provided approximately 100-150 mA/cm^2. The positive side of the power supply was connected to a thin sheet of platinum foil (anode) [Sawatzky,1960].

At the cathode, hydrogen gas was produced,

$$Zr + 1.6H^+ + 1.6e^- \Rightarrow ZrH_{1.6}$$
$$2H^+ + 2e^- \Rightarrow H_2$$
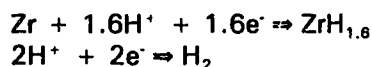
and at the anode,

$$2H_2O \Rightarrow 4H^+ + O_2 + 4e^-$$
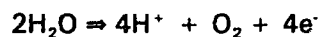
oxygen gas was produced.
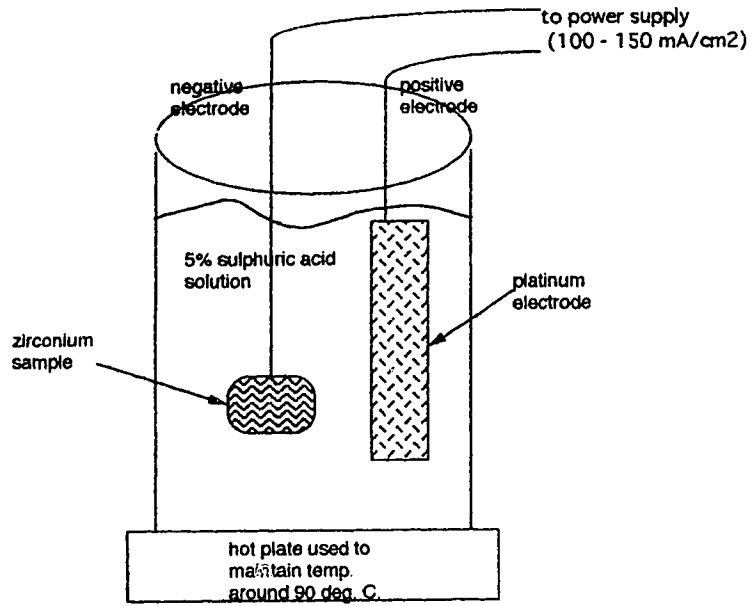
Figure 3.1: Electrolytic Hydriding Set-Up.
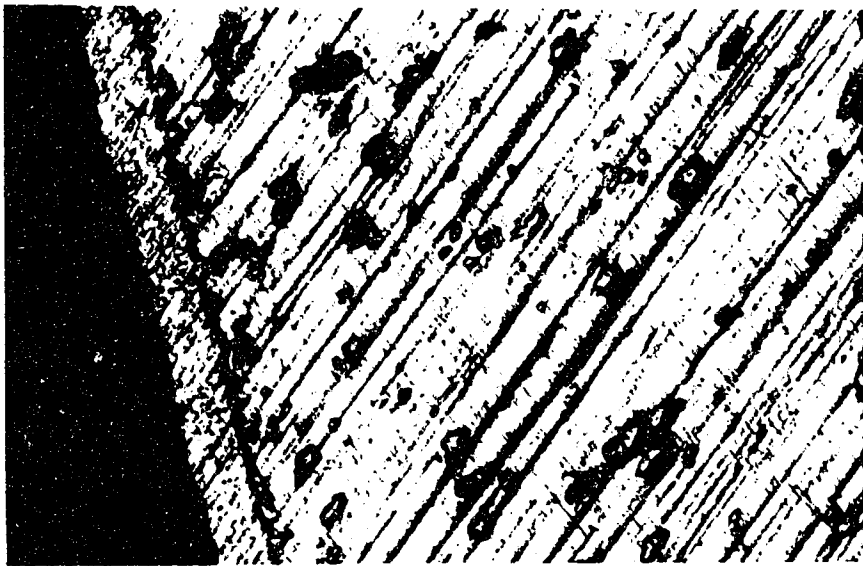
Figure 3.2: Photo of Hydride Layer before Anneal, Sample A3, 185X.

This particular process was later modified by eliminating the pickling stage and preparing the sample surface by using a glass bead blasting process. In the beading process a high pressure spray of glass beads bombards the sample. This assists in removing the surface oxide layer (this method is similar to the process which is used to sandblast bricks on the face of an old building) without significant work hardening. This was again followed by a thorough scrubbing with alumina powder. This final technique produced the best results (figure 3.2).

3.22 Diffusion Anneal

Following hydriding, a diffusion anneal was necessary to introduce hydrogen into the sample. The terminal solid solubility (TSS) curve was consulted to determine that a minimum temperature of 613 K was required to introduce 90 ppm of hydrogen in the specimens [Kearns, 1967]. A diffusion coefficient, D_H = 2.19 X 10^{-10} m^2/s, was calculated using the expression [Eadie, Tashiro, Harrington and Leger, *1992*].

$$D_H = 4.1 \times 10^{-7} \exp \{-4618.72/T(K)\} \text{ m}^2/\text{s} \tag{3}$$

The expression,$X = C(Dt)^{1/2}$, where X is the diffusion distance, t is the time required and C a constant calculated from previous work [Eadie, Li, Shek and Sagat, 1993], was used to calculate the time required at temperature T for hydrogen diffusion. At 613 K, it was determined that approximately 96 hours were necessary to produce a sample containing 80 ppm hydrogen uniformly throughout. Solutions to the diffusion expression, $X = C(Dt)^{1/2}$, [Crank, 1975] indicate that a reduction in the actual time required by 1/2 would make little change to the final concentration obtained at the centre of the sample. Therfore it was estimated that 48 hours would be sufficient to obtain enough hydrogen in the interior of the sample. Similar methods were used to calculate the time and temperature requirements for the specimens with higher hydrogen contents (36 hours at 673 K for 160 ppm). Several samples were prepared, producing different hydrogen contents varying from 40 ppm to 210 ppm hydrogen. These samples were examined metallographically following the diffusion anneal to estimate the hydrogen content (Figure 3.3), then the surfaces were ground down slightly to remove any remaining hydride layer.

Figure 3.3:   Photo of hydrides in sample, sample A3, 115X.

3.23 Tapered Double Cantilever Beam/Constant K Sample

The samples were machined into double cantilever beam or "constant K" samples (Figure 3.4), which were oriented such that cracking would occur along the axial direction of the pressure tube material (Figure 3.5). The design of the tapered double cantilever beam sample is such that it provides a constant stress intensity factor (constant K) as long as testing remains in the tapered region. The sides of the sample are tapered to provide a stress intensity value which is independent of crack length (figure 3.5).

Sample cutting was done using electro-spark discharge machining (EDM) by Excell Wire Erosion in Brampton, Ontario.

A more quantitative hydrogen analysis was done following machining using both microcalorimetric and inert gas fusion methods.
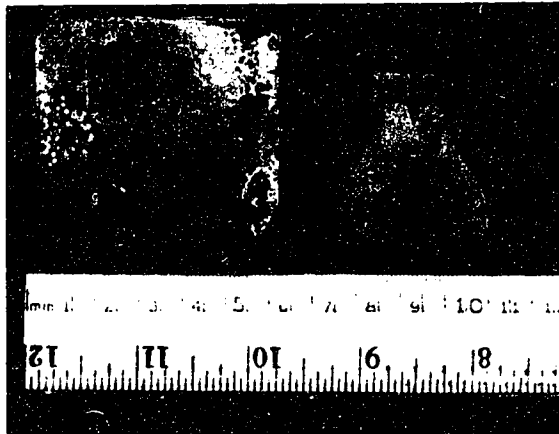

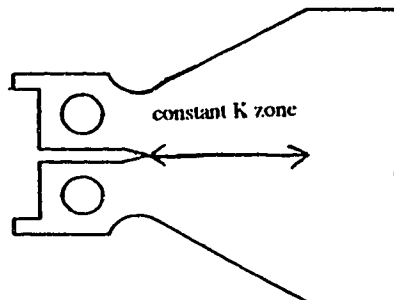Figure 3.4:   Sample - before and after machining.

Figure 3.5:   Tapered double cantilever beam/constant K testing specimen.

3.3 Fatigue

The constant K samples were carefully fatigued from 0.2 to 13 MPa(m)$^{1/2}$ using a Material Testing System (MTS) 810 to produce a sharp crack in the notched area. Care was taken to avoid exceeding the testing K value of 17 MPa(m)$^{1/2}$.

3.4 DHC Test Rig Setup

The sample testing rig is shown in Figure 3.6. It consisted of two loading rods, the lower, fixed in position and the upper, connected to a lever-type of arrangement. Figure 3.7 is a schematic diagram of a sample mounted in the loading rods. A K-type themocouple was spot-welded to the sample for precise temperature control at the crack location.

3.41 Furnace tuning

A Eurotherm, model 815 controller/programmer was used to control the temperature to an electrical resistance-type furnace. The accuracy of the thermocouple used during material testing was verified with a Wahl Thermocouple Calibration Standard C-65. Following furnace tuning, a series of tests were done to check the size of the constant temperature zone within the furnace (Table 3.1). The size of the constant temperature zone, located near the centre of the furnace, was approximately 80 mm X 80 mm.

Table 3.1: Results of Furnace Testing at 300° C and 350° C.

	Left of Centre - 40 mm	Centre of Furnace	Right of Centre - 40 mm
Up 40 mm	300/350	300/350	300/350
Centre of Furnace	302/350	302/350	302/350
Down 40 mm	300/350	300/350	300/350

3.42 Acoustic Emission (AE) Equipment

The following Dunegan/Endevco acoustic emission equipment was used: Model 302A Dual Amplifier, Model 303 Dual counter, Model 1801- 170B Preamplifier (using 0.1 to 0.3 MHz) and Model D150M 144 Transducer (Figure 3.8 & Figure 3.9).

The transducer was mounted in a bracket at the end of the lower loading rod (Figure 3.10). It was held lightly in place (approximately 300 grams pressure) with a small piece of foam rubber and some high temperature vacuum grease. This loading rod served as a waveguide to transmit any AE signals which originated from the sample during the cracking process.

3.43 Potential Drop (PD) Equipment

A Hewlett Packard HP 6263 DC power source was used to supply a constant current of ~8 Amps. The power to the sample was supplied through copper wire which was fastened
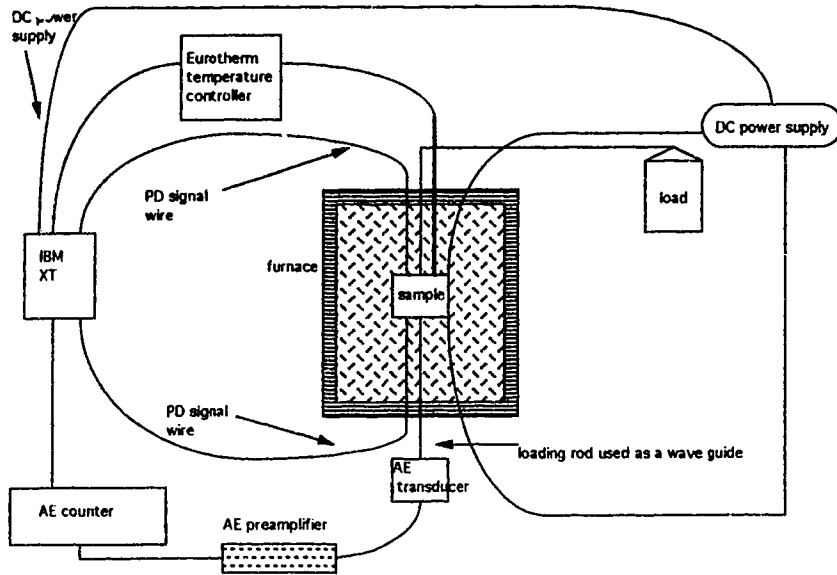
Figure 3.6:   Schematic of Test Rig Setup
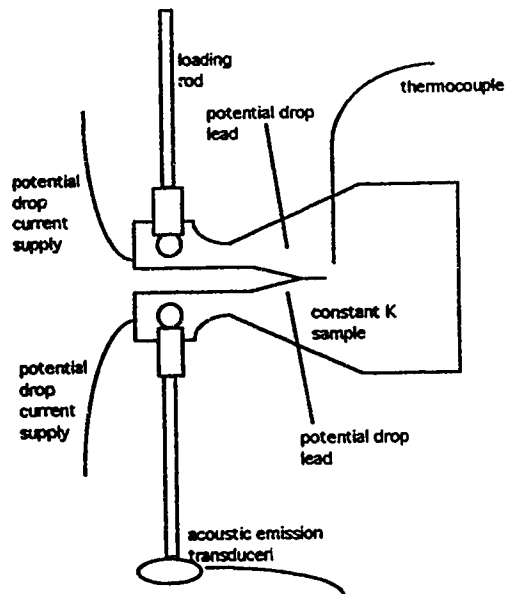
Figure 3.7: Constant "K" Sample with Attachments

to the sample near the crack opening with screw-type connectors. The actual PD signal was carried through thin strips of Chromel A which were spot welded to the sample on either side of the crack.

3.44 Computer Recording System

Data from the temperature controller, acoustic emission counter, DC power supply and potential drop signal were collected and stored on an IBM XT-type computer. (Figure 3.6) A computer program, written in BASIC, was used to record the data from the above sources.
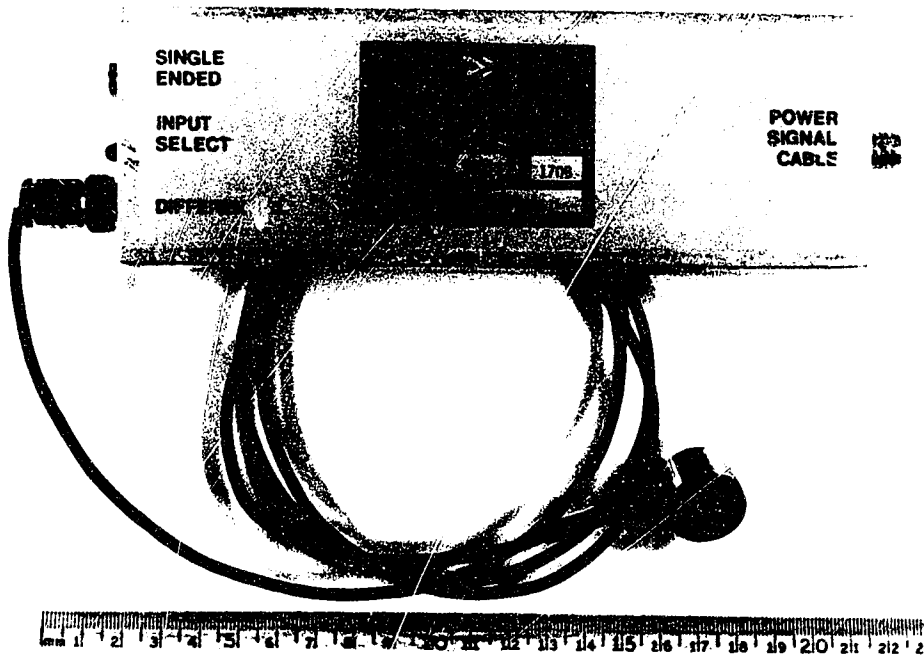
Figure 3.8: AE preamplifier and transducer.
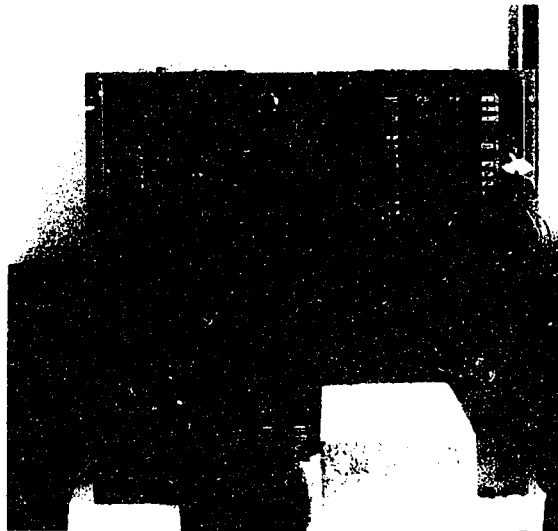
Figure 3.9:   Dunegan/Endevco Acoustic emission equipment.
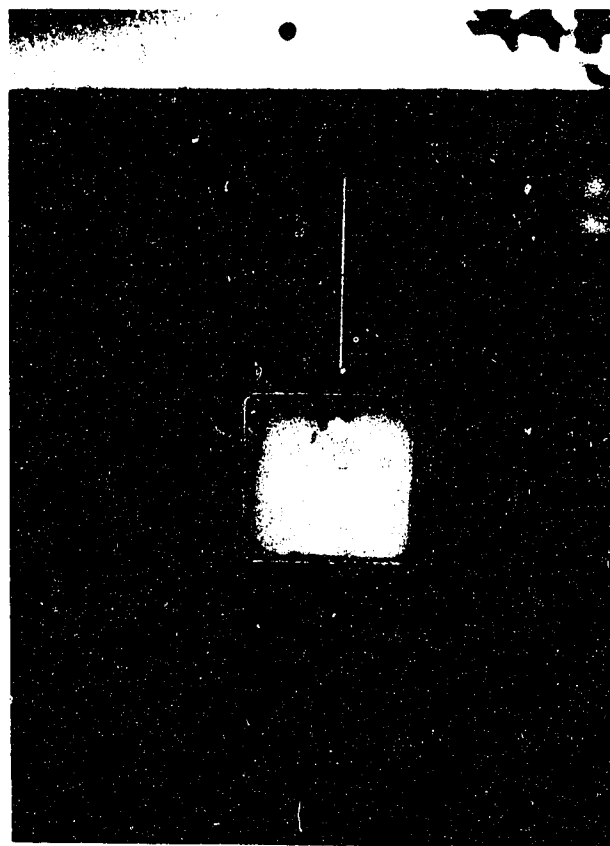
Figure 3.10:   Transducer held in place on loading rod.

3.5 Material Testing

Initially a series of runs was made on the testing apparatus with a "dummy" compact toughness (CT) specimen composed of steel. This was followed by testing on the samples prepared from the Zr-2.5% Nb pressure tube material.

3.51 Steel Dummy Sample

A series of heating and cooling tests were programmed into the temperature controller to simulate a testing cycle. Testing began initially with a gain setting of 95 decibels (dbs) on the AE equipment and a test rig load of 1.5 kg to check for background noise on the AE equipment. The AE preamplifier had a built-in gain setting of 40 dbs and the remaining 55 dbs were made up on the AE dual amplifier. This gain setting was gradually reduced to 88 dbs total (Figure 3.11). The same type of test was repeated with a mass of about 15 kgs to simulate actual testing conditions at 17 MPa $(m)^{1/2}$ (Figure 3.12). This final test was done under actual loading conditions. A maximum of about 6.8 kilocounts was accumulated over 30 hours of testing and several periods of temperature cycling. It was determined that this would be an acceptable amount of background noise, less than 5% of the total kilocounts, when compared with previous AE results (Eadie, Li, and Shek, 1993).

3.52 As-manufactured Zr-Nb Samples

All the testing on as-manufactured samples was done at a mass of approximately 10 to 12 kgs to produce a K_{Ic} of 17 $MPa(m)^{1/2}$. The K_{Ic} was calculated using the expression [Davies and Stearns, 1981];

$$K_{Ic} = 10.9 \ P/[B(w)^{1/2}] \qquad \qquad (4)$$

where P was the applied load (Newtons), B the sample thickness and w the sample width. The gain was set on the AE equipment at 88 dbs based on results from testing of the steel dummy sample (figures 3.11 & 3.12).

A typical cracking run consisted of a climb from room temperature at 5° C/min. to a hold temperature. The hold temperature, determined by the TSS curve plus a superheat of approximately 70 to 90°, was held for 3 hours in order to dissolve a large proportion of the hydrogen in the sample. The sample was then cooled at a rate of 2.5° C/min to the testing temperature until cracking started. Cracking was allowed to continue for either several hours or several days depending on the test temperature. Figure 3.13 shows a typical heating and cooling cycle along with some AE data.

The test was stopped when it was determined that enough cracking had occurred to allow easy measurment of the crack area by the use of an optical microscope. This was done by estimating cracking times by the use of the following expression for average delayed hydride crack velocity (DHCV) of as-manufactured material taken from Eadie, Li, and Shek, 1993:

$$\text{ave DHCV} = 7.9446 \times 10^6 \ (nm/s) \ \exp\{-6246.38/T\}. \qquad (5)$$

This rough calculation was used to estimate cracking velocity and thus ensure cracking remained in the constant K zone of the sample (figure 3.5). Cracking was arrested by removing the load from the sample.
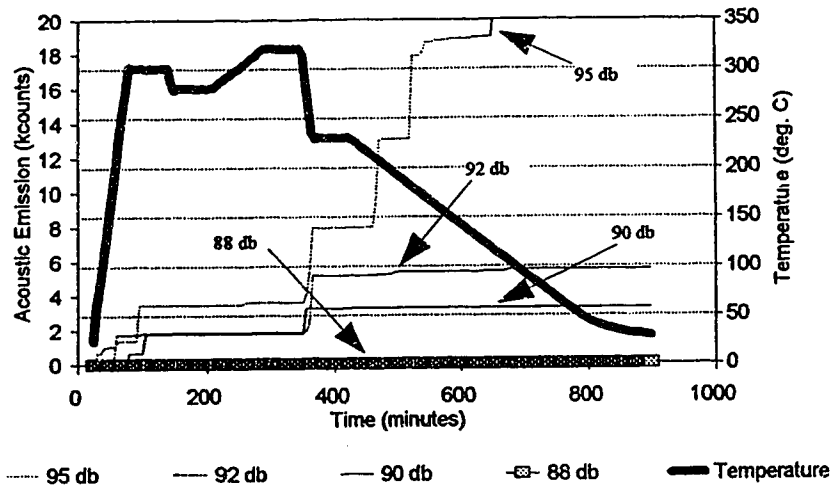
Figure 3.11:   AE and temperature vs time for different gain settings - 1.5 kg load using dummy steel sample.
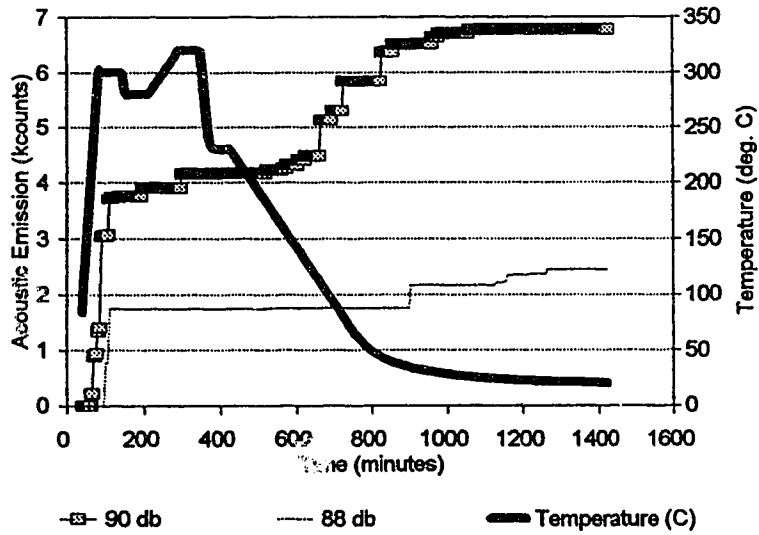

Figure 3.12:   AE and temperature vs time for different gain settings - 15.08 kg load using dummy steel sample.

Multiple tests were conducted on each sample. Identification of individual tests was made easier by heat tinting the sample following each test. During the heat tinting process, the sample was exposed to a temperature significantly higher than the test temperature for a short period of time (30 minutes) to produce a thick oxide coating on the fracture surface. Progressively lower temperatures were used for each tinting process, giving thinner oxide layers each time. This was done to produce a different oxide colour on the sample surface during each tinting procedure. This process allowed easier identification of the individual test runs following the end of testing a sample. It was determined, following testing of the first two samples, that the optimum number of tests which could be performed on each sample was about five. Difficulties arose in identifying a particular fracture surface with a particular test if more than five tests were attempted.

Isothermal testing was attempted at the following temperatures; 100, 120, 130, 140, 150, 165, 170, 195, 200, 210, 220, 250, 260, 270 degrees Celsius.

The first two samples were tested using a combined crack detection system of both AE and potential drop techniques. At this point, it was determined that some type of electronic interference was affecting the AE equipment. There were two other testing rigs receiving the potential drop signal at the time and it was suspected that the source of this interference was most likely related to the potential drop signal. When the potential drop equipment was removed, no further detectable interference was found.

When testing was concluded on a sample, it was removed from the rig and broken apart. The fracture surfaces were examined using an optical microscope. Photographs were taken and the individual test distances were identified and measured (Figure 3.14).

3.53 Cold Worked Zr-Nb Samples

An as-manufactured specimen of Zr-2.5 Nb pressure tube material was cold worked an additional 40% by rolling in the axial direction. This resulted in a final condition of ~70% cold work. This sample was prepared to contain approximately 160 ppm hydrogen. A constant "K" sample was prepared in a manner similar to the as-manufactured material.

Results from the research done by Eadie, Li and Shek, 1993 indicated that the average delayed hydride crack velocity was higher for the cold worked material than the as-manufactured material. Therfore the following expression was used in the estimation of cracking distance in a procedure similar to that used for the as-manufactured material [Eadie, Li, and Shek, 1993];

$$DHCV = 1.1769 \times 10^7 \text{ (nm/s) exp} \{-5885.7/T\} \tag{6}$$

This sample was also tested, measured and examined optically in a manner similar to the as-manufactured samples.

3.6 Examination of Striation Spacing

A scanning electron microscope (SEM), Hitachi S - 2700, was used to examine striation spacings on several of the samples following testing. The samples were examined using secondary electrons at a voltage of 20 kV.
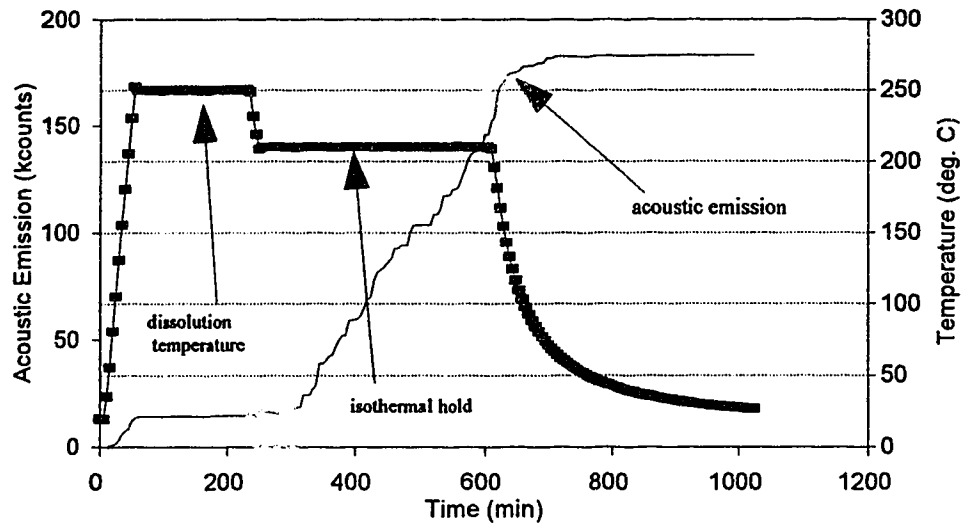
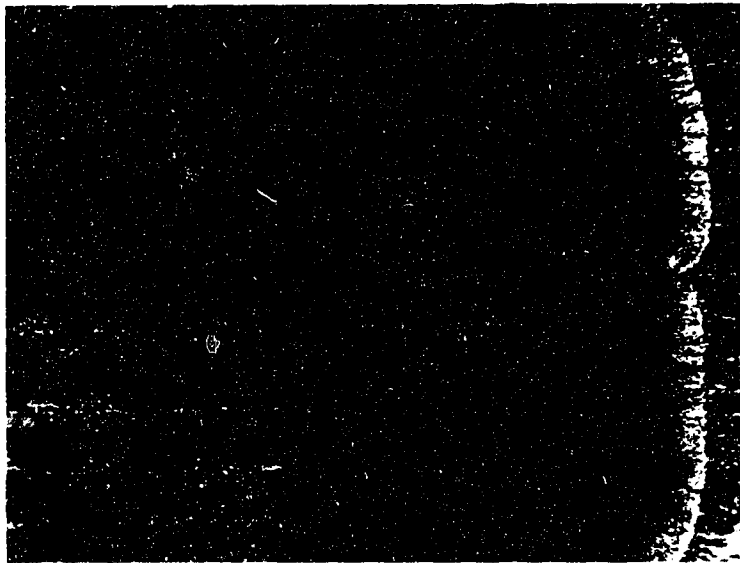Figure 3.13: Typical Heating and Cooling Cycle ($K_I = 17$ mpa $(m)^{1/2}$, 22 ppm H)

Figure 3.14: Fracture Surface showing Multiple Testing as indicated by Heat Tinting

4.0 RESULTS

4.1 Hydrogen Analysis

Hydriding a sample to obtain an adequate surface layer of zirconium hydride appeared to be more of an "art" than an exact science. Each batch of samples behaved differently during the hydriding process. Listed below in Table 4.1 are the results of hydrogen analysis following the diffusion anneal.

Table 4.1: Hydrogen Analysis

Sample no.	Proposed hydrogen level	Actual hydrogen level
A1	80	22
A2	80	54
A3	160	232
A4	160	207
A5	80	80
A6	80	82
A7	80	96
A8	80	94
SW1	160	147

*samples prepared with hydride layer removed prior to electrospark discharge machining

4.2 As Manufactured and Cold Worked Samples - AE Testing Results

An actual test consisted of an initial dissolution heating followed by controlled cooling to test temperatures ranging from 100° C to 265° C under applied stress. During the early stages of testing, acoustic emissions versus time were plotted to give an indication of how many emissions were collected on the cool down portion of testing. Figure 4.1 is an example of a test where a large amount of AE was produced during the cooldown to test temperature. This early plotting of data was particularly important on some of the low temperature tests where preliminary results were used to provide estimates on how long a test should be conducted. An attempt was made to produce tests where at least 80% of the AE were attained on the isothermal part of the testing. This was done to ensure that most of the cracking occurred isothermally (Figure 4.2). In an attempt to reduce the amount of DHC and subsequent AE during the cooldown portion of some of the low temperature tests, dissolution temperatures were reduced to cause only enough hydrogen to go into solution for DHC to occur. In this manner, any unnecessary AE during cooling was avoided. Figure 4.3 illustrates a test where little AE is produced during the cooldown portion of testing.
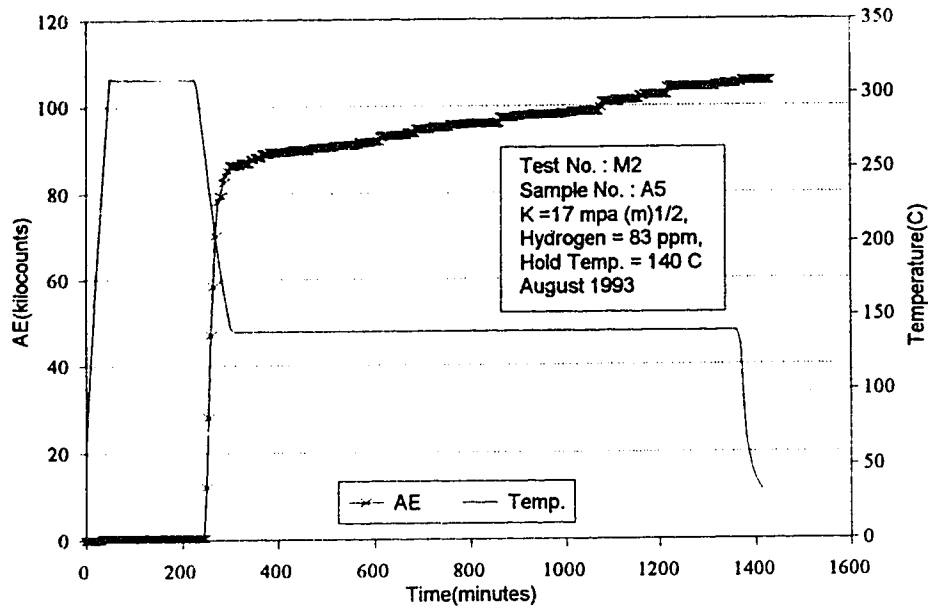
Figure 4.1: Isothermal Hold indicating Significant AE Activity during Cooldown Portion of Testing.
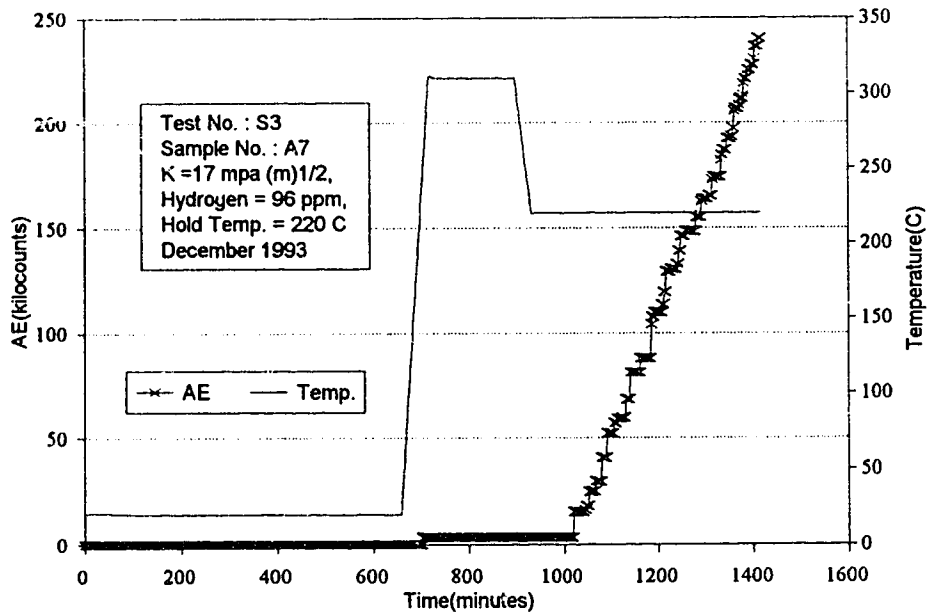

Figure 4.2: DHC Testing indicating >80% of AE Activity during Isothermal Holding.
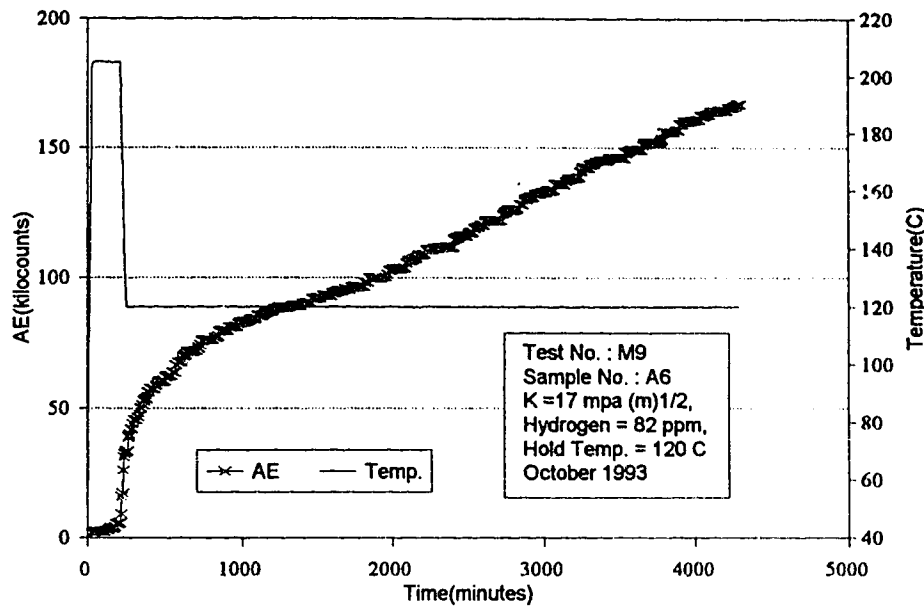
Figure 4.3: Low superheat on low temperature test showing little AE activitiy during cooldown part of testing.

The remaining preliminary AE results for both the as manufactured and cold worked samples were plotted and are located in Appendix 1.

4.21 Abnormal Results

As previously discussed, initial DHC testing was done with a combination of AE and potential drop techniques. As illustrated in Figures 4.4 and 4.5, some interference was encountered between the two techniques. After removal of the potential drop equipment the AE results appeared to return to values which were expected (Figure 4.6) for the temperature which was being tested.

4.3 Estimation of Area Cracked

Following each series of tests, the sample was broken apart along the crack face and the area cracked was measured. For each sample the crack velocity and kilocounts per mm^2 of crack advance were calculated. It was expected that cracking might occur during the cooldown portion of the test. In order to ensure all cracking occurred isothermally, the total area cracked per test was multiplied by a weighting factor. This weighting factor was obtained by dividing the total number of kilocounts accumulated during the isothermal part of the test by the total number of kilocounts accumulated during the entire cracking period. This AE crack ratio was calculated for each test temperature. If this ratio was less than 0.8, the test was not used in the final results (that is, at least 80% of the acoustic emission had
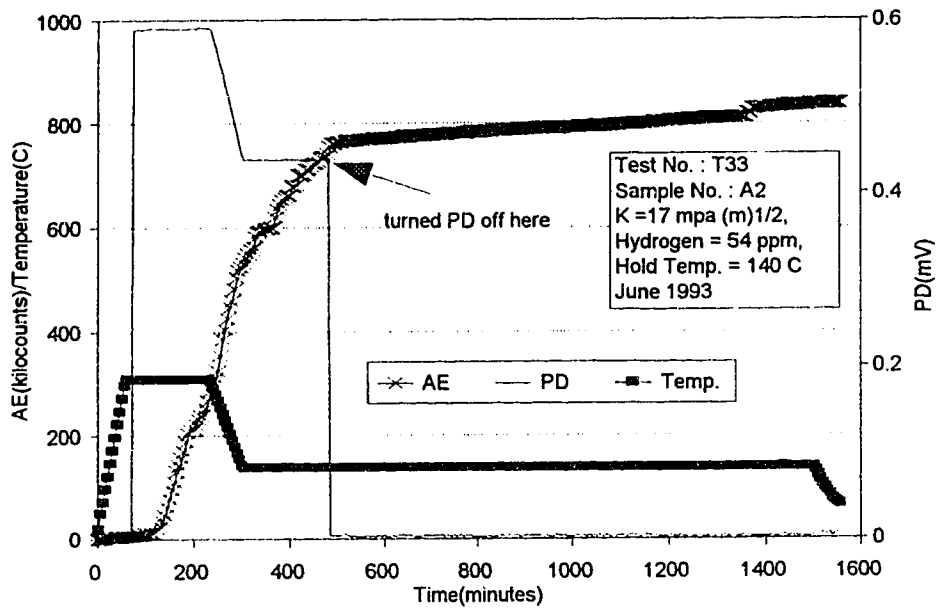
Figure 4.4:   AE results before and after removal of potential drop equipment.
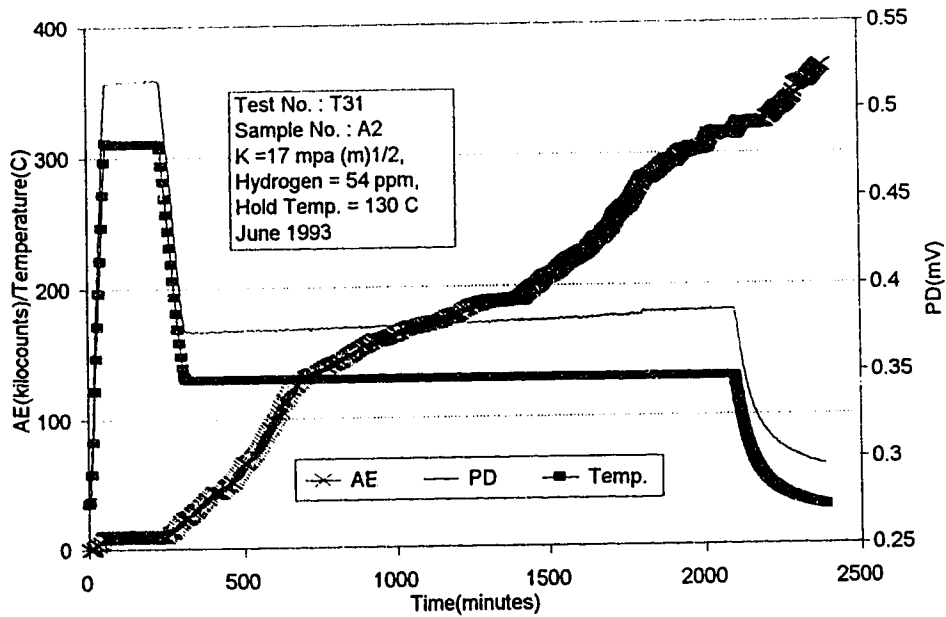

Figure 4.5:   Possible anomalous AE results - due to interference with potential drop equipment.

to be isothermal). This AE crack ratio is shown in Table 4.2. The test done at 210 °C, with an AE crack ratio of 0.495 is a test which was discarded because too much cracking had occurred while cooling the sample down to test temperature.

Cracking distances for each individual test were measured from the surface of the crack face using an optical microscope. These distances were multiplied by the AE crack ratio to come up with an adjusted crack distance which was used as the isothermal crack distance. An example of this type of calculation is done in Table 4.2. It is this adjusted crack distance which was used in the following plots of crack velocities and AE per mm^2 vs test temperatures (Figures 4.7 to 4.22).

Table 4.2: Adjusted Crack Distances,

Test temp. (C)	Total crack AE (kcounts)	Isothermal AE (kcounts)	AE Crack Ratio AE (iso AE /total crack AE)	Measured Crack Dist. (mm)	Adjusted Crack Distance (mm)
210*	53.56	26.53	.495	.07	.495 X.07 = .035
100	7.049	6.749	.957	.629	.957 X.63 = .602

* this test was discarded.

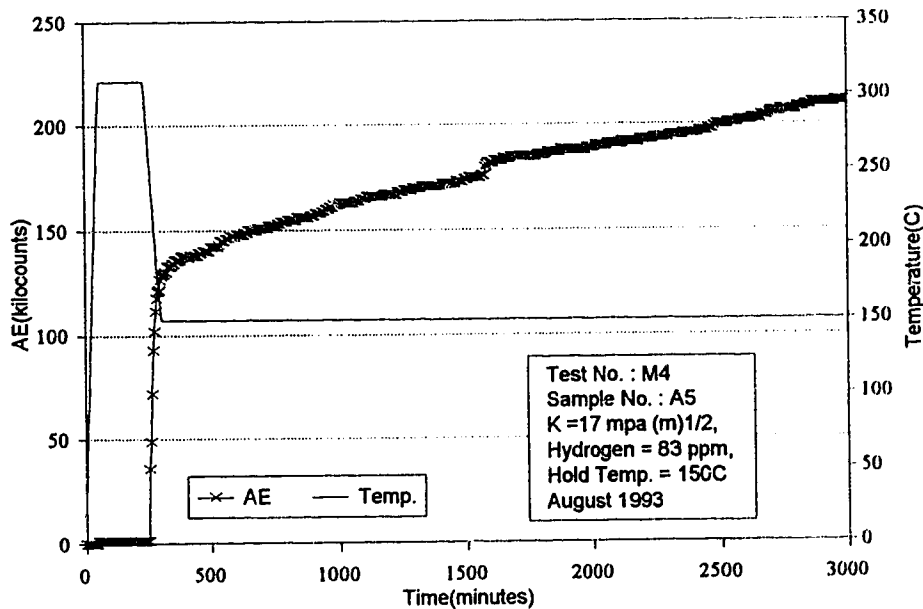Figure 4.6: Typical set of AE results for the temperature at which the sample was tested.

Figure 4.7: As-manufactured material, experimental crack velocities - sample A1.

Figure 4.8: As-manufactured material, experimental kilocounts/mm**2 - sample A1.

Figure 4.9: As-manufactured material, experimental crack velocities - sample A2.

Figure 4.10: As-manufactured material, experimental kilocounts/mm**2 - sample A2

Figure 4.11: As-manufactured material, experimental crack velocities - sample A4.

Figure 4.12: As-manufactured material, experimental kilocounts/mm**2 - sample A4.
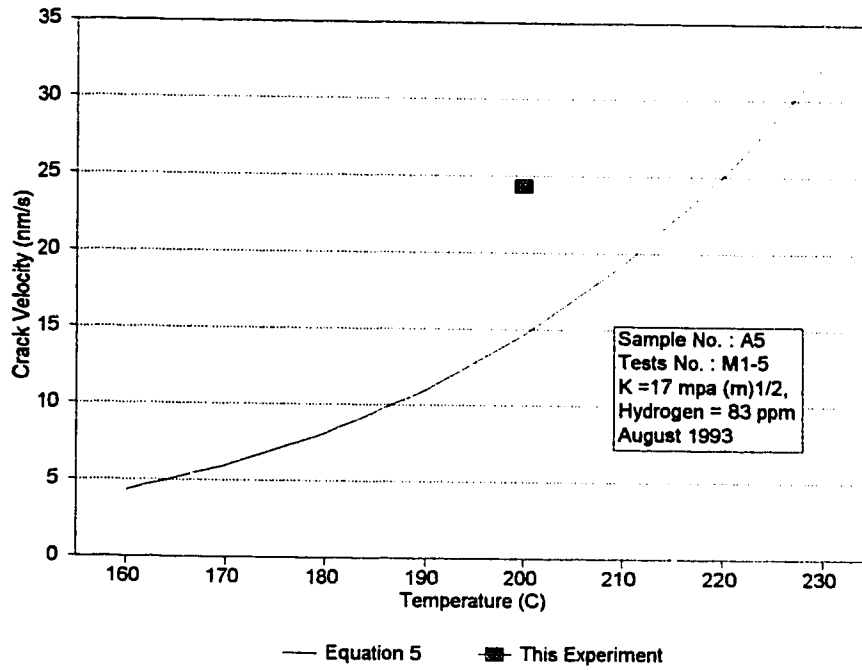
Figure 4.13: As-manufactured material, experimental crack velocities - sample A5.
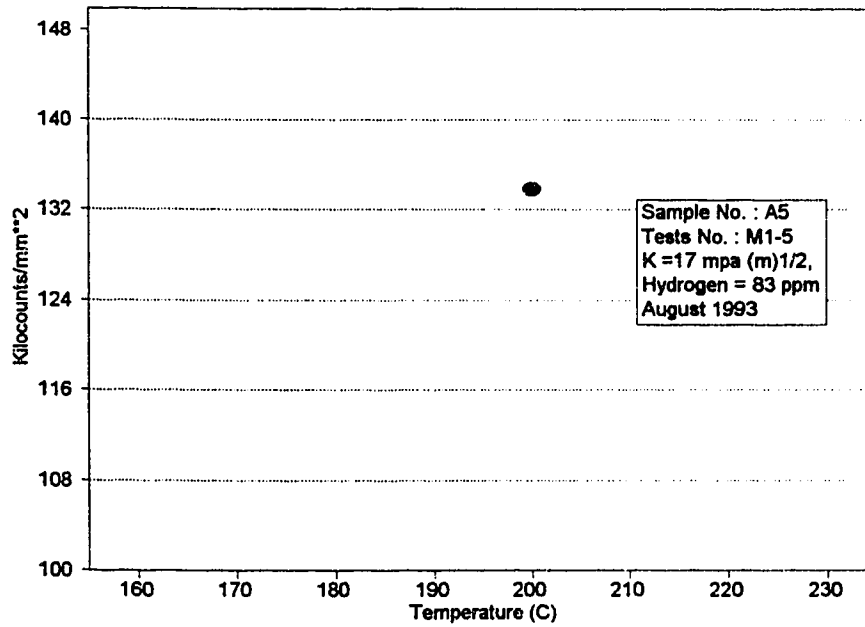
Figure 4.14: As-manufactured material, experimental kilocounts/mm**2 - sample A5.
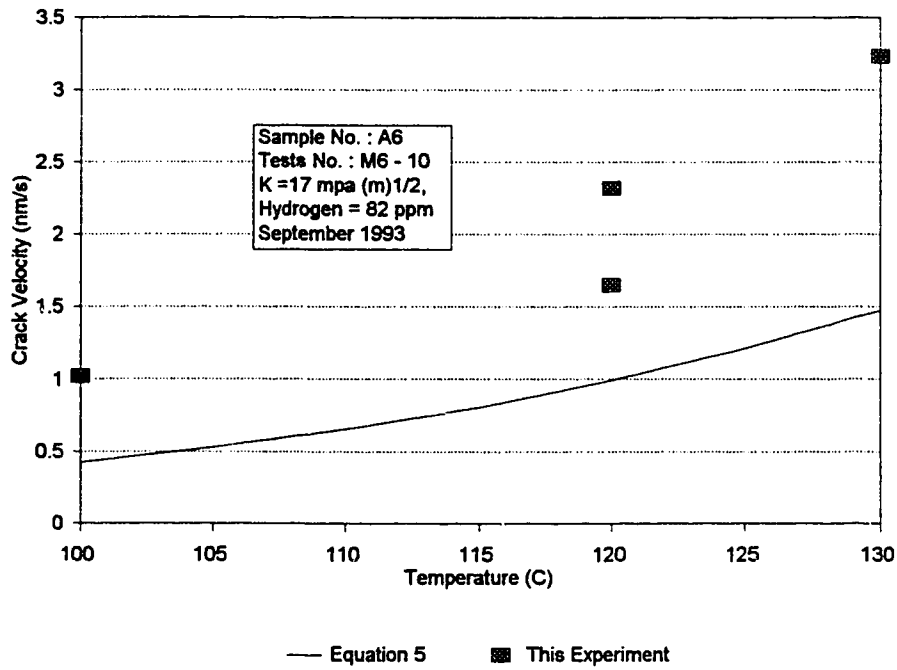
Figure 4.15: As-manufactured material, experimental crack velocities - sample A6.
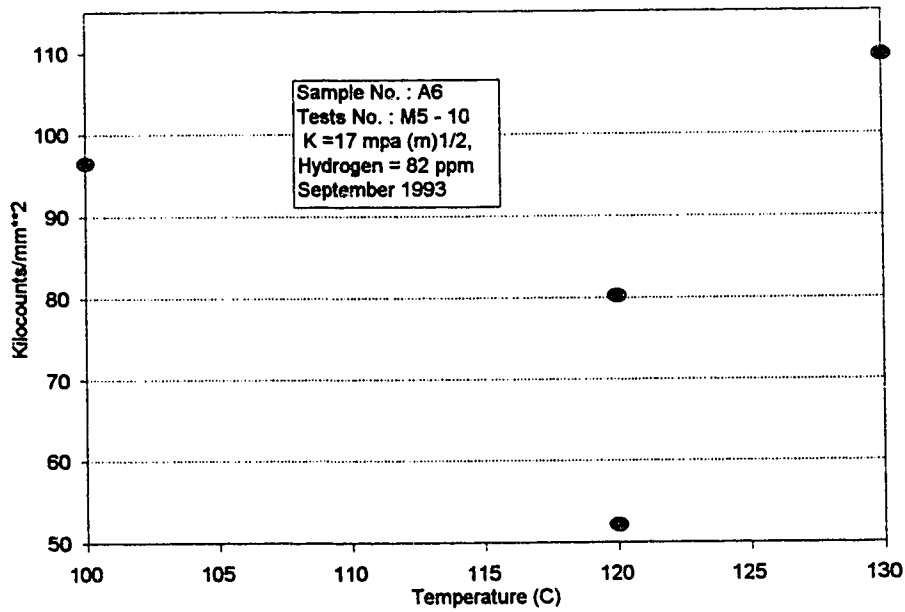
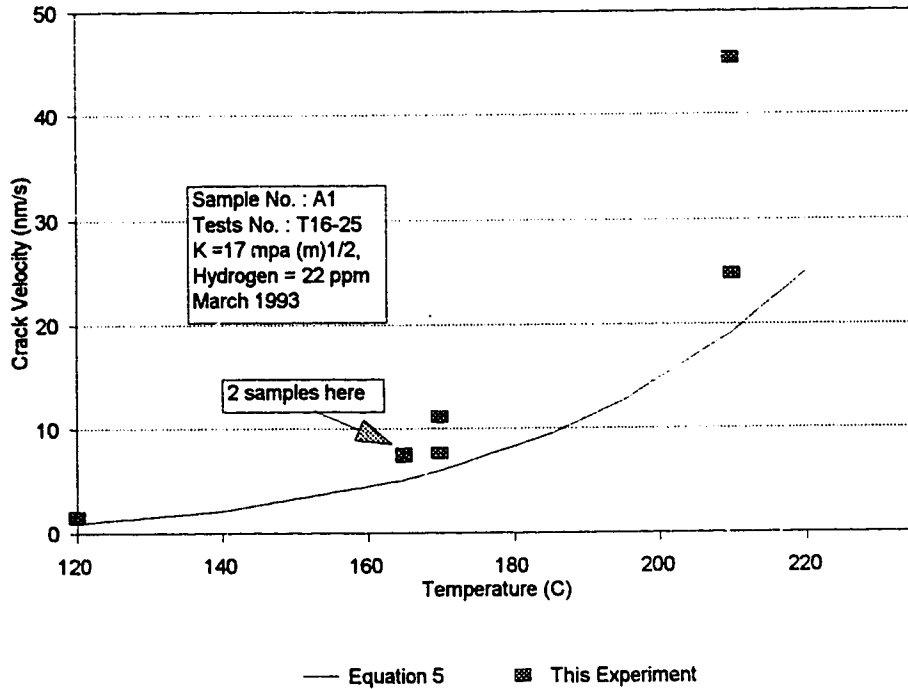Figure 4.16: As-manufactured material, experimental kilocounts/mm**2 - sample A6.
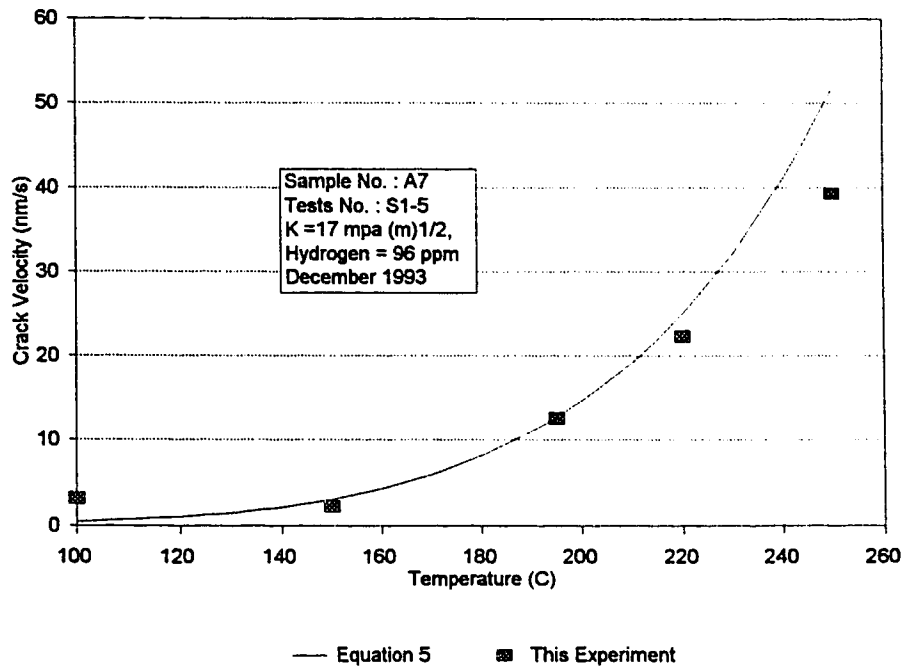
Figure 4.17: As-manufactured material, experimental crack velocities - sample A7.
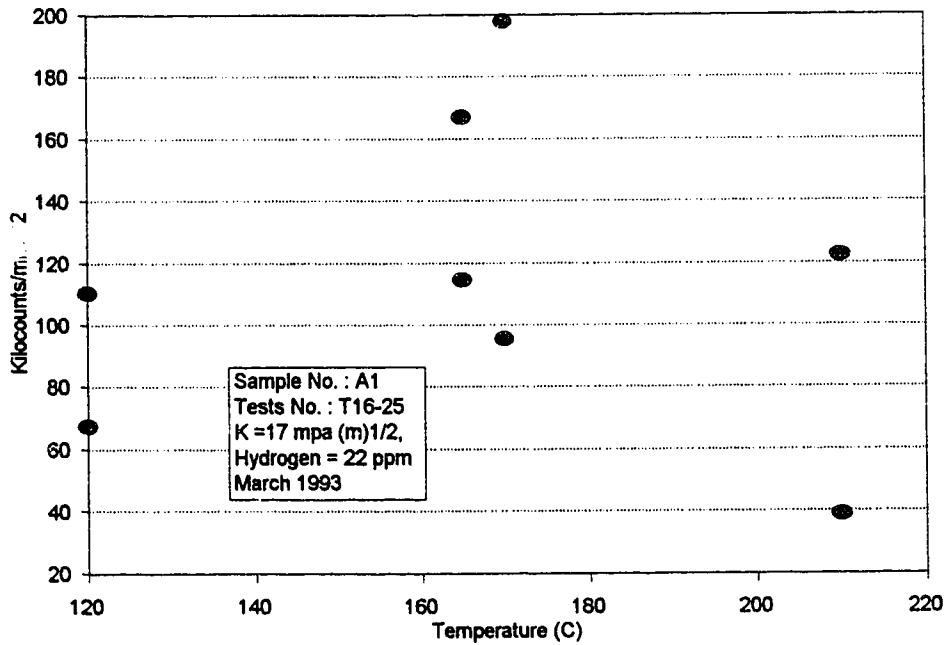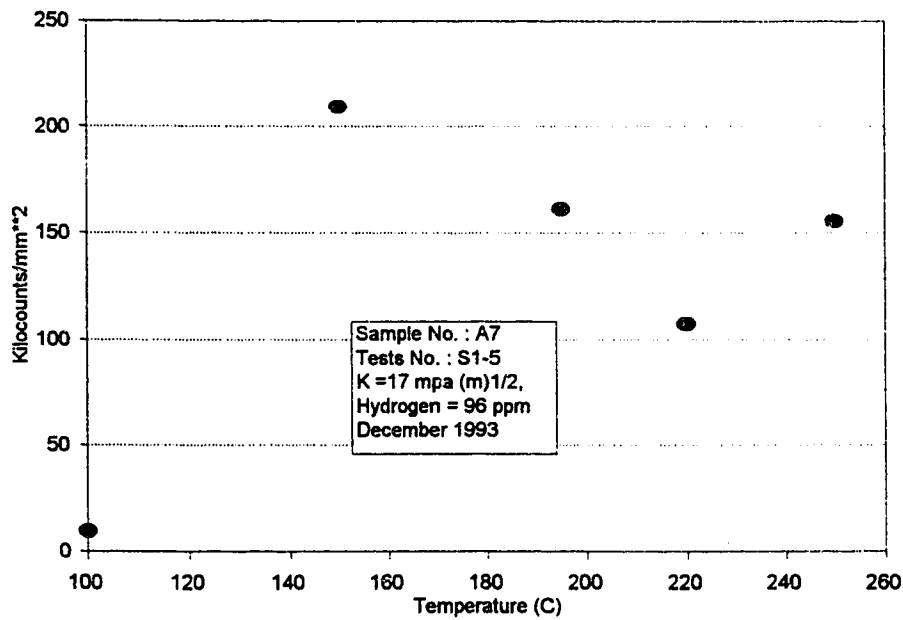

Figure 4.18: As-manufactured material, experimental kilocounts/mm**2 - sample A7.
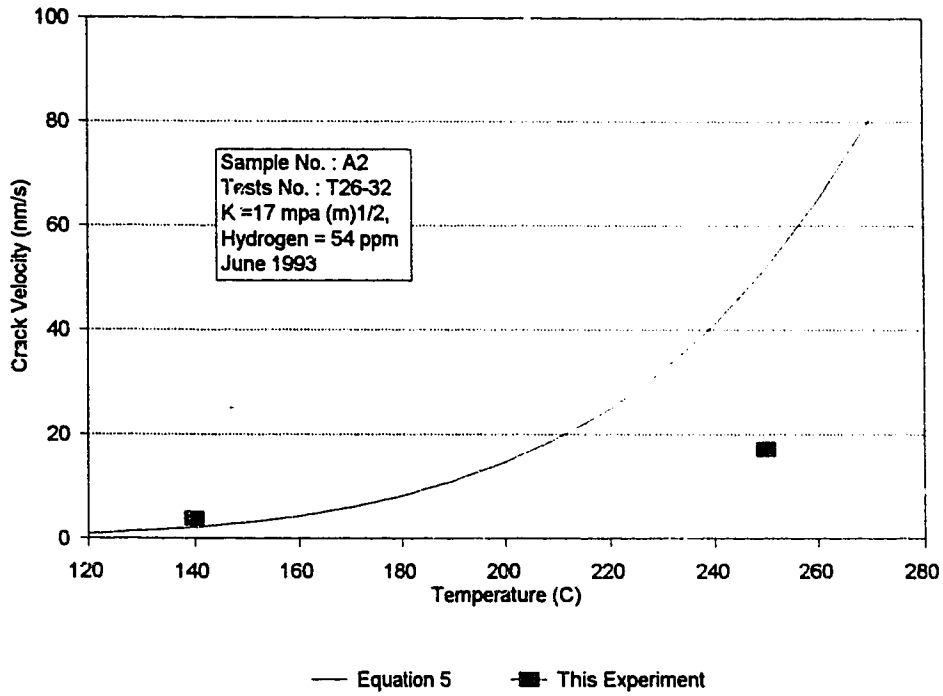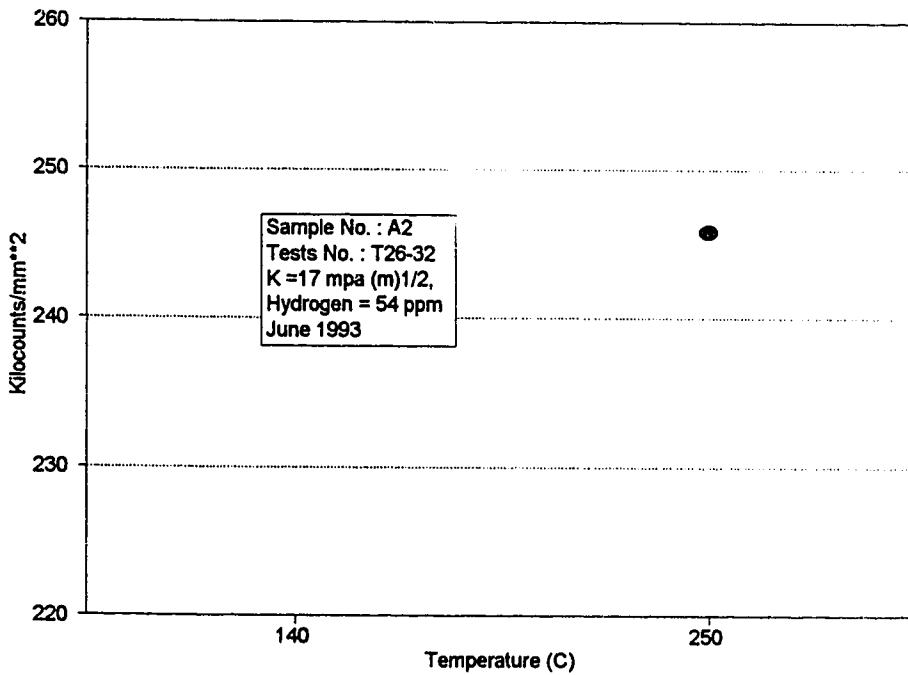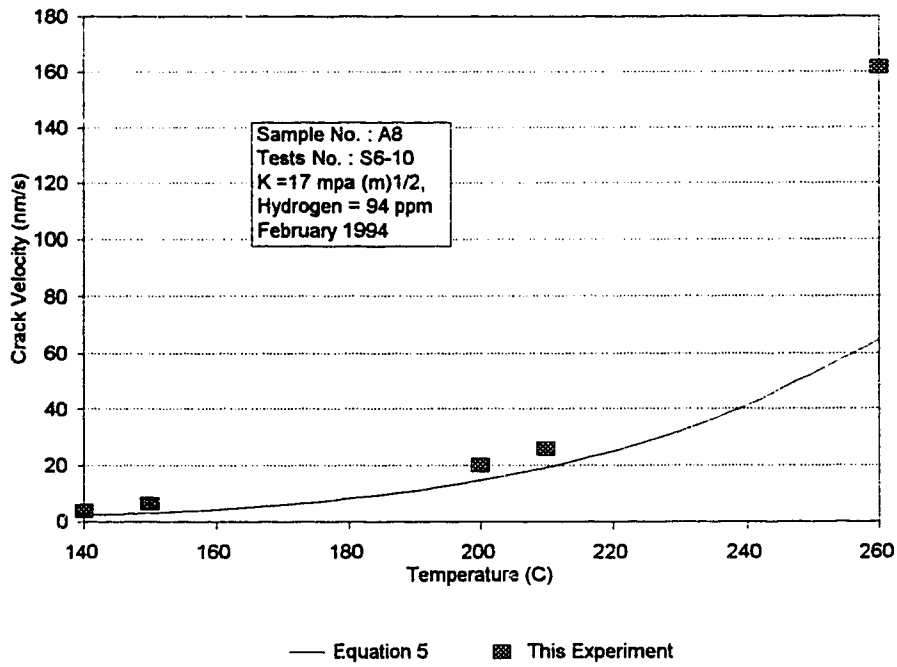
Figure 4.19: As-manufactured material, experimental crack velocities - sample A8.

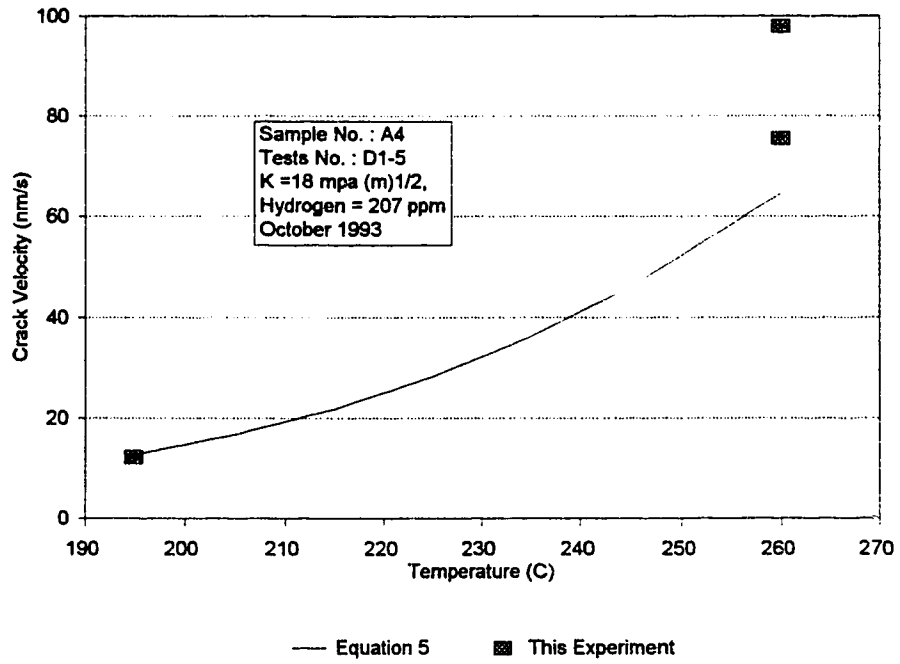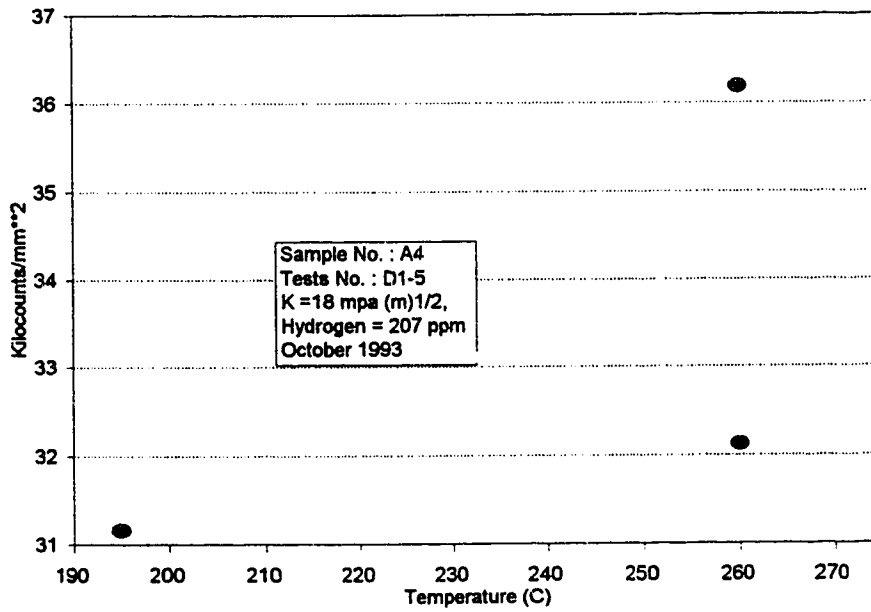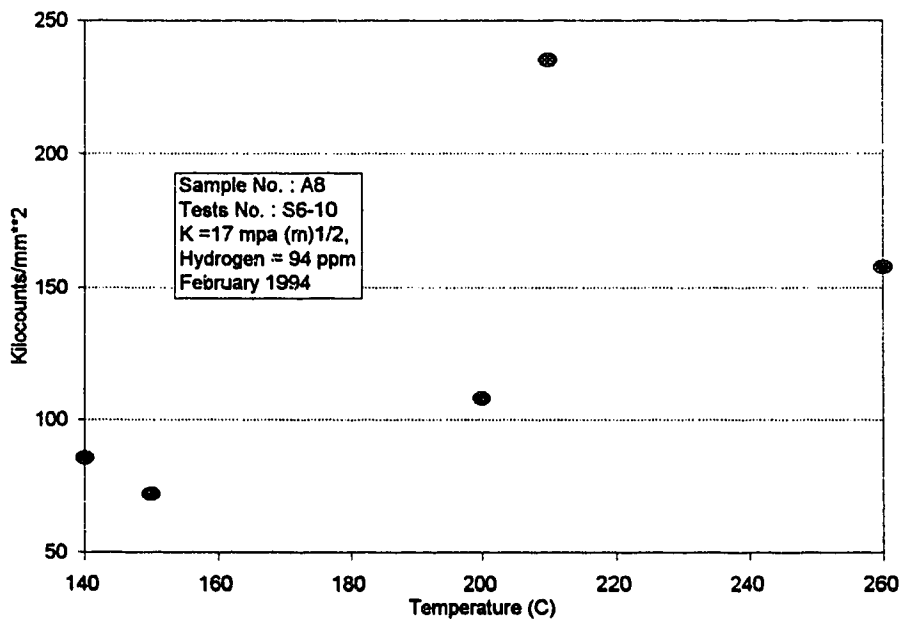Figure 4.20: As-manufactured material, experimental kilocounts/mm**2 - sample A8.
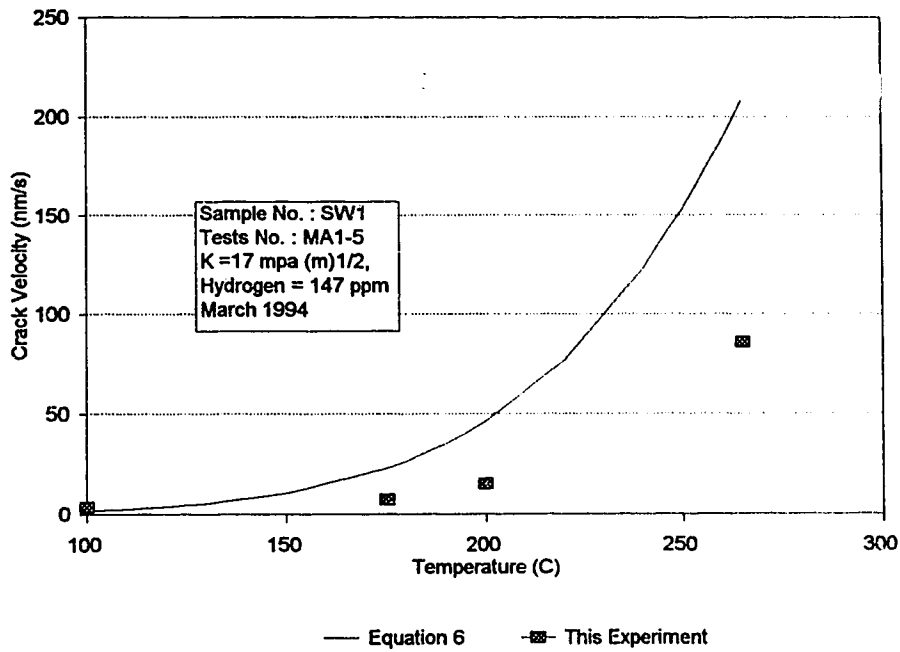
Figure 4.21: Cold worked material, experimental crack velocities - sample SW1.
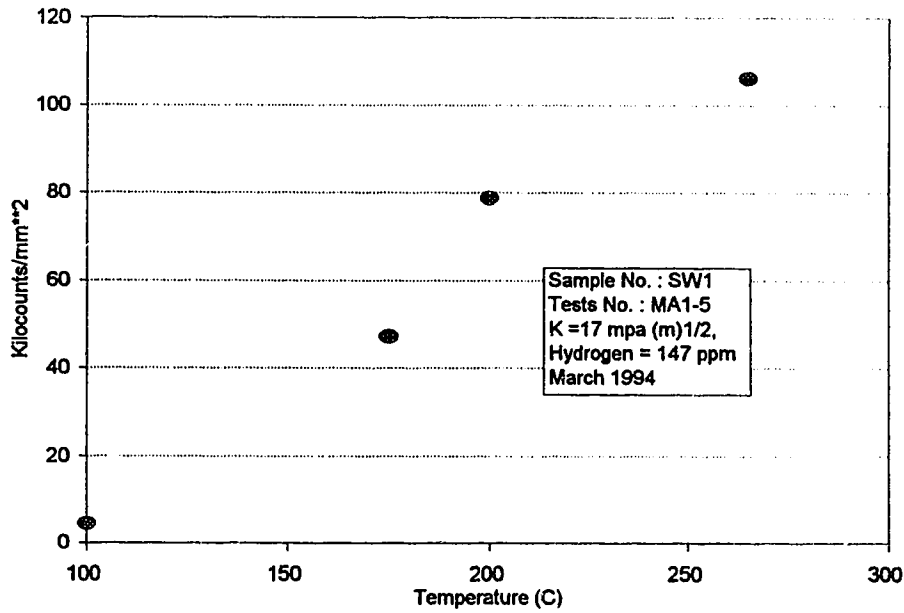
Figure 4.22: Cold worked material, experimental kilocounts/mm² - sample SW 1.

4.4 AE per mm² versus Test Temperatures

A summary of all the tests which were done in this study is found on Figure 4.23. In this figure a separation was made between the as-manufactured samples - low hydrogen (less than 100 ppm) and high hydrogen (approximately 160 to 207 ppm hydrogen) and the 40% cold worked material (with 147 ppm hydrogen).
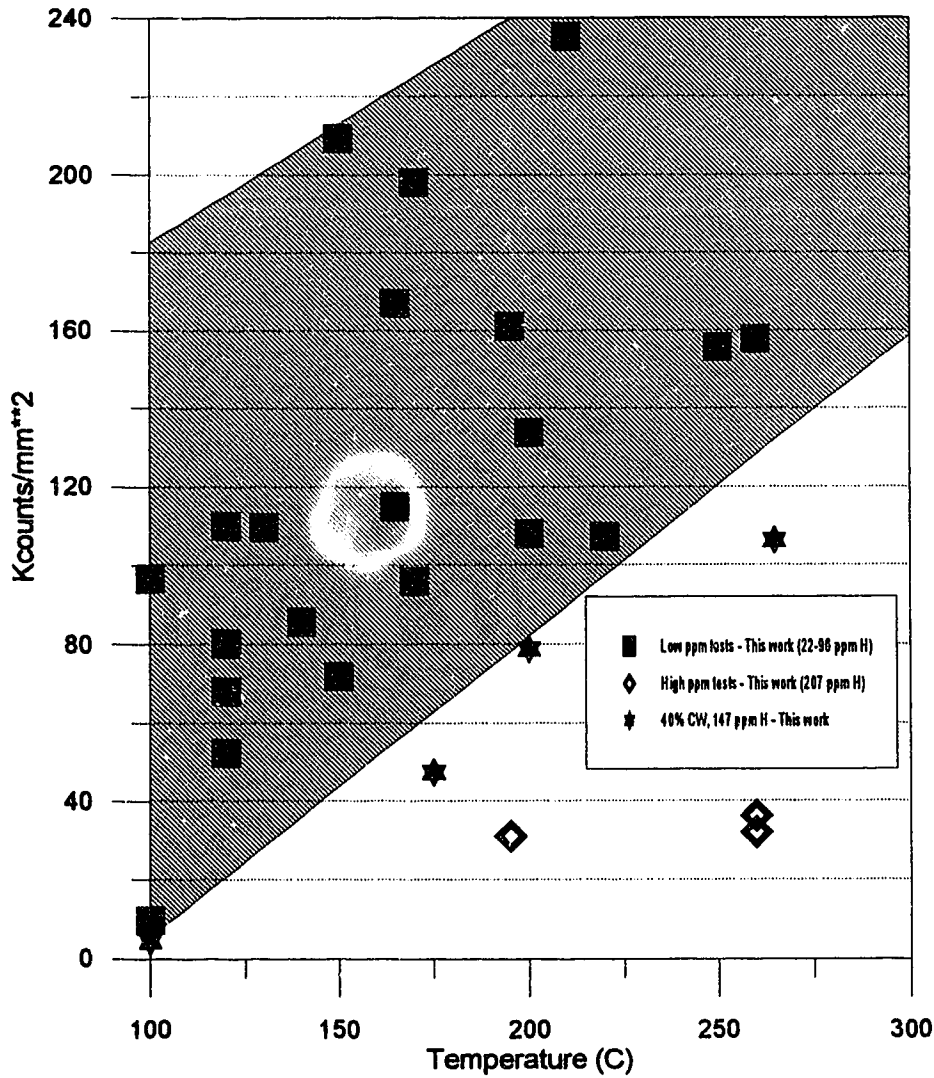
Figure 4.23: Summary of as-manufactured and cold worked material testing - kilocounts per mm² versus temperature from this work.

Figure 4.24 is a summary of the crack velocities calculated from the as-manufactured material tested in this work as compared to theoretical values derived from the expression [Eadie, Li, and Shek, 1993];

$$\text{ave. DHCV} = 7.9446 \times 10^6 \text{ (nm/s) exp } \{-6246.38/T(K)\}. \tag{5}$$

Figure 4.21 is a similar plot for the cold worked samples using the expression [Eadie, Li, and Shek, 1993];

$$\text{ave. DHCV} = 1.1769 \times 10^7 \text{ (nm/s) exp } \{-5885.7/T(K)\}. \tag{6}$$

The crack velocities which were determined in this study were used only to assist in analyzing the AE results. For example, if the AE counts appeared low on a particular test the crack velocity for that test was examined to determined if cracking was slower or had actually stopped.
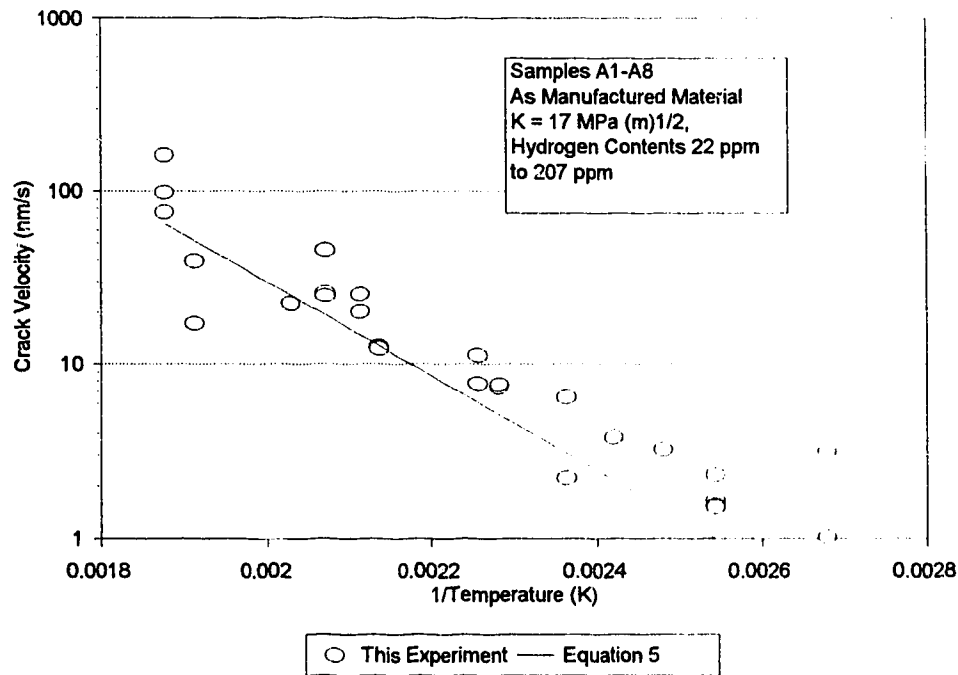
Figure 4.24: Summary of experimental crack velocities as compared to theoretical values [Eadie, Li and Shek, 1993] - as-manufactured material.

4.5 SEM Examination of Fracture Surface

The fracture surfaces of several of the samples were examined in detail using the secondary electron imaging capability of the SEM.

4.51 Secondary/Lengthwise Cracks

Secondary cracks, running parallel to the hoop/axial plane of the sample (Figures 4.25, 4.26 and 4.27) appeared in many of the samples which were examined. These cracks, which were quite distinct at high magnifications (6,000 to 10,000X), were referred to as lengthwise cracks. The presence of these cracks appeared to be independent of the hydrogen content of the sample. Up to 5 independent tests were performed on each sample. On these multiple test samples, lengthwise cracks were present on all but the final test which was done on each sample regardless of temperature. Examination of the fracture surface from the final test on all samples revealed very few, if any, lengthwise cracks (Figures 4.28 and 4.29).

In an effort to assess the universality of these crack, fracture surfaces were examined from recent unpublished results done on axial - cantilever beam samples. DHC on these samples had been initiated with the presence of a notch. These samples had not been fatigued nor had they been post-fracture heat-tinted. No lengthwise cracks were detected on these samples.
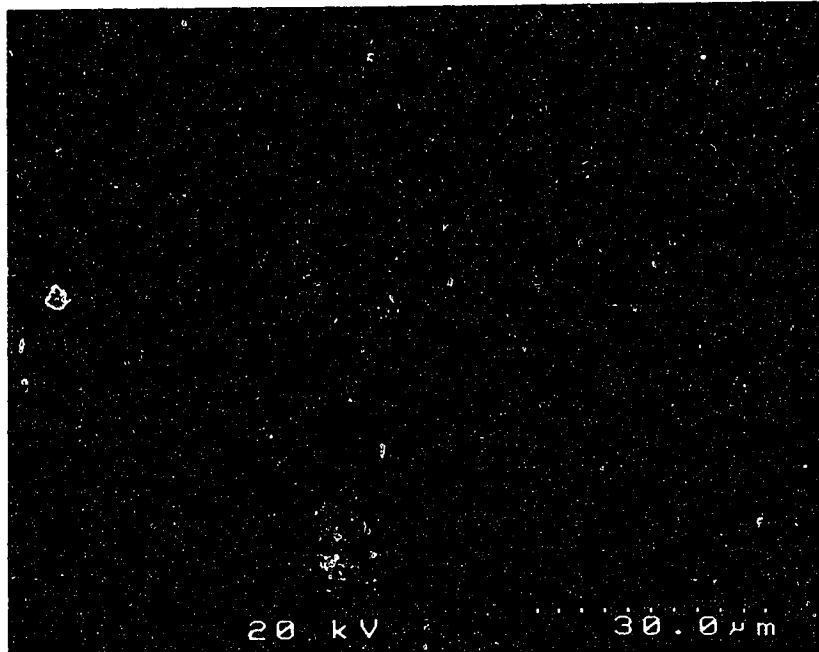
Figure 4.25: Sample SW1 - 40% cold worked, 147 ppm hydrogen, SEM photograph taken looking down on radial/hoop face (perpendicular to main DHC cracking direction) showing hydrides parallel to secondary cracks, 1000X.
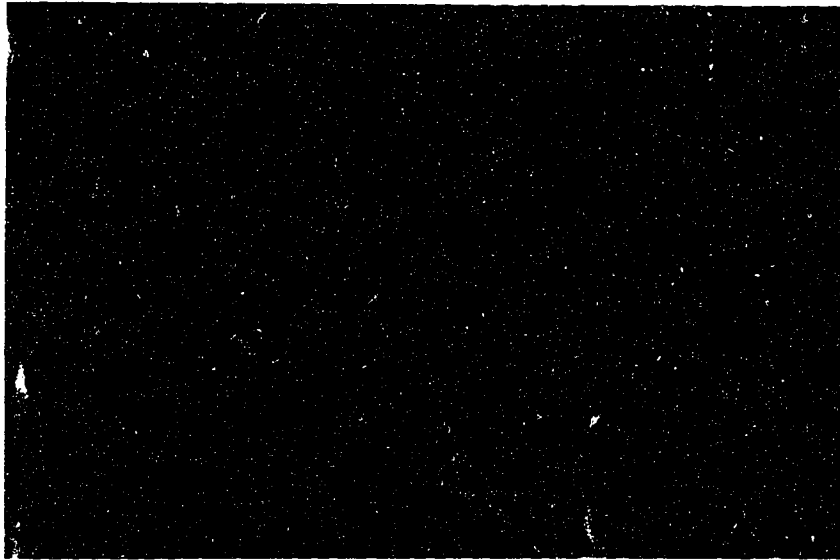
Figure 4.26: Sample A4 - as-manufactured, 207 ppm hydrogen, testing done at 260°C. SEM photograph taken looking down on the fracture surface (radial/axial plane) showing lengthwise cracking along the hoop/axial plane. Cracking direction is from top to bottom. 6,000X.
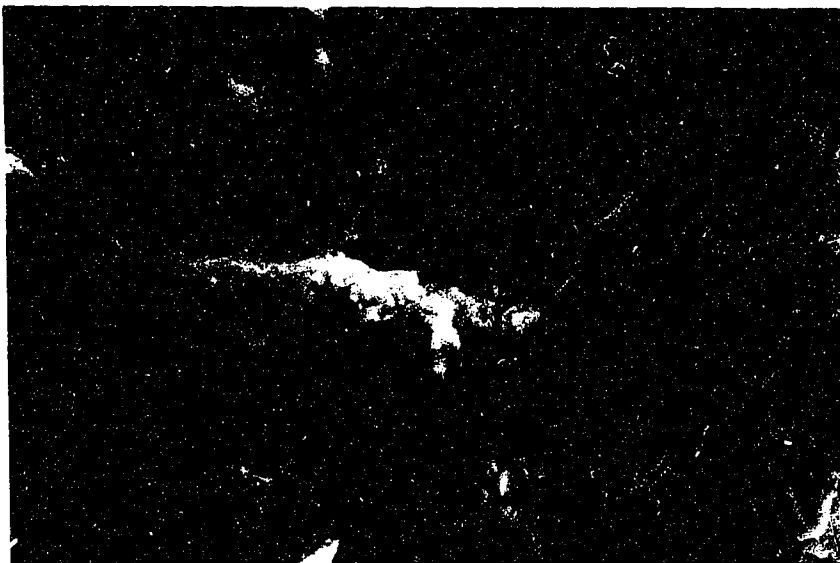
Figure 4.27: Sample SW1 - 40% cold worked, 147 ppm hydrogen, testing done at 100°C. SEM photograph taken looking down on the fracture surface (radial/axial plane) showing lengthwise cracking along the hoop/axial plane. Cracking direction is from top to bottom. 10,000X.
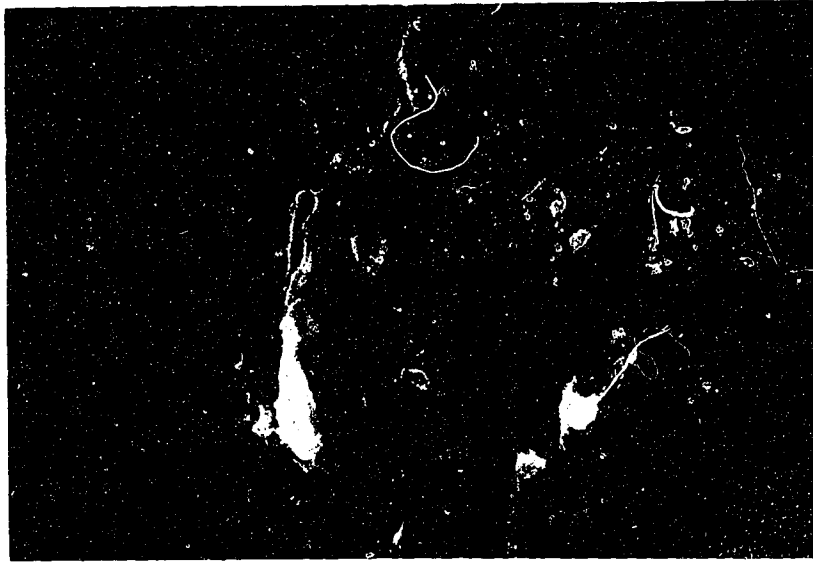
Figure 4.28: Sample A4 - as-manufactured, 207 ppm hydrogen, final test done on sample, testing done at 195°C. SEM photograph taken looking down on the fracture surface (radial/axial plane). Few, if any lengthwise cracks visible. Cracking direction is from top to bottom. 6,000X.

Figure 4.29: Sample SW1 - 40% cold worked, 147 ppm hydrogen, final test done on sample, testing done at 265°C. SEM photograph taken looking down on the fracture surface (radial/axial plane). Few, if any lengthwises cracks visible. Cracking direction is from top to bottom. 6,000X.

4.52 Measurement of Striation Spacing

Striation spacing was measured on several samples of as-manufactured material of different hydrogen contents; A4 - 207 ppm hydrogen (Figure 4.30), sample A7 - 96 ppm hydrogen (Figure 4.31), sample A8 - 94 ppm and sample A1 - 22 ppm. The results, found on Figure 4.32, illustrate a trend toward decreasing striation spacing with increasing hydrogen content. These tests were all performed at a stress intensity of approximately 17 MPa√m.

↓ striations
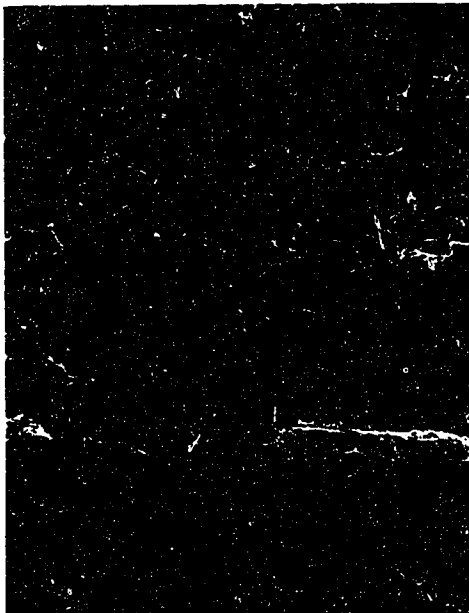
Figure 4.30: Sample A4 - as manufactured sample containing 207 ppm H (test temperature 195°C) - individual striations are visible on fracture surface. Cracking direction is from left to right. 400X.

↓ striations
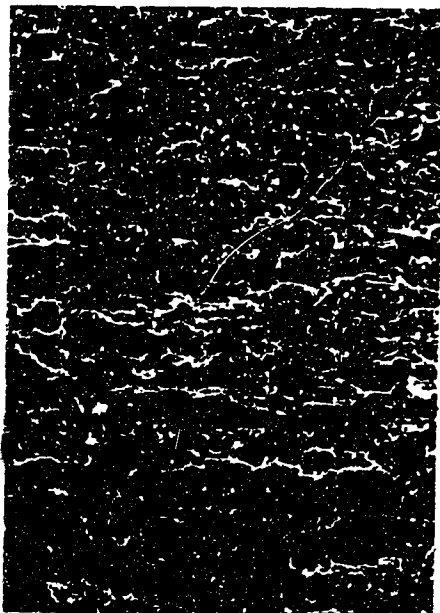
Figure 4.31: Sample A7 - as manufactured sample containing 96 ppm H (test temperature 195°C) - striation spacing is noticeably larger than sample A4. Cracking direction is from left to right. 400X.
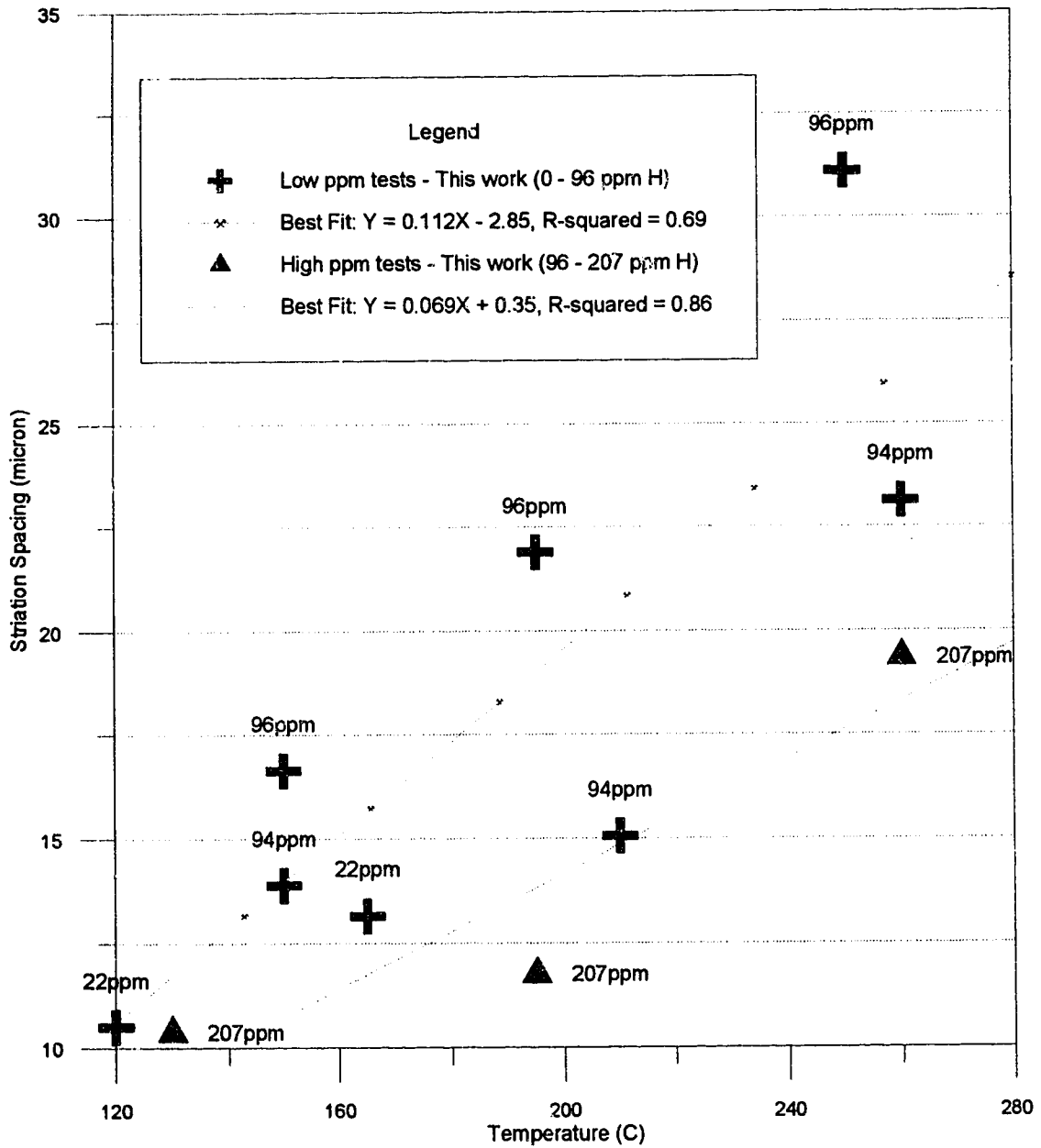
Figure 4.32: Striation spacing vs temperature. There is a trend toward a decrease in spacing with increasing hydrogen content. All tests were done at a constant K of 17 MPa(m)$^{1/2}$.

5.0 DISCUSSION

5.1 Hydriding Results

Sample preparation for DHC testing is a lengthy process, requiring periodic metallographic examination to achieve a desired hydrogen value. It is only after viewing many samples that one can make an adequate guess whether a hydride layer is thick enough to ultimately produce a sample containing 180 or 150 ppm hydrogen.

In the course of this study several samples did not yield hydrogen values as anticipated (Table 4.1). Several possibilities for these discrepancies are listed below.

Initially some samples were sent for electro-spark discharge machining (EDM) with the outside hydride layer still intact. The EDM process may have caused some of this hydride layer to diffuse into the sample causing significantly higher hydrogen values [Foecke et al., 1993]. This may have been the case for samples A3 and A4.

Samples A7 and A8, which were sent for machining with the surface hydride layer removed, were hydrided successfully. These results suggest that removal of the outer hydride layer prior to machining is a necessity.

Samples A1 and A2, were hydrided by another researcher and it is possible that they may not have had a thick enough hydride layer on them initially to produce the desired 80 ppm of hydrogen.

The cold worked sample, SW1, was hydrided with a target hydrogen level of 180 ppm hydrogen, but only 147 ppm were obtained. It is possible that the sample was not uniformly hydrided, resulting in a discontinuous hydride layer. This would not necessarily have been detected during a routine metallurgical examination of the sample. This could have produced a sample with a lower than anticipated hydrogen content.

Accuracy of hydrogen analysis was not considered to be a source of error when assessing hydriding problems, as several samples were analyzed in duplicate as a quality check.

5.2 Scatter of Data

Variables in the AE equipment were examined in an attempt to account for some of the considerable amount of scatter in the data (Figure 5.1). The same transducer, preamplifier, event recorder and testing rig were used for all the tests. Therefore, these variables were deemed less suspect in having caused the scatter.

During testing, it was necessary to displace the AE transducer when the sample was removed from the loading rod following each series of 5 tests. Although care was taken in re-attaching the AE transducer/waveguide after individual tests, it is possible that the transducer may not have been positioned directly under the loading rod. This could have produced a slightly different AE signal during testing. A sponge/grease arrangement was used to hold the transducer in place. Over the course of a year and a half of sample testing,

it is possible that this sponge compacted somewhat causing slight variations in the pressure being applied to the transducer.

Most of the studies, which have been reported in regard to transducer/sample contact, state that attachment of the transducer to the sample and variations in the thickness of the couplant are the main source of problems with reproducibility of work [Hill and El-Dardiry, 1981].

Alternate sources of AE noise, which can occur within the frequency range (0.1 to 0.3 MHz) were considered when assessing the problems of scatter in the data. In a university research environment many sources of noise within this frequency range are present, including hydraulic noise (500 kHz to 1 MHz), machinery noise (not usually above 100 kHz) and electrical interference (which can occur anywhere within the frequency range). In some circumstances this type of interference was easily identified and corrected. (eg. potential drop signal interference which was discussed in section 4.21). It was thought that poor connections at the potential drop power supply/sample connection was the cause of the signal problems. Although precautions were taken during testing, it is possible that not all the sources of this type of interference were identified and that some may have contributed to the scatter in the data.

5.3 Acoustic Emission - As Manufactured Material

In Figure 5.1, data from the testing of as manufactured material in this work are compared to similar results produced by Eadie, Li and Shek, 1993 on as manufactured material containing approximately 160 ppm hydrogen. Although there is considerable scatter in both sets of results, (R^2 values of 0.3 and 0.4 for least squares linear best fit) some definite trends are apparent. The first trend is a distinct increase in AE with increasing test temperature (Figure 5.1). The other main trend is that the material with a higher hydrogen content (>100 ppm H) has a much lower overall number of AE per mm^2 when compared with the material tested with a lower hydrogen content (<100 ppm H) (Figure 5.1, 5.2). These trends are in agreement with the work done by Eadie, Li and Shek, 1993.

5.31 Effects of Temperature on AE

Previous work [Tangri, 1977, Coleman, 1986] suggests that brittle zirconium hydrides fracturing intermittently produce AE and, that the zirconium alloy matrix is ductile and therefore quiet. Studies by Eadie, Jovanovic and Ma, 1994 have been able to relate the fracture of these clusters of hydride platelets to particular AE steps.

Dutton, Woo, Nuttall, Simpson and Puls, 1977; Eadie, Jovanovic and Ma, 1994; Anderson and Ma, 1994 have all pointed out that the distance between striations along a DHC fracture surface increases with temperature. Similar results were also obtained in the present work. If interstriation distance corresponds with the length of a hydride cluster [Yuan and Tangri, 1982], this lends support for the concept that larger clusters of hydride(s) [Eadie, Jovanovic and Ma, 1994] form at elevated temperatures. Eadie, Jovanovic and Ma, 1994 have also pointed out that these hydride clusters grow in thickness as well as length at higher temperatures (~250°C).
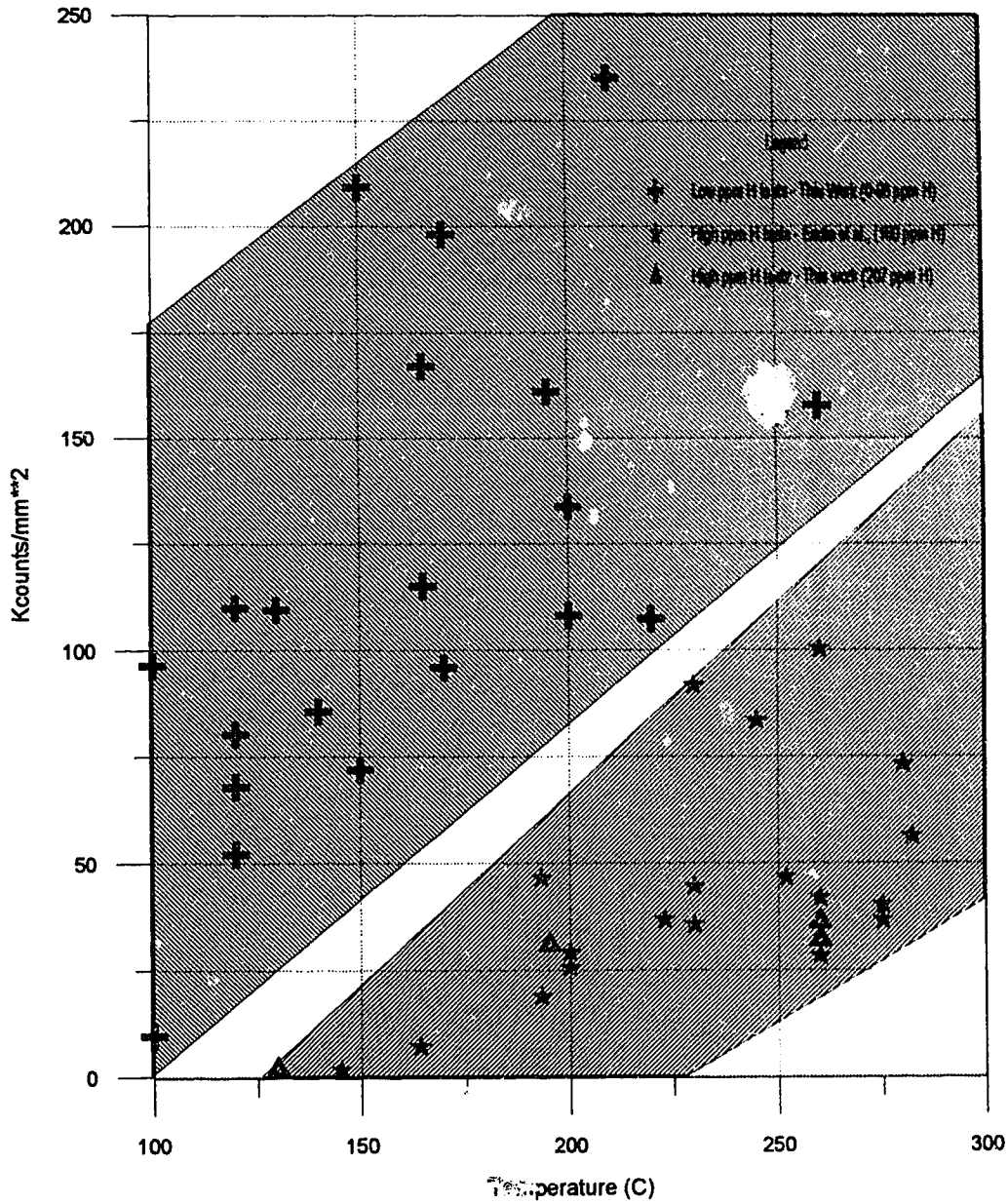
Figure 5.1:   Summary of as-manufactured material testing - kilocounts per mm² versus temperature, (this work compared to Eadie, Li and Shek, 1993).

These clusters of hydrides are able to grow longer before a "critical" fracture length is reached because the peak stress at the crack tip is lower at elevated temperatures. This is mainly due to the overall lowering of the yield strength of the material at elevated temperatures and a corresponding lowering of the hydrostatic stress [Puls, 1990]. Also contributing to this effect is a softening of the zirconium hydride(s) at elevated temperatures [Choubey and Puls, 1994].

If an AE event is occurring when an individual zirconium hydride platelet is fracturing, then the presence of longer and/or thicker clusters (i.e. a greater volume) of platelets per mm^2 of crack surface, at elevated temperatures could produce more AE per mm^2. This would be possible if the crack is propagating in a discontinuous manner through a thick layer of hydride platelets. In this situation a postmortem fracture surface analysis might not be successful in obtaining evidence of additional hydrides due to the loss of brittle hydride material during fracture.

A *postmortem* analysis of the fracture surface did not reveal any effect, with respect to temperature, in the size of the brittle facets found on the crack face [Eadie, Jovanovic and Ma, 1994]. Detailed metallography performed with the use of the secondary electron mode of the SEM was unsuccessful in identifying zirconium hydrides on the fracture surface.

Due to the nature of the method of detection of AE done in this study, cumulative counting, it was not possible to detect whether one large hydride or several smaller hydrides "clustered" together have fractured. AE is collected if the amplitude of an acoustic emission is high enough to pass over a detection threshold. One large AE event of high amplitude could possibly produce the same number of counts as several events of smaller amplitude (Figure 5.3). Amouzouvi and Clegg, 1988 reported the production of higher amplitude AE signals in zirconium samples with increasing test temperature. This research supports the presence of a longer, thicker clusters of hydrides. Amplitude distribution studies were not done in the present work.

A difference in the fracture characteristics of these hydrides could create a change in frequency of the AE signal being produced at higher temperatures. This change in AE frequency could also contribute to the increase in AE per mm^2 at elevated temperatures. Brittle to ductile fracture of different materials (mainly steels) have reportedly produced AE which has been hundreds of kHz apart and at opposite ends of the frequency range [Ono, Stern, and Long, 1972; Spanner, 1972]. This effect could influence the amount of AE per mm^2 detected as the equipment which was used in this study also gated the frequencies which were detected between a range of 0.1 to 0.3 MHz.

5.32 Effects of Hydrogen on AE

Although these samples contained a higher concentration of hydrogen prior to testing, only a specific amount of this hydrogen was available to contribute to DHC. This amount is dependent on the concentration of hydrogen in solution at a particular temperature regardless of overall hydrogen content. The concentration of dissolved hydrogen can vary anywhere between the precipitation solvus and the dissolution solvus due to the presence of the hysteresis in the zirconium - hydrogen TSS. The thermal history of the sample is thus a factor in determining the amount of hydrogen available for DHC.
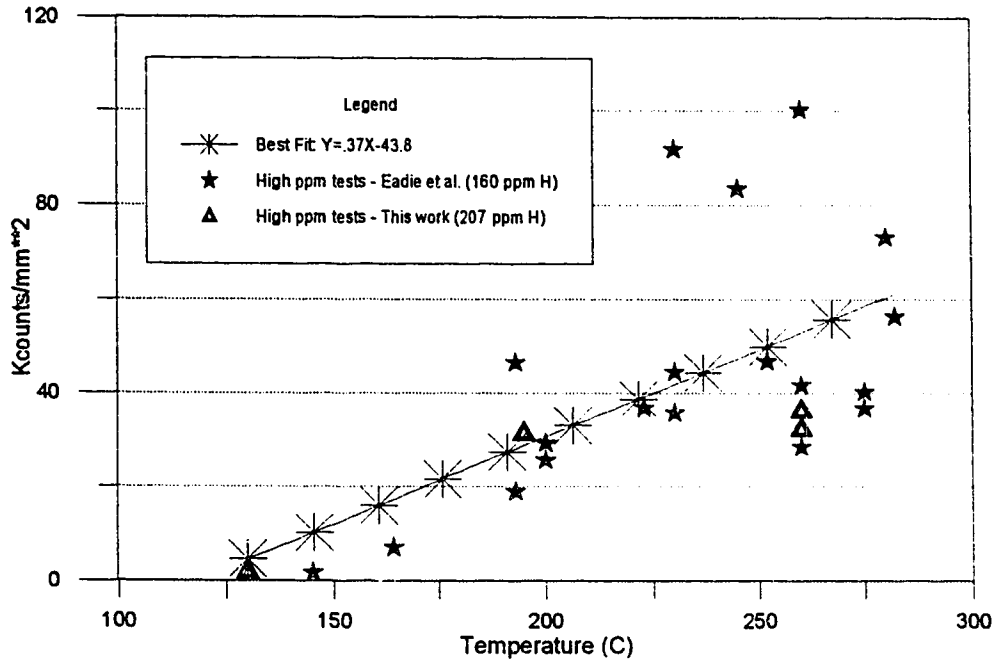
Figure 5.2: High hydrogen sample (207 ppm H), (this work, compared to the work of Eadie, Li and Shek, 1993).
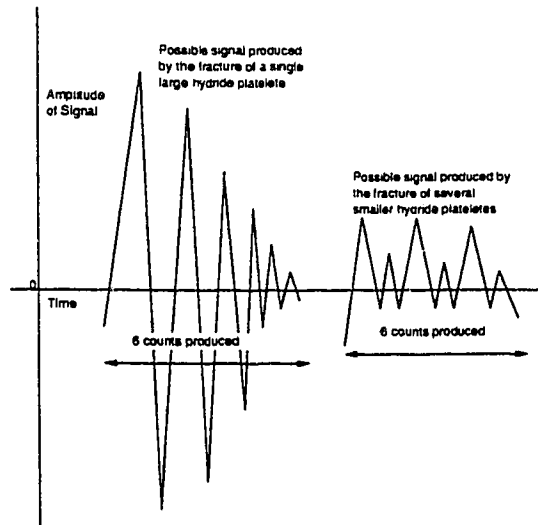

Figure 5.3: Comparison of amplitude of AE signals.

One possible explanation for the lower AE with increased hydrogen values is the presence of fewer or thinner clusters of hydride platelets at the crack tip. This can be explained in a similar manner to that used for the temperature and striation size effect. A reduction in the size or thickness of the cluster of hydride(s) at the crack tip could have caused an AE signal of lower amplitude to be produced. This lower amplitude signal would not be counted if it was not above the detection threshold of the AE equipment resulting in few kilocounts per mm.

The results shown in Figure 5.4 reveal a possible relationship between striation spacing and hydrogen content. Although results were few, due to difficulties in obtaining measurements, there is an indication of a decrease in striation spacing with increasing hydrogen values. These tests were all performed at constant stress (~ 17 MPa(m)$^{1/2}$. Recent unpublished work of Anderson and Ma, 1994 (included in Figure 5.4) also reflects these results. These results can be explained by a shorter critical hydride cluster length (corresponding to striation spacing) before fracture. Possible reasons for shorter hydride clusters will be discussed further in Section 5.4.

The low and high hydrogen curves from Figures 5.1 and 5.4 were compared at varying temperatures. Figure 5.4, at 240°C, shows a difference between the striation spacings of the two hydrogen curves of ~ 7 μm. From Figure 5.1, at 240° C these two curves are $\sim$ 125 kilocounts/mm^2 apart. In other words, roughly 125 kilocounts/mm^2 made a difference of 7 μm in the striation spacing between the low hydrogen and high hydrogen curves. A reduction of 7 μm on the low hydrogen curve of Figure 5.4 ($\sim$ 180°C) produced a corresponding drop of only 40 kilocounts/mm^2 on the low hydrogen curve of Figure 5.1. A reduction of 7 μm on the high hydrogen curve of Figure 5.4 ($\sim$ 170°C) produced a corresponding drop of only 45 kilocounts/mm^2 on the high hydrogen curve of Figure 5.1. In summary a 7 μm striation spacing produced a 125 kilocount per mm^2 difference when hydrogen content was taken into account while a similar spacing produced only a change of 40 to 45 kilocounts per mm^2 with respect to temperature. These results suggest that whatever is causing the increase in AE per mm^2 with temperature is not the same as that which is causing the change in AE with hydrogen content and that there is some additional or combination of effects occurring.

In conclusion, the actual reason for the decrease in AE per mm^2 in the samples with a higher hydrogen content was unresolved although a relationship does appear to be between striation spacing (hydride cluster length) and AE.

5.4 Beta Phase

As suggested earlier, a shorter hydride cluster length and hence a shorter striation spacing in the samples with higher hydrogen contents might possibly explain the resulting lower overall AE per mm^2 for these samples. These shorter hydride clusters could be related to the fact that in the production of the higher hydrogen samples, extended periods of time at elevated temperatures ($\sim$ 00°C for $\sim$ 48 hours) were used.

Perovic and Weatherly, 1982; Perovic, Weatherly and Simpson, 1983; and Eadie, Jovanovic, Ma and Shek, 1994 have described the effect of heat treatment on zirconium - 2.5% niobium as causing a breakdown of the beta (β) zirconium phase. The breakdown in turn affects the interface between the alpha (α) and beta (β) zirconium phases. With this
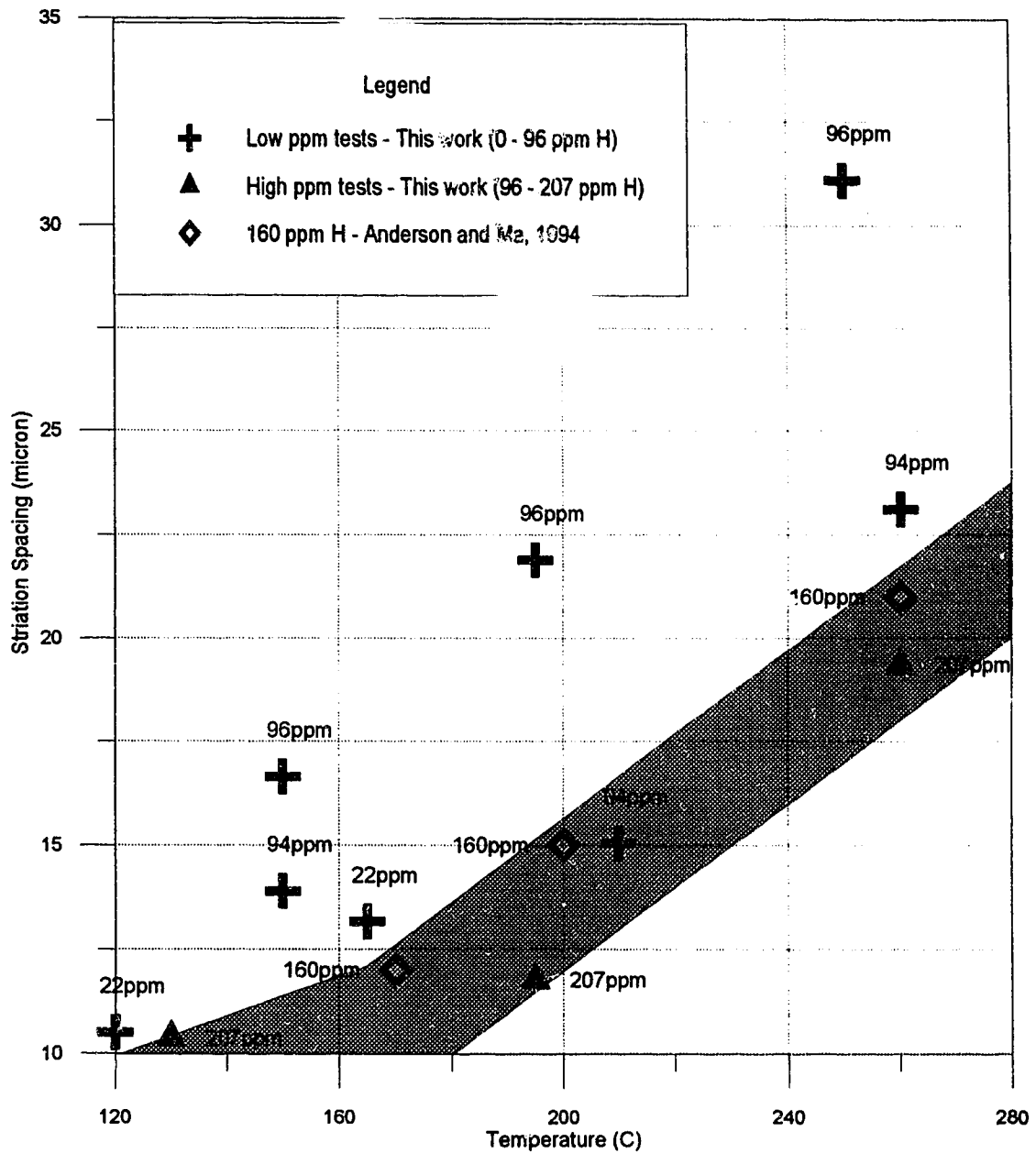
Figure 5.4: Striation spacing versus temperature - decrease in spacing with increasing hydrogen content. All tests were done at a constant K of 17 MPa(m)$^{1/2}$. Included are results from work of Anderson and Ma, 1994.

particular effect comes a possible influence on hydride morphology, as the a - β interface has been found to influence the nucleation of zirconium hydrides [Perovic and Weatherly, 1982; Perovic, Weatherly and Simpson, 1983].

A plot of kilocounts per mm^2 versus heat treatment required to produce a noticeable change in the alpha (a) and beta (β) zirconium interface (Figure 5.5) suggests a trend toward lower AE counts per mm^2 with increasing amounts of heat treatment (testing done with cantilever beam samples). This trend is particularly noticeable at the lower testing temperatures (Figures 5.6, 5.7 and 5.8) around 24 hours of heat treatment. Further testing is necessary to refine these trends due to the scatter in the AE data.
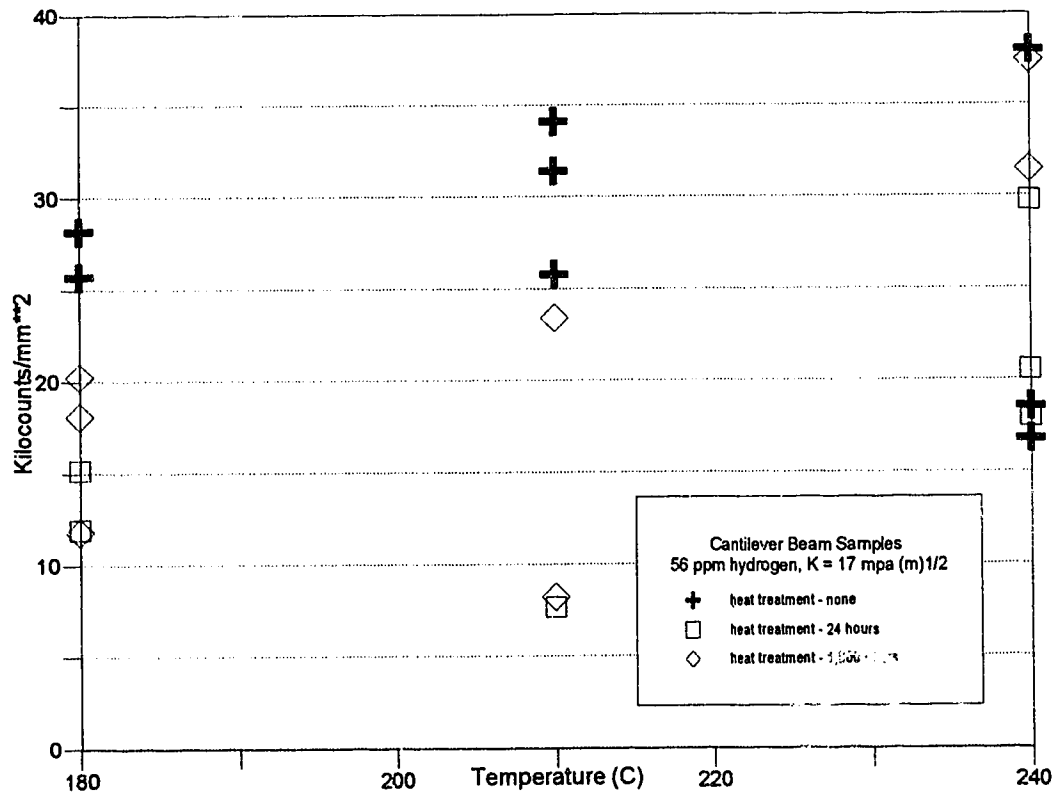

Figure 5.5: Kilocounts per mm^2 versus temperature [Eadie, Jovanovic, Ma and Shek, 1994].
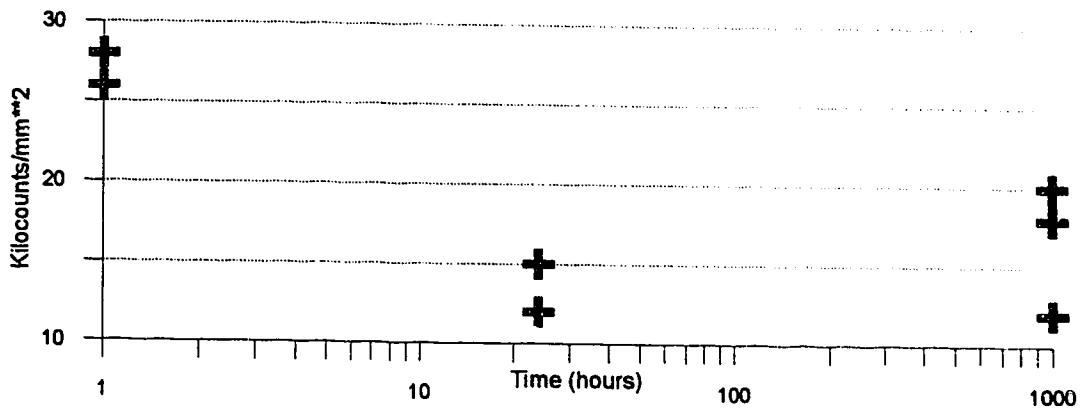
Figure 5.6: Hours of heat treatment versus kilocounts per mm² - test temperature 180° C [Eadie, Jovanovic, Ma and Shek, 1994].
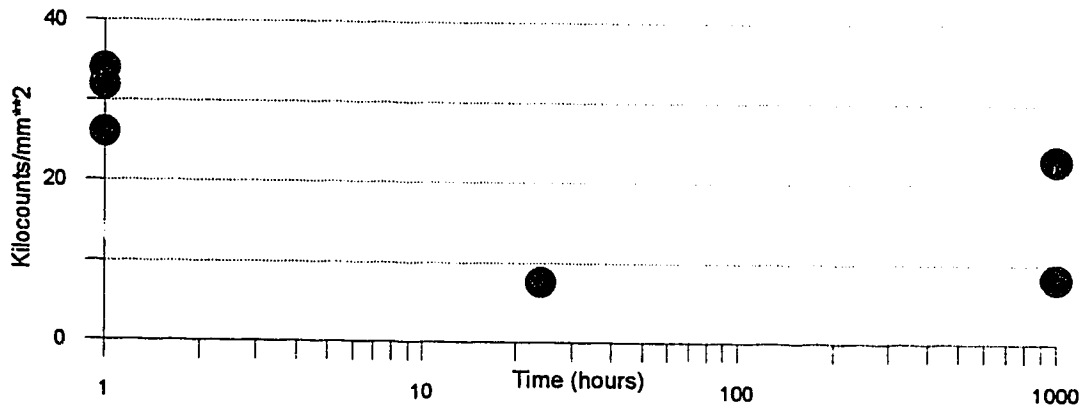

Figure 5.7: Hours of heat treatment versus kilocounts per mm² - test temperature 210° C [Eadie, Jovanovic, Ma and Shek, 1994].
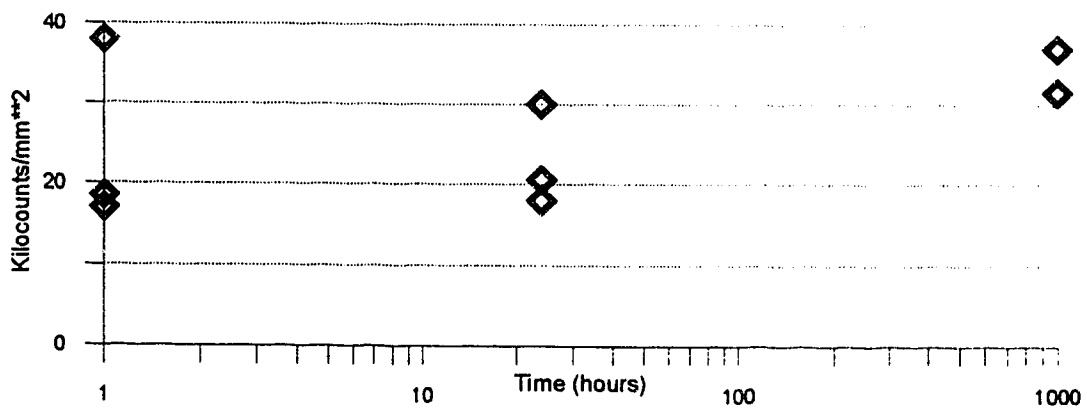

Figure 5.8: Hours of heat treatment versus kilocounts per mm² - test temperature 240° C [Eadie, Jovanovic, Ma and Shek, 1994].

5.5 Secondary Cracking

DHC occurs along the axial/radial plane of the sample (Figure 2.3). The secondary cracks, which were identified by Wilkins and Nuttall, were located along the hoop (circumferential)/axial plane of the sample (Figure 2.3). Secondary cracks were also found in this study. Figure 4.25, looking down on radial/hoop face (perpendicular to the main DHC direction), shows non-stress re-oriented hydrides associated with a secondary crack.

Wilkins and Nuttall, 1978 have suggested that the presence of a continuous sheet of hydride presents a path of low fracture resistance and favours the propagation of secondary cracks. This suggests that material which has been cold worked or contains more hydrogen should have more secondary cracking.

With the exception of Figure 4.25, most of the photos of the secondary cracks presented in this study (Figures 4.26 to 4.29) have been taken at a much higher magnification (5,000 - 10,000X) than the work done by Wilkins and Nuttall, 1978 (200 to 300X). It was difficult to associate many of these finer secondary cracks with hydrides, therefore these cracks were referred to separately as lengthwise cracks.

5.51 Lengthwise Cracking

Examination of the crack face following DHC, did not reveal any relationship between the amount of cracking and hydrogen content or the amount of cold work. The only distinct trend which showed up in all the samples was that little if any lengthwise cracking was visible on the very last test on the each sample. Two features were common to all these last tests: no thermal cycles of any type had been performed following testing and they were farthest in distance from the initial prefatigue zone.

Further testing by Eadie, Jovanovic, Ma and Shek, 1994 suggests that this lengthwise cracking was related to the thermal cycling which was done on a given sample between testing. This explanation suggests lengthwise cracking is unrelated to DHC and would not produce any AE during sample testing.

5.52 Secondary Cracking and AE

No relationship appeared to exist between secondary cracking and AE in this study. These results are in contrast to the results described by Arora and Tangri, 1981. Arora and Tangri stated that the zone of higher AE at the beginning of an individual DHC test can be accounted for by secondary cracking.

Wilkins and Nuttall, 1978 have suggested that this secondary cracking during DHC testing is most prominent near the prefatigue zone of a sample and does not extend very far into the DHC zone. If secondary cracking is causing the zone of higher AE at the beginning of a test, one would expect this zone to decrease in size during successive testing on the same sample.

On multiple test samples used in this study, an initial zone of high AE was sometimes found on tests which were performed at distances which were far from the prefatigue zone. This evidence suggests that secondary cracking effects alone cannot be causing this zone of higher than expected AE activity.

It is likely that this higher rate of AE is related to the higher DHC velocities which occur during the cool down to test temperature. AE results shown on Figure 5.9, (isothermal testing done on as manufactured material at 195°C), show a distinct zone of higher AE at what appears to be the beginning of the isothermal hold. Upon closer examination it is seen that the zone of higher AE actually occurs during the cool down portion of testing which was higher in temperature.

Another possible effect is that secondary cracking may somehow be interfering with the AE signal. This could be caused by breaking up some of the larger hydrides in the samples with higher hydrogen contents and creating a shorter striation spacing. If secondary cracking is predominantly occurring near the prefatigue zone of a sample as suggested by Wilkins and Nuttall, it cannot be a major factor in the reduction of AE in the samples with higher hydrogen levels.

5.6 Cold Worked Material

Figure 5.10 is a comparison of the results of tests done on cold worked and as manufactured material. These results indicate that the cold worked material appears to lie somewhere in the middle of the results of the as manufactured material. A comparison with the work of Eadie, Li and Shek, 1993, yields similar results to this study.

This cold worked material also exhibits an increase in AE and striation spacing with increasing temperature in a manner similar to the as manufactured material. The overall striation spacings were smaller than the as manufactured material, as expected for material of a higher yield strength. In this study, not enough testing was done on the cold worked material to show any distinct trends in AE characteristics between material with different hydrogen contents (Figure 5.11).
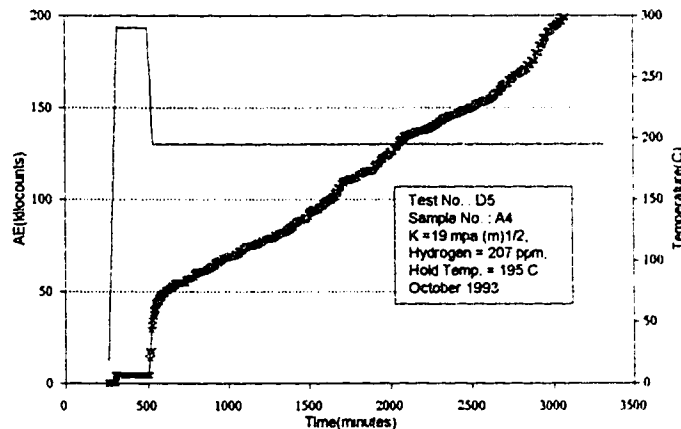

Figure 5.9: AE versus time for isothermal testing done at 195°C on as manufactured material showing high rate of AE just prior to the beginning of the isothermal hold. Examination of the corresponding fracture surface yielded few secondary cracks.
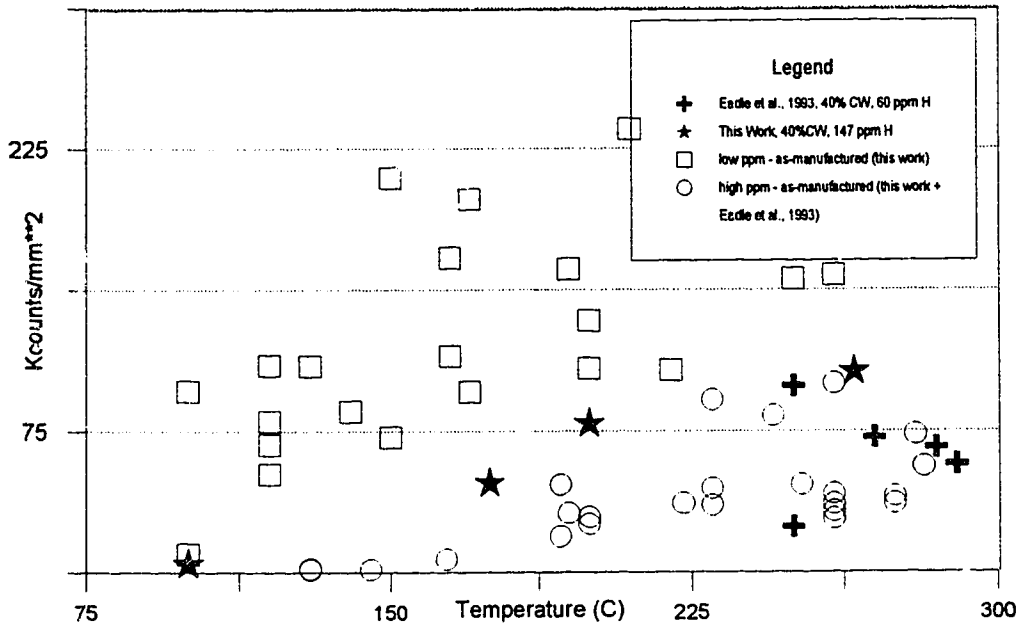
Figure 5.10:   Kilocounts per mm² for both the as-manufactured data and cold worked
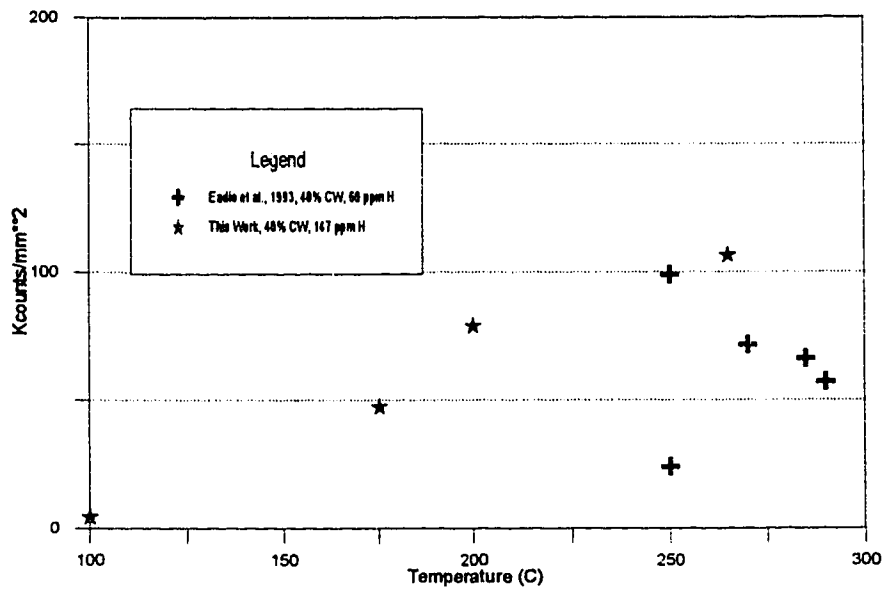   data, (this   rk compared to work of Eadie, Li, and Shek, 1993).

Figure 5.11:   Kilocounts per mm² for the cold worked data for both this work and the
               work of Eadie, Li, and Shek, 1993

5.7 AE and Low Temperature Testing

Inconsistent behaviour in the AE results was observed in some of the testing which was carried out at temperatures below 130°C. Figure 5.12 illustrates a DHC test carried out at a temperature of 100° where the AE appears to drop off entirely during the period of testing. The results in Figure 5.13 are similar to higher temperature tests where AE increases steadily throughout the period of testing. This effect appeared in both as manufactured and cold worked samples.

An examination of the crack velocities for these samples did not reveal any slowing down of cracking, therefore it was concluded that DHC was still occurring during the entire period of testing even though AE results in Figure 5.12 were low.

With these abnormalities occurring, the possibility of an AE signal problem was once again suspected. Either AE was not being produced or the signal was not being detected due to a possible frequency or amplitude change or combination of effects.

5.8 Crack Velocities

The crack velocities calculated for as-manufactured material (Figure 4.24) from this study are in close agreement with the formula for the average DHC velocity [Eadie, Li, and Shek; 1993]:

$$\text{ave. DHCV} = 7.9446 \times 10^6 \text{ (nm/s) exp } \{-6246.38/T\}. \tag{5}$$

While the crack velocities for the as-manufactured material are in relatively good agreement with predicted results, the cold worked material tested in this study was lower in velocity than that predicted by the formula [Eadie, Li, and Shek; 1993];

$$\text{ave. DHCV} = 1.1769 \times 10^7 \text{ (nm/s) exp } \{-5885.7/T\}. \tag{6}$$

Only one cold worked sample was tested in this study, clearly more work needs to be done to make a reasonable comparison with the work of Eadie, Li and Shek; 1993. Possible reasons for the discrepancy may lie in the amount of cold work which was present in the sample. An increase in the amount of cold work has been shown to raise the crack velocity [Eadie, Li and Shek; 1993].
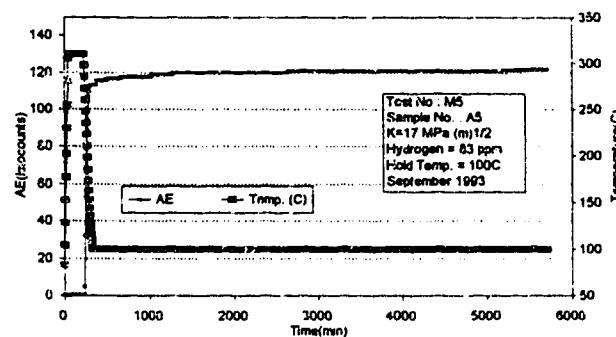

Figure 5.12:   AE versus time for isothermal testing done at 100°C on as-manufactured material. AE appears to drop off entirely during the period of testing.
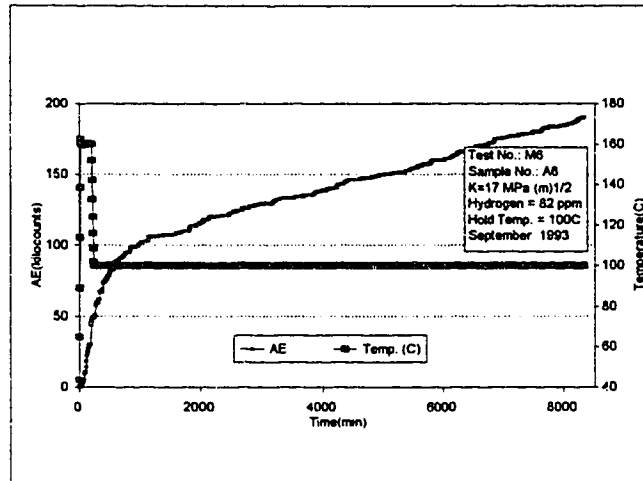
Figure 5.13:   AE versus ime for isothermal testing done at 100°C on as-manufactured
               material. Cumulative counts increase steadily throughout the period of
               testing.

5.9 Loss of AE Signal

One of the concerns encountered during the course of this research was the possibility of a
loss or the appearance of a loss of AE signal. The evidence which was taken from crack
velocity data suggested that DHC was still occurring, thus it was suspected that for some
reason AE was not being recorded by the equipment. A variation in the frequency of the AE
which was produced was suggested as a cause of the possible loss of signal under certain
testing conditions. AE has been observed to span a wide range of frequencies depending
on the mechanism of fracture (ductile or brittle) [Fowler and Papadakis, 197℃; Ono, Stern,
and Long, 1972; Spanner, 1972]. Testing in this study was conducted over a limited range
of frequencies due to equipment limitations. The transducer which was used was capable
of detecting AE over a wide range of frequencies, but the signal was then gated between
0.1 to 0.3 MHz in the preamplifier.

The transducer was then connected to the sample via a waveguide which was constructed
out of the sample loading rod. This particular equipment arrangement was utilized because
a high temperature transducer was not available at the time of testing. AE produced by
DHC cracking was transmitted from the sample through the waveguide to the transducer.

Fowler and Papadakis, 1972 discuss the dispersive nature of AE in some engineering structures, particularly rods and plates. Spanner, 1972; and Anderson, Gavin, Karvinen, Price and Reimann, 1972 also discuss the effect of a cylindrical shape on the attenuation of an AE signal. It is thought that a tube behaves similar to a bandpass filter, limiting the passage of higher frequencies when compared to a wire bundle [Anderson, Gavin, Karvinen, Price and Reimann, 1972].

The waveguide used in this study was a solid cylindrical-shaped rod, therefore it is possible that some AE was attenuated before reaching the transducer. These gating-type effects could possibly create AE signal losses which would occur during all phases of sample testing.

5.10 Comparison with Previous Work

The data collected by Eadie, Li and Shek, 1993 was acquired with a slightly different testing set up than this study. A different transducer/couplant arrangement, over the same frequency range (0.1 to 0.3 MHz) was used. Their work was also done at a higher gain setting than this study, thus making quantitative comparisons of results difficult.

In spite of the variations in testing rig set-ups and different AE equipment, all the results from this study and the work of Eadie, Li and Shek, 1993 contradict the work of Arora and Tangri 1979 and Coleman, 1986. This study and the work of Eadie, Li and Shek, 1993 indicate an increase in AE per mm^2 of sample cracked with temperature (Figure 5.3). The work of Arora and Tangri, 1981; Tangri and Yuan, 1982; Coleman, 1986; and Sagat, Ambler and C.E. Coleman, 1986, on as-manufactured material, all outline a nearly constant relationship between AE cumulative counts and area cracked over a range of temperatures. In addition, Arora and Tangri, 1981 describe that their results held constant over conditions of varying stress and hydrogen content. In this study there appeared to be a variation in AE related to hydrogen content developing.

If AE is strongly dependent on temperature, delayed hydride crack velocity (DHCV) can not be correlated directly with area cracked and AE, as the second term in equation 7, Area/AE constantly changes with temperature.

$$\text{DHCV} = \frac{d(AE)}{d(TIME_{isothermal})} \times \left(\frac{AREA}{AE}\right) \frac{1}{WIDTH\ OF\ SAMPLE} \tag{7}$$

Another important difference between this work and the work done by Arora and Tangri, 1981 and by Tangri and Yuan, 1982 is that this work did not find any indication of three distinct regimes or areas of variable AE (Figure 2.9) during the isothermal part of testing.

6.0 CONCLUSIONS

1   There is a distinct increase in AE per mm^2 of area cracked with increasing test temperature for both as-manufactured and cold worked Zr - 2.5% Nb material.

2   The samples containing higher amounts of hydrogen (greater than about 160 ppm hydrogen) produced lower overall number of kilocounts per mm^2 when compared with the material tested with a lower hydrogen content. Both conclusions 1 and 2, agree with the results of Eadie, Li and Shek, 1993.

3   There was no indication of three distinct regimes or areas of variable AE as described by Arora and Tangri, 1981 and by Tangri and Yuan, 1982 during the isothermal part of testing during this study.

4   The spacing between striations appeared to increase/decrease in a manner corresponding with the increase/decrease in AE per mm^2.

5   The spacing between striations appeared to be slightly shorter with higher overall hydrogen values at constant K and temperature. This result suggests a shorter critical hydride length before fracture with increased hydrogen values.

6   The decrease in striation spacing with higher overall hydrogen values appeared to correspond with changes in the alpha - beta hydride interface.

7   Considerable scatter (R^2 values of 0.3 and 0.4) was present in the AE data in spite of the care which was taken in an attempt to obtain reproducible data.

8   The relationship between AE per mm^2 of area cracked with increasing temperature and hydrogen content suggest that AE testing can only be used at best as semi-quantitative tool to indicate the start/stop of DHC.

7.0 PROPOSALS FOR FUTURE WORK

More testing needs to be done to confirm the results which indicate lower AE in the samples with higher overall hydrogen levels. In addition, more work should be done on samples with varying amounts of cold work.

Further work needs to be done to confirm the relationship which appeared to exist between striation spacing (hydride(s) size) and AE counts per mm^2. Detailed studies of the fracture surface are also necessary to relate the degree of ductility to AE frequencies.

The effect of heat treatment on the alpha - beta hydride phase interface could be explored further. Additional striation spacing measurements should be taken to confirm preliminary results determined in this study.

Secondary cracking events (caused by non-stress re-oriented hydrides) should be studied further to detect what influence is felt beyond the fatigue zone.

More work needs to be done on AE frequency analysis to determine if there is actually any signal loss during testing. Ideally, testing needs to be done with a spectrum analyzing digital oscilloscope which can do fast Fourier analysis over ranges from at least 50 kHz to 5 MHz. The equipment should be able to take a sound (AE event) and actually determine the frequency spectrum. This equipment should also be able to store events in order to compare different samples or different tests. In the event that this equipment is unavailable, a combination of several narrow band pass filters (preamplifier) could be used simultaneously [Ono, Stern and Long, 1972]. This work should be combined with some analysis of AE signal amplitudes.

More experimental work is necessary on varying waveguides, transducers and positions of mounting them. For example the use of a wire bundle as a waveguide or a high temperature transducer fixed directly on sample. The AE transducer should be fixed in a manner where the pressure can be reproduced consistently.

In general there is a need to increase the reproducibility of AE testing.

8.0 REFERENCES

Nuclear Training Course 427, Ontario Hydro Internal Document, July 1978.

Ambler, J.F.R., *Effect of Direction of Approach to Temperature on the Delayed Hydrogen Cracking Behaviour of Cold-Worked Zr-2.5Nb*, Zirconium in the Nuclear Industry: Sixth International Symposium, ASTM STP 824, pp. 653-674, 1984

Amouzouvi, K.F. and Clegg, L.J., *Peak Amplitude distribution of Acoustic Emission Events during Delayed Hydride Cracking of Zr-2.5% Nb Alloy*, Proceeding of the International Symposium on Fracture Mechanics, 1987, Vol. 6, Proceedings of the Metallurgical Society of the Canadian Institute of Mining and Metallurgy, pp. 107-118, Pergammon Press, 1988.

Anderson, M. J. and Ma, Y., *Effect of Cold Work and Hydrogen Content on Striation Spacing in Zr-2.5Nb Pressure Tube Material*, unpublished, 1994.

Anderson,T.T., Gavin, A.P., Gavin, J.R., Karvinen, J.R., Price, C.C. and Reimann, K.J., *Detecting Acoustic Emission in Large Liquid Metal Cooled Fast Breeder Reactors*, Acoustic Emission, ASTM STP 505, pp. 250-269, 1972.

Arora, A, *M.Sc. Thesis*, University of Manitoba, Winnipeg, Canada, 1978.

Arora, A and Tangri, K., *On Methods of Structural Evaluation by Acoustic Emission*, International Journal of Fracture, Vol. 15, pp. R93-R95, 1979.

A) Arora, A and Tangri, K, *Acoustic Emission: A Means of Measuring Crack Growth at Elevated Temperatures*, Experimental Mechanics, pp. 261-267, October 1981.

B) Arora, A and Tangri, K, *Acoustic Emission Studies of Nucleation and Propagation of Subcritical Cracks*, International Advance in Nondestructive Testing, Vol. 8, pp.217-236, Gordon and Breach, Science Publishers, 1981.

Beatty, A. G., *Acoustic Emission Couplants I: The ASTM Survey*, Journal of Acoustic Emission, Vol. 2, pp. 67-68, 1983.

Beatty, A.G. Baron, J.A, Algera, R.S. and Feng, C.C. *Acoustic Emission Couplants II: Coupling Efficiencies of Assorted Materials*, Journal of Acoustic Emission, Vol. 2, pp. 69-70, 1983.

Bradford, S.A., *Corrosion Control*, Van Nostrand Reinhold, New York, 1993.

Cheadle, B.A., Coleman, C.E. and Licht, H. *CANDU-PHW Pressure Tubes: Their Manufacture, Inspection, and Properties*, Nuclear Technology, Vol. 57, pp. 413-425, June 1982.

Coleman, C.E., *Effect of Texture on Hydride Reorientation and Delayed Hydrogen Cracking in Cold-Worked Zr-2.5Nb*, ASTM STP 754, pp. 393-411, 1982.

Coleman, C.E., Cheadle, B.A., Ambler, J.F.R., Lichtenberger, P.C. and Eadie, R.L., *Minimizing Hydride Cracking in Zirconium Alloys*, Canadian Metallurgical Quarterly, Vol. 24, No. 3, pp. 245-250, 1985.

Coleman, C.E., Acoustic Emission from Zirconium Alloys During Mechanical and Fracture Testing, Atomic Energy of Canada Limited (AECL) - 9111, October 1986.

Choubey, R., and Puls, M.P., *Crack Initiation at Long Radial Hydrides in Zr-2.5% Nb Pressure Tube Material at Elevated Temperatures*, Metallurgical and Materials Transaction A, Vol. 25A, pp. 993-1004, May 1994.

Crank, J., *The Mathematics of Diffusion*, Clarendon Press, 1975.

Davies, P.H. and Stearns, C.P., *Experimental Compliance Calibration of a Tapered DCB (Constant K) Specimen*, Ontario Hydro Research Report No. 81-389-K, November 1981, unpublished report.

Dutton, R., Woo, C.H., Nuttal, K., Simpson, L.A. and Puls, M.P., *The Mechanism of Hydrogen-Induced Delayed Cracking in Zirconium Alloys*, Hydrogen in Metals, Paper 3C6, Second International Congress on Hydrogen in Metals, Pergammon Press, pp. 1-8, 1978.

Foecke, T., Marsh, P.G., Moody, N.R. and Gerberich, W.W., *A Sample Fabrication-Induced Hydrogen Artifact in Fracture Experiments*, Scripta Metallurgica et Materialia, Vol. 28, pp. 77-80, 1993.

Frederick, J.R. and Felbeck, D.K., *Dislocation Motion as a Source of Acoustic Emission*, Acoustic Emission, ASTM STP 505, pp. 129-130, 1972.

Eadie, R.L. and Smith, R.R., *Modelling Delayed Hydride Cracking in Zirconium Alloys*, Canadian Metallurgical Quarterly, Vol. 27, pp. 213-223, 1988.

Eadie, R.L. and C.E. Coleman, *Effect of Stress on Hydride Precipitation in Zr-2.5% Nb and on Delayed Hydride Cracking*, Scripta METALLURGICA et MATERIALIA, Vol. 23, pp. 1865-1870, 1989.

Eadie, R.L., and Ellyin, F., *The Effect of Hydride Precipitation on the Stresses Near the Crack Tip in a Delayed Hydride Crack in Zr-2.5% Nb*, Scripta METALLURGICA et MATERIALIA, Vol. 23, pp. 585-592, 1989.

Eadie, R.L., Mok, D., Scarth, D. and Leger, M., *The Hydrostatic Stress Field Around the Crack Tip in Zirconium 2.5% Niobium and Implications for Delayed Hydride Cracking*, Scripta METALLURGICA et MATERIALIA, Vol. 25, pp. 497-502, 1991.

Eadie, R.L., Tashiro, K., Harrington, D. and Leger, M., *The Determination of the Partial Molar Volume of Hydrogen in Zirconium in a Simple Stress Gradient Using Comparative Microcalorimetry*, Scripta METALLURGICA et MATERIALIA, Vol. 26, pp. 231-236, Pergamon Press plc., 1992.

Eadie, R.L., Li, D. and Shek, G.K., *Delayed Hydride Cracking During Temperature Transients in As-Manufactured Zr - 2.5% Niobium Pressure Tube Material and in the Same Material Cold Worked an Additional 40%*, unpublished report, November 1993.

Eadie, R.L., Metzger, D., and Leger, M., *The Thermal Ratchetting of Hydrogen in Zirconium-Niobium - an Illustration using Finite Element Modelling*, Scripta Metallurgica et Materialia, Vol. 29, pp. 335-340, 1993.

Eadie, R.L., Jovanovic, M., Li, D. and Ma, Y., *Experimental Report on DHC in T 101*, unpublished results, 1994.

Eadie, R.L., Jovanovic, M. and Ma, Y., *Report on Fractography of Zr - 2.5% Nb Alloy*, unpublished 1994.

Fontana, M.A., *Corrosion Engineering*, McGraw-Hill, 1986.

Fowler, K.A. and Papadakis, E.P., *Observation and Analysis of Simulated Ultrasonic Acoustic Emission Waves in Plates and Complex Structures*, Acoustic Emission, ASTM STP 505, pp. 222-237, 1972.

Frederick, J.R. and Felbeck, D.K., *Dislocation Motion as a Source of Acoustic Emission*, Acoustic Emission, ASTM STP 505, pp. 129-139, 1972.

Hardie, D. and Shanahan, M.W., *Stress Reorientation of Hydrides in Zirconium-2.5% Niobium*, Journal of Nuclear Materials, Vol. 55, pp. 1-13, 1975.

Hart, S.D., *Inspection of Selected Areas of Engineering Structures by Acoustic Emission*, Acoustic Emission, pp 65-68, Applied Science Publishers 1976.

Kearns, J.J., *Terminal Solubility and Partitioning of Hydrogen in the Alpha Phase of Zirconium, Zircaloy - 2, and Zircaloy - 4*, Journal of Nuclear Materials, Vol. 22, pp. 292 - 303, North-Holland Publishing, 1967.

Li, J.C.M., Oriani, R.A. and Darken, L.A., *The Thermodynamics of Stressed Solids*, Zeitschrift fur Physikalisched Chemie Neue Folge, Bd. 49, pp. 271-290, 1966.

Northwood, D.O. and Kosasih, U., *Hydrides and Delayed Hydrogen Cracking in Zirconium and its Alloys*, International Metals Reviews, Vol. 28, pp. 92-121, ASM, 1983.

Ono, K., Stern, R. and Long Jr. M., *Application of Correlation Analysis to Acoustic Emission*, Acoustic Emission, ASTM STP 505, pp. 152-163, 1972.

Perovic, V. and Weatherly, G.C., *On the Formation and Reorientation of Stacks of Hydride Precipitates in Zr-2.5% Nb Pressure Tubes*, Ontario Hydro Research Paper No. 82-319-K, 1982.

Perovic, V., Weatherly, G.C. and Simpson, C.J., *Hydride Precipitation in α/β Zirconium Alloys*, Acta Metallurgica, Vol. 31, No. 9, pp. 1381-1391, 1983.

Perryman, E.C.W., *Pickering Pre:s're tube Cracking Experience,* Nuclear Energy, Vol. 17, pp. 95-105, April 1978.

Puls, M.P., *Elastic and Plastic Accommodation Effects on Metal-Hydride Solubility,* Acta Metall.,Vol. 32, No. 8, pp. 1259-1269, Pergamon Press Ltd., 1984.

Puls, M.P., *On the Consequences of Hydrogen Supersaturation Effects in Zr Alloys to Hydrogen Ingress and Delayed Hydride Cracking,* Journal of Nuclear Materials, Vol. 165, pp. 128-41, North-Holland Publishing Co., Amsterdam, Holland, 1989.

Puls, M.P., *Effects of Crack Tip Stress States and Hydride-Matrix Interaction Stresses on Delayed Hydride Cracking,* Metallurgical Transactions A, Vol. 21A, pp. 2905-17, Ministry of Supply and Services, November 1990.

Sagat, S., Ambler, J.F.R and Coleman, C.E., *Application of Acoustic Emission to Hydride Cracking,* Atomic Energy of Canada Limited (AECL) - 9258, July 1986.

Sawatzky, A., *Hydriding Zircaloy-2 by Electrolysis,* AECL Publication No. 1046, June 1960.

Schemel, J.H., *ASTM Manual on Zirconium and Hafnium,* ASTM STP 639, 1977.

Shek, G.K. and Graham, D.B., *Effects of Loading and Thermal Manoeuvres on Delayed Hydride Cracking in Zr-2.5 Nb Alloys,* ASTM STP 1023, pp. 89-110, 1989.

Simpson, L.A. and Clark, C.F., *Application of the Potential-Drop Method to Measurements of Hydrogen-Induced Sub-Critical Crack Growth in Zr-2.5 wt % Nb,* Atomic Energy of Canada Limited (AECL) - 5815, Oct 1977.

Simpson, L.A. and Nuttal, K., *Factors Controlling Hydrogen Assisted Subcritical Crack Growth in Zr-2.5 Nb Alloys,* Zirconium and the Nuclear Industry, ASTM STP 633, pp. 608-629, 1977.

Simpson, L.A., *The Critical Propagation Event for Hydrogen-Induced Slow Crack Growth* in Zr-2.5% Nb, ICM 3, Vol. 2, pp. 445-455, 1979.

Slattery, G.F., *The Terminal Solubility of Hydrogen in Zirconium Alloys between 30 and 400°C,* Journal of the Institute of Metals, Vol. 95, pp. 43-47, 1967.

Spanner, J.C., *Acoustic Emission, Techniques and Applications,* Intex Publishing Co., pp. 56-57, 177-183, 1974.

Tangri, K., *Acoustic Emission Investigation of Sub-Critical Crack Growth in Zr-2.5 Nb,* Proceedings of the Institute of Acoustics, pp 4.17.1-4.17.4, 1977.

Tangri, K. and Yuan, X.Q., *Acoustic Emission Study of the Various Stages of Hydrogen Induced Cracking in Zr - 2.5% Nb Alloy,* Fracture Problems and Solutions in the Energy Industry, pp. 27-37, Pergammon Press, 1982.

Wilkins, B.J.S. and Nuttall, K., *Secondary Cracking in Hydrided Zr - 2.5 Wt% Nb Alloys*, Journal of Nuclear Materials, Vol. 75, pp. 125-130, 1978.

Yuan, X.Q. and Tangri, K., *Metallographic Observations on the Developing Hydride Morphology at the Crack Tip during Hydrogen Induced Delayed Cracking in a Zr-2.5% Nb Alloy*, Journal of Nuclear Materials, Vol. 105, pp. 310-317, 1982.
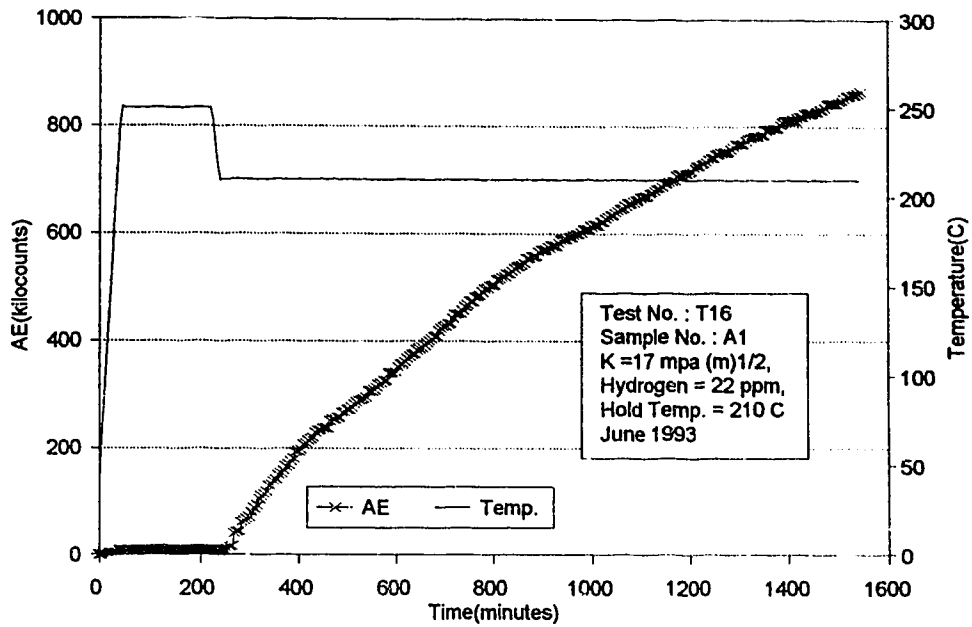
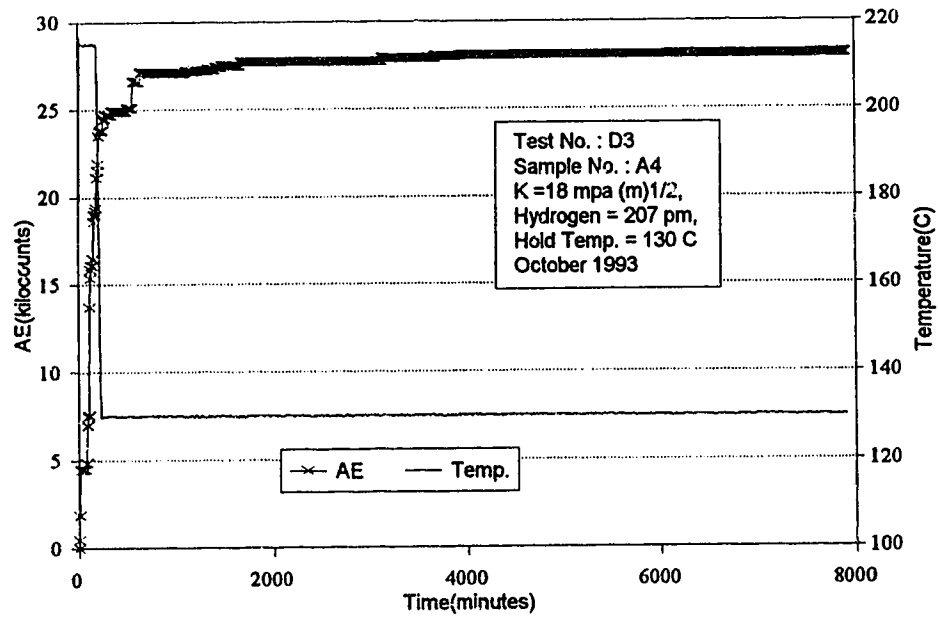Figure A1.1: "As Manufactured" Material, Acoustic Emission & Temperature vs Time - Sample A1, Test No. T16, Isothermal Hold = 210° C.
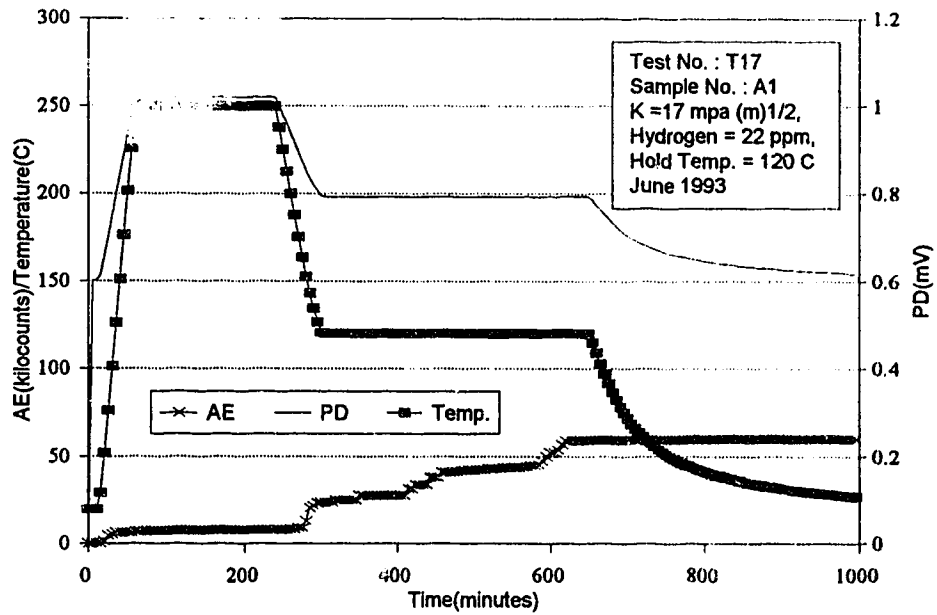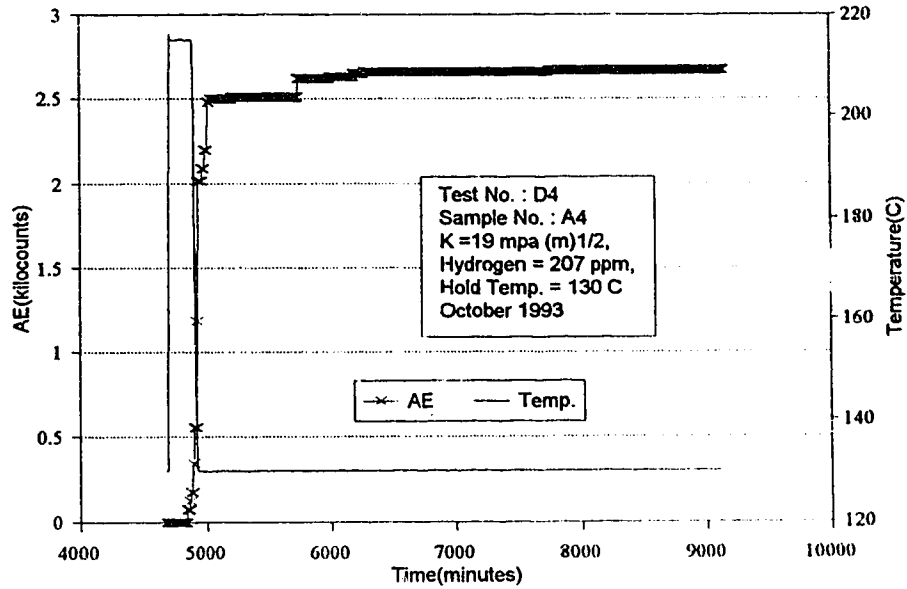

Figure A1.2: "As Manufactured" Material, Acoustic Emission & Temperature vs Time - Sample A1, Test No. T17, Isothermal Hold = 120° C.
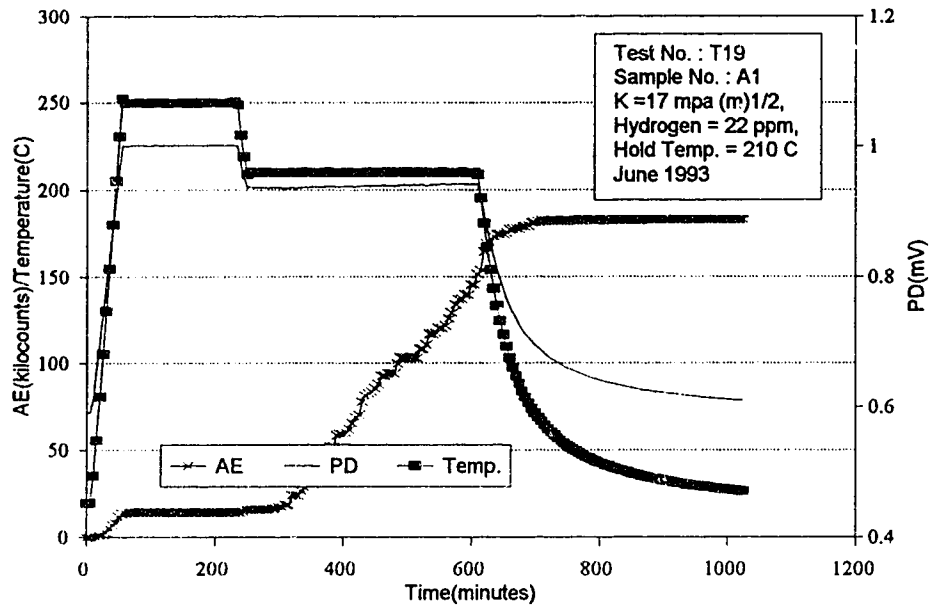
Figure A1.3:   "As Manufactured" Material, Acoustic Emission & Temperature vs Time -
Sample A1, Test No. T19, Isothermal Hold = 210° C.
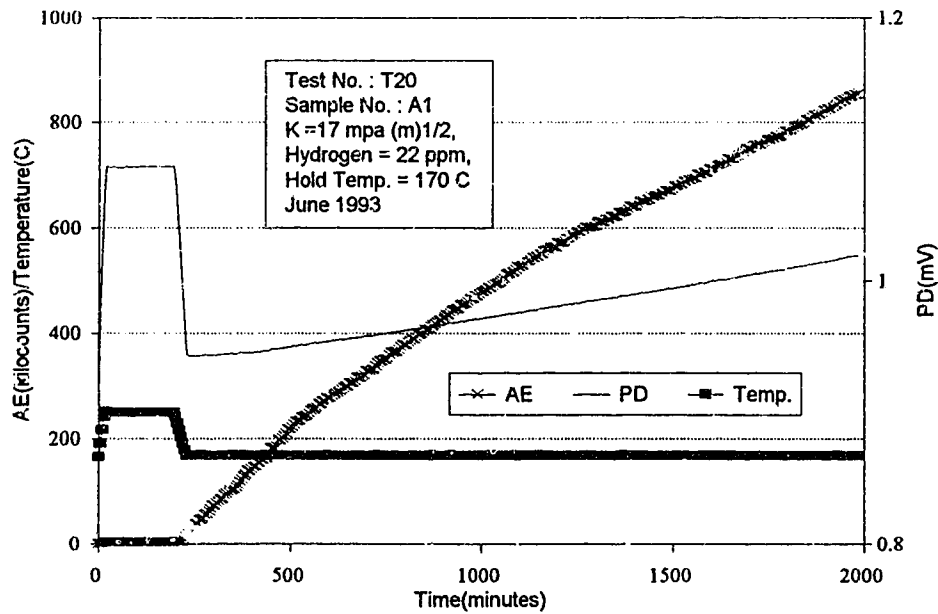
Figure A1.4:   "As Manufactured" Material, Acoustic Emission & Temperature vs Time -
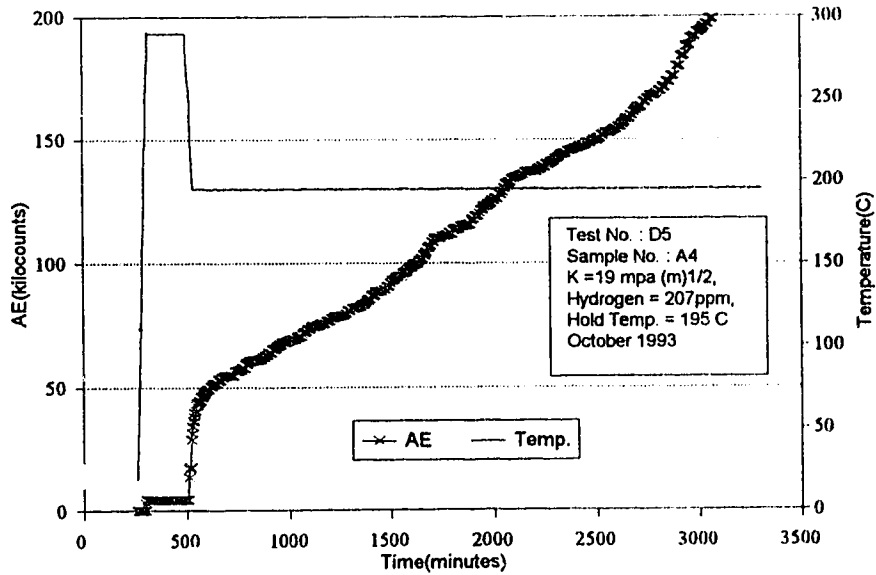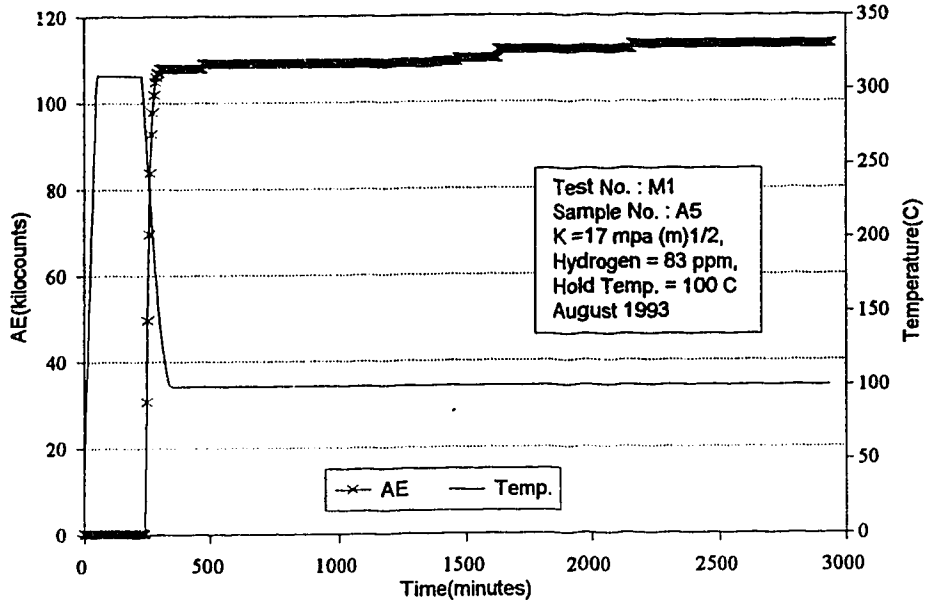Sample A1, Test No. T20, Isothermal Hold = 170° C.
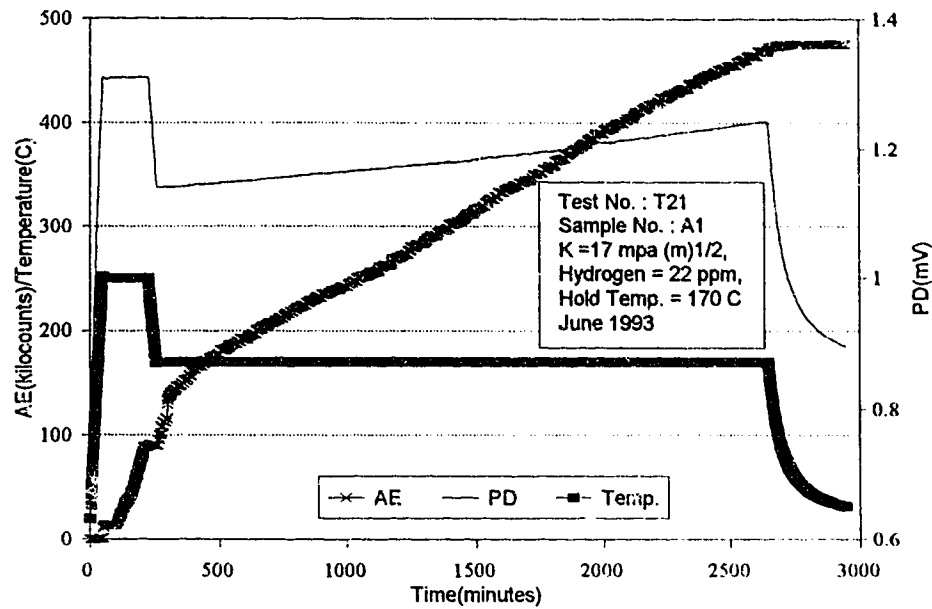
Figure A1.5:   "As Manufactured" Material, Acoustic Emission & Temperature vs Time - SampleA1, Test No. T21, Isothermal Hold = 170° C.
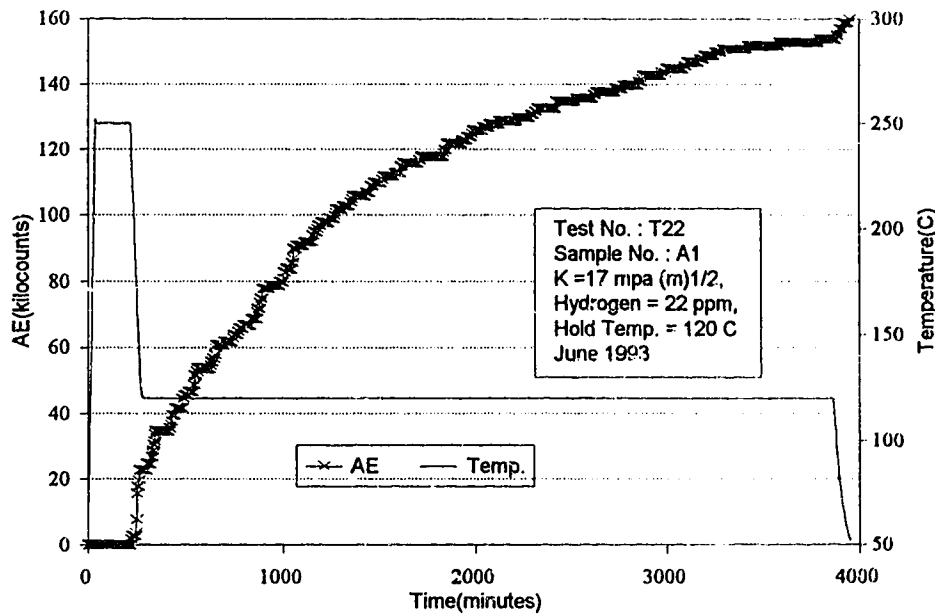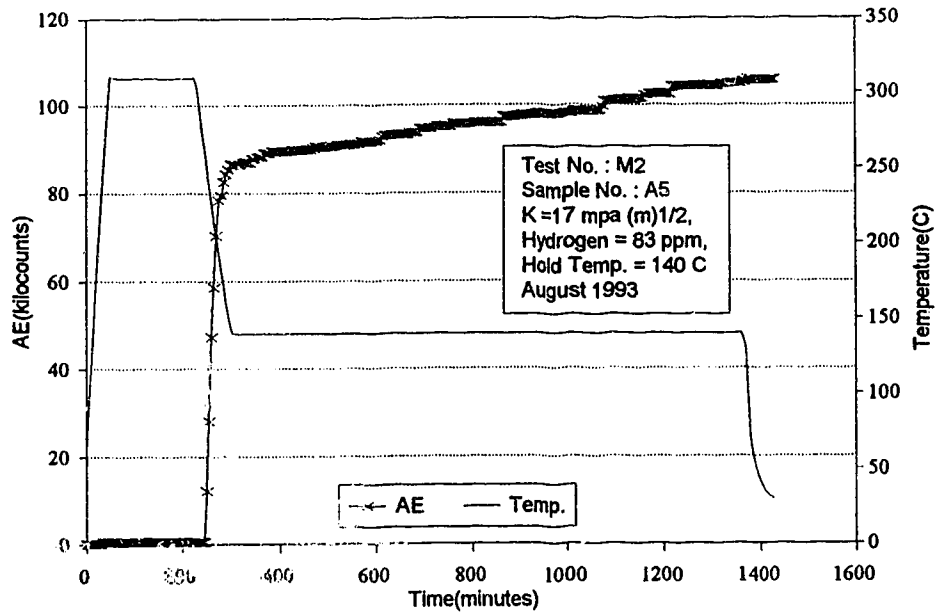

Figure A1.6:   "As Manufactured" Material, Acoustic Emission & Temperature vs Time - Sample A1, Test No. T22, Isothermal Hold = 120° C.
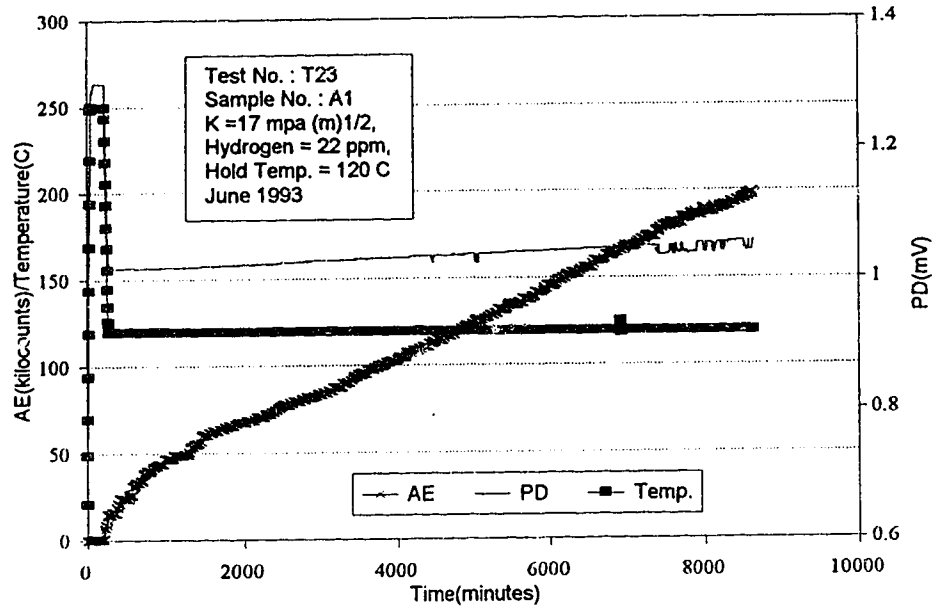
Figure A1.7:   "As Manufactured" Material, Acoustic Emission & Temperature vs Time - Sample A1, Test No. T23, Isothermal Hold = 120° C.
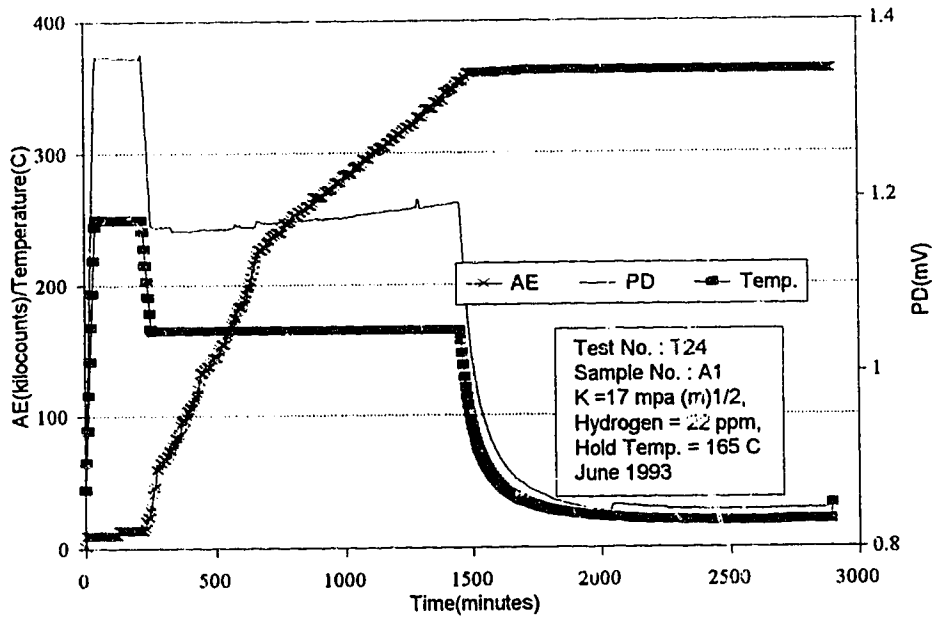
Figure A1.8:   "As Manufactured" Material, Acoustic Emission & Temperature vs Time - Sample A1, Test No. T24, Isothermal Hold = 165° C.
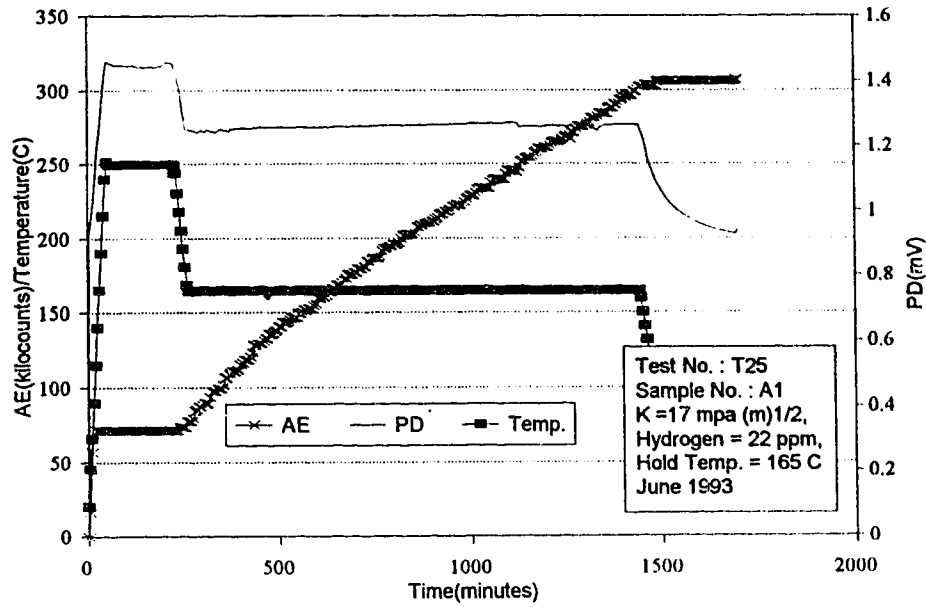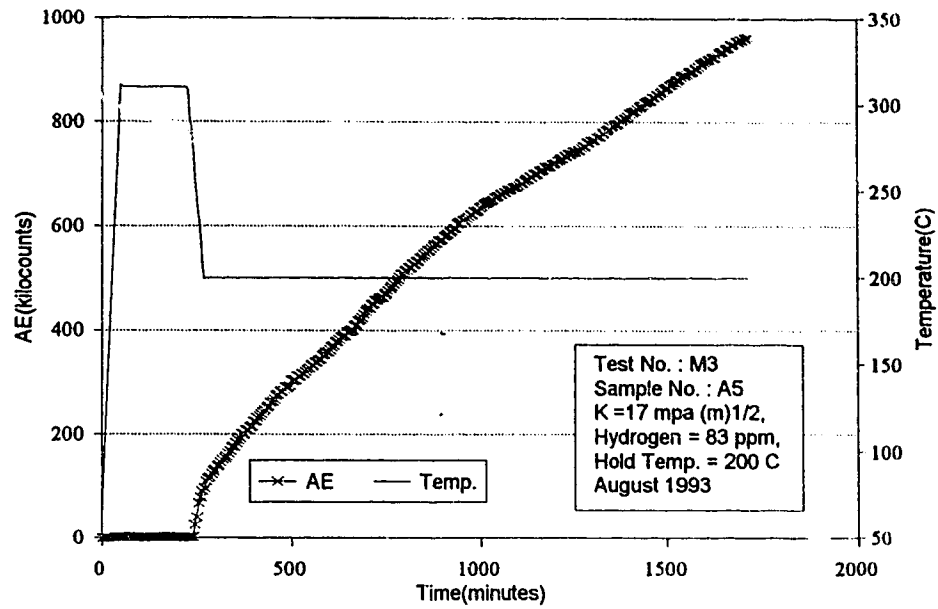
Figure A1.9:   "As Manufactured" Material, Acoustic Emission & Temperature vs Time -
Sample A1, Test No. T25, Isothermal Hold = 165° C.
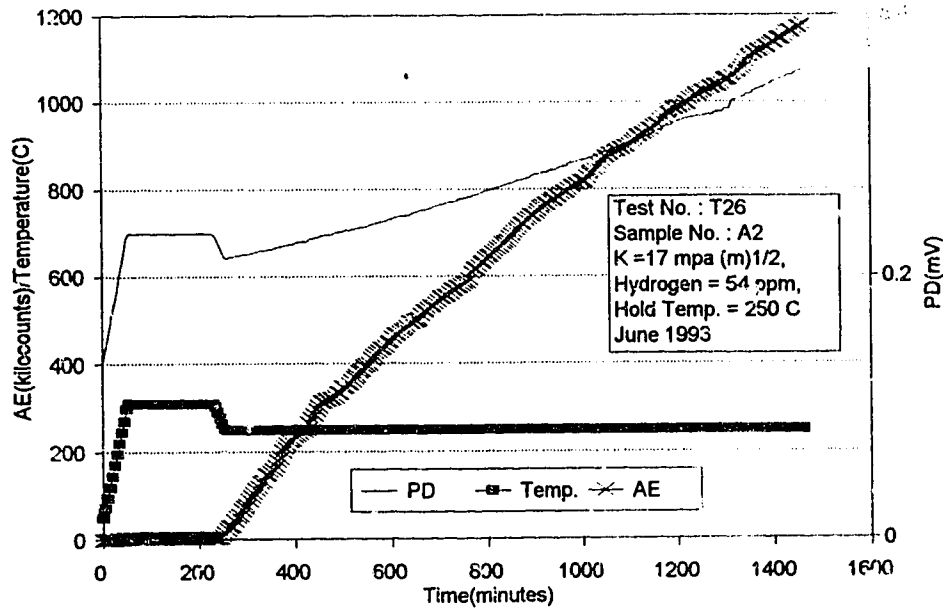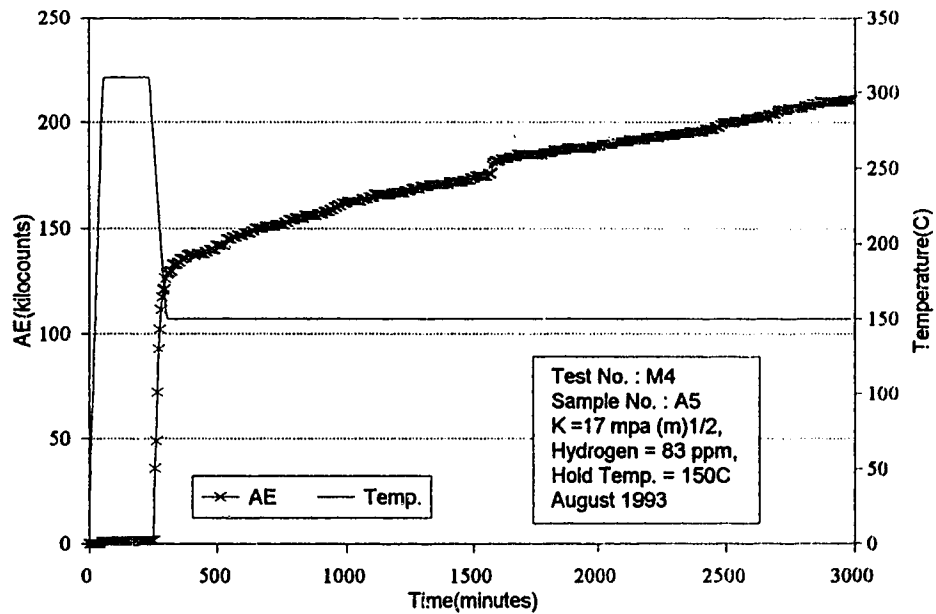

Figure A1.10:   "As Manufactured" Material, Acoustic Emission & Temperature vs Time -
Sample A2, Test No. T26, Isothermal Hold = 250° C.
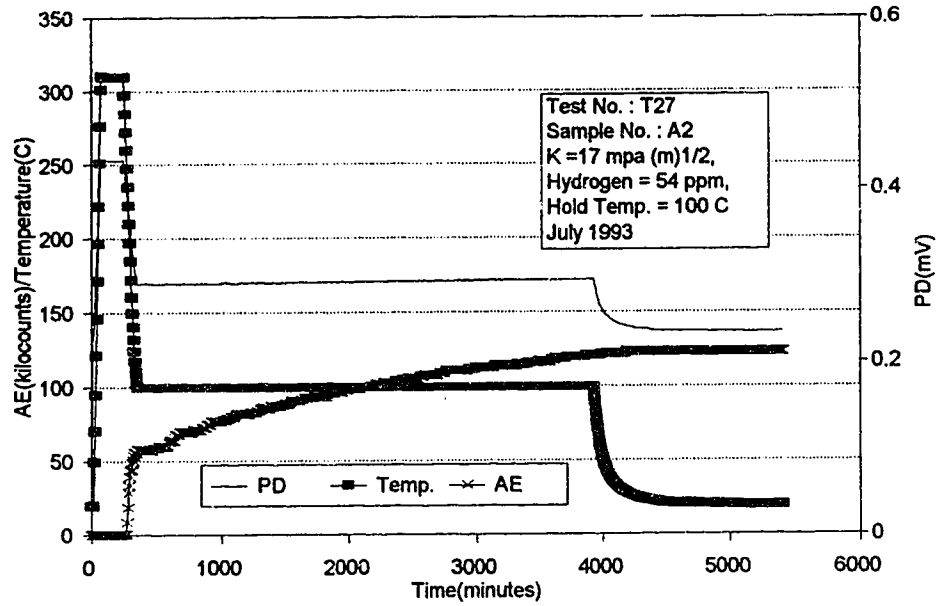
Figure A1.11: "As Manufactured" Material, Acoustic Emission & Temperature vs Time - Sample A2, Test No. T27, Isothermal Hold = 100° C.
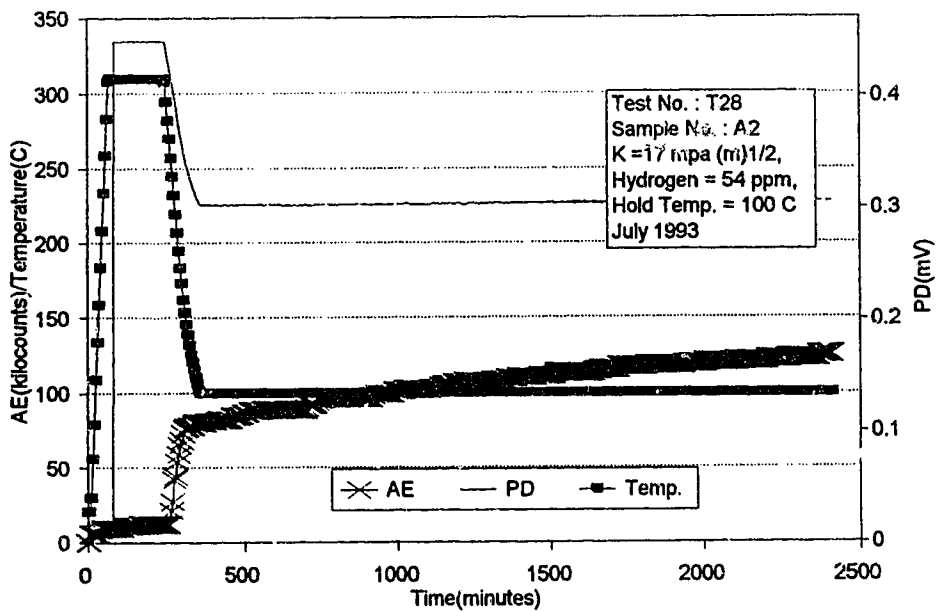
Figure A1 12: "As Manufactured" Material, Acoustic Emission & Temperature vs Time - Sample A2, Test No. T28, Isothermal Hold = 100° C.
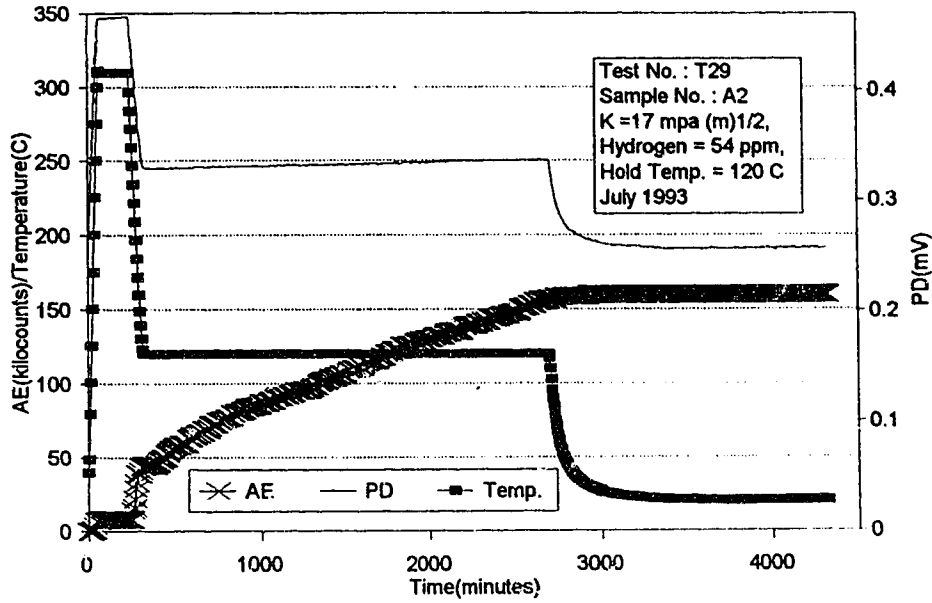
Figure A1.13: "As Manufactured" Material, Acoustic Emission & Temperature vs Time - Sample A2, Test No. T29, Isothermal Hold = 120° C.
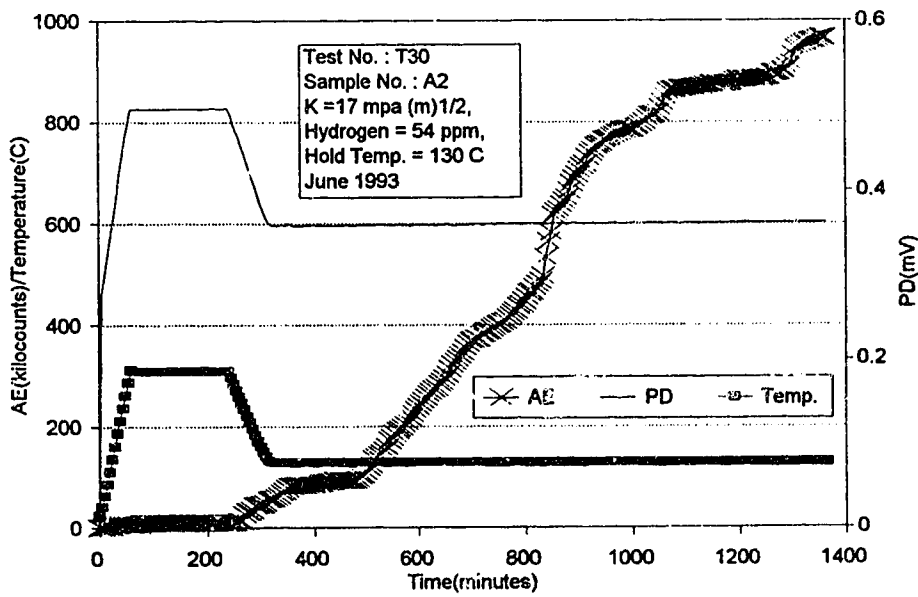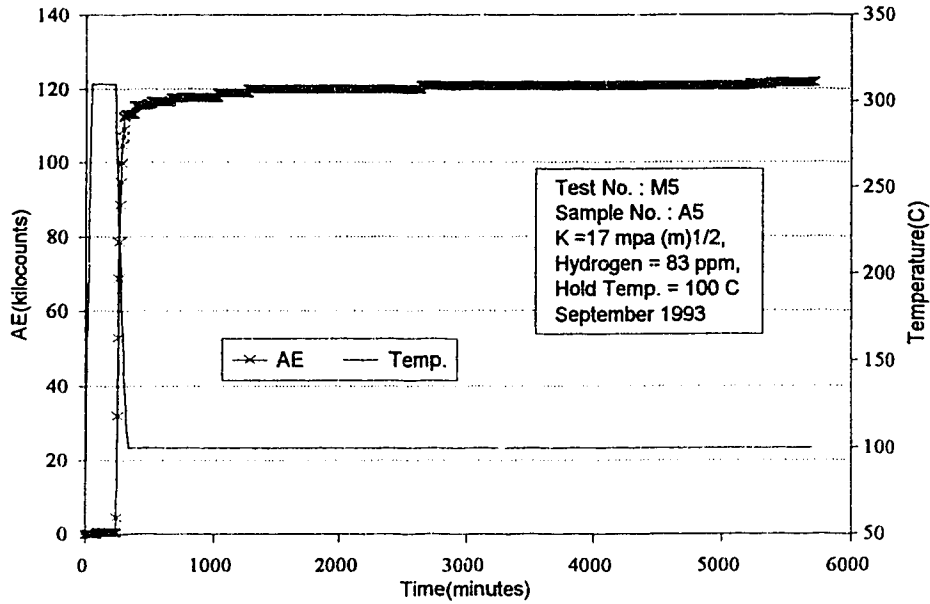

Figure A1.14: "As Manufactured" Material, Acoustic Emission & Temperature vs Time - Sample A2, Test No. T30, Isothermal Hold = 130° C.
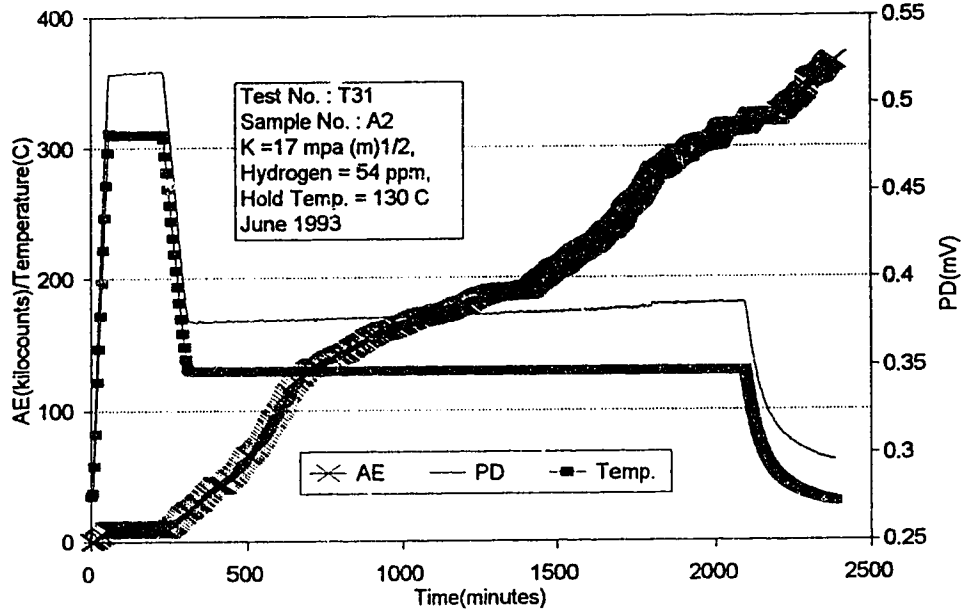
Figure A1.15: "As Manufactured" Material, Acoustic Emission & Temperature vs Time - Sample A2, Test No. T31, Isothermal Hold = 130° C.
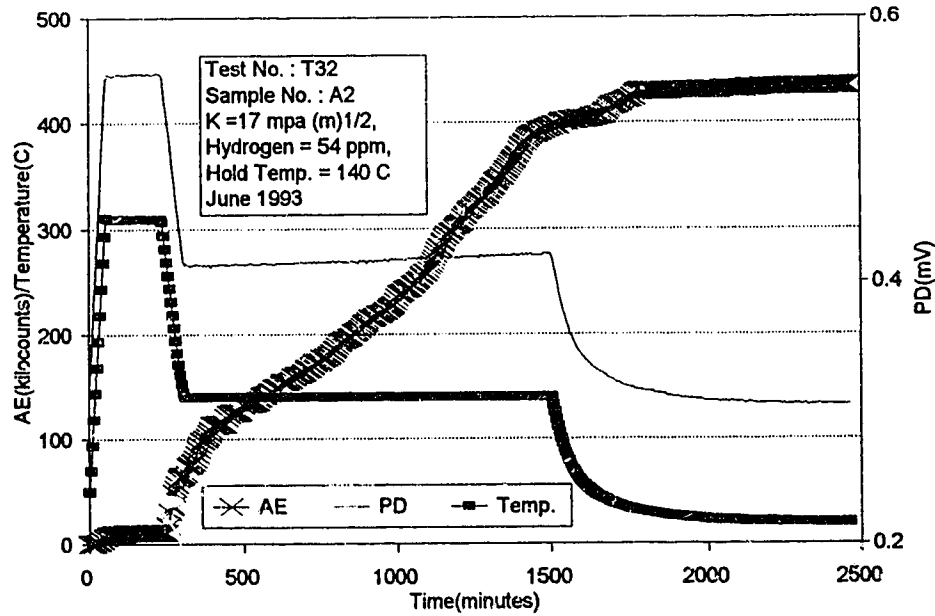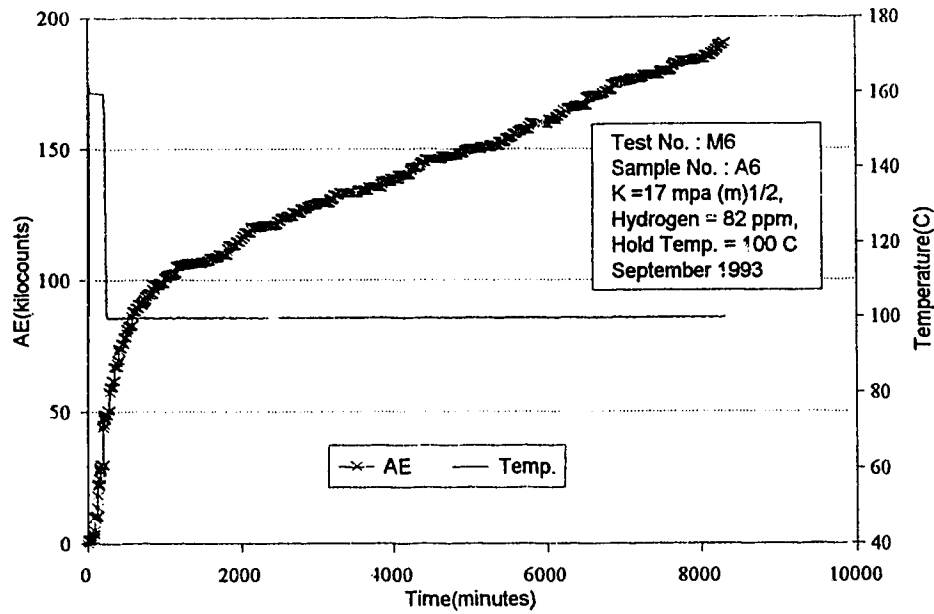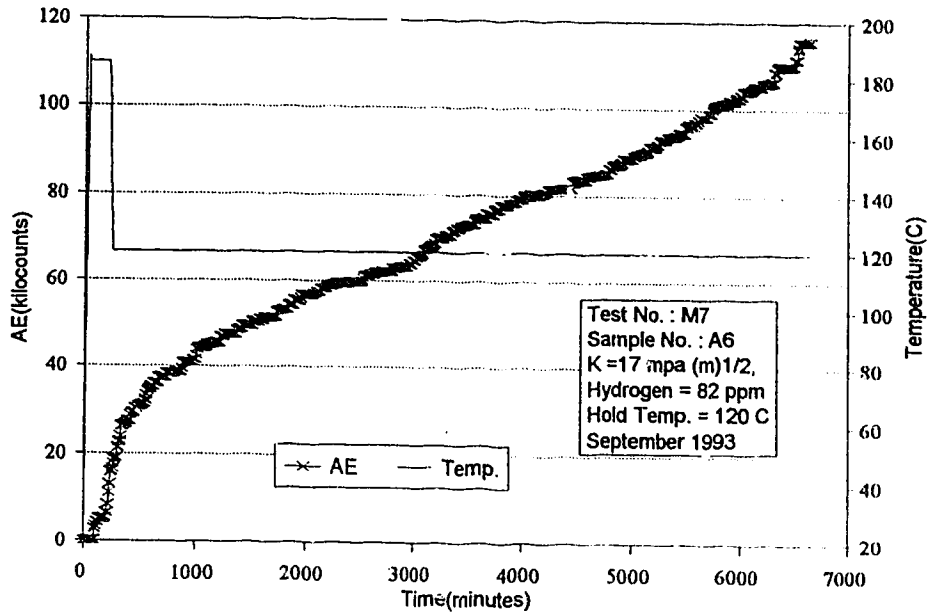

Figure A1.16: "As Manufactured" Material, Acoustic Emission & Temperature vs Time - Sample A2, Test No. T32, Isothermal Hold = 140° C.
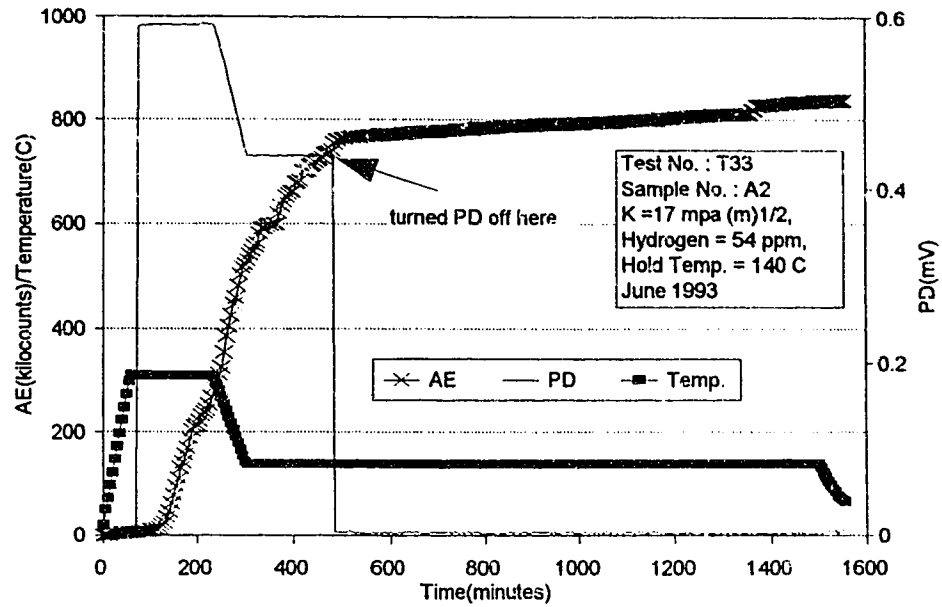
Figure A1.17: "As Manufactured" Material, Acoustic Emission & Temperature vs Time - Sample A2, Test No. T33, Isothermal Hold = 145° C.
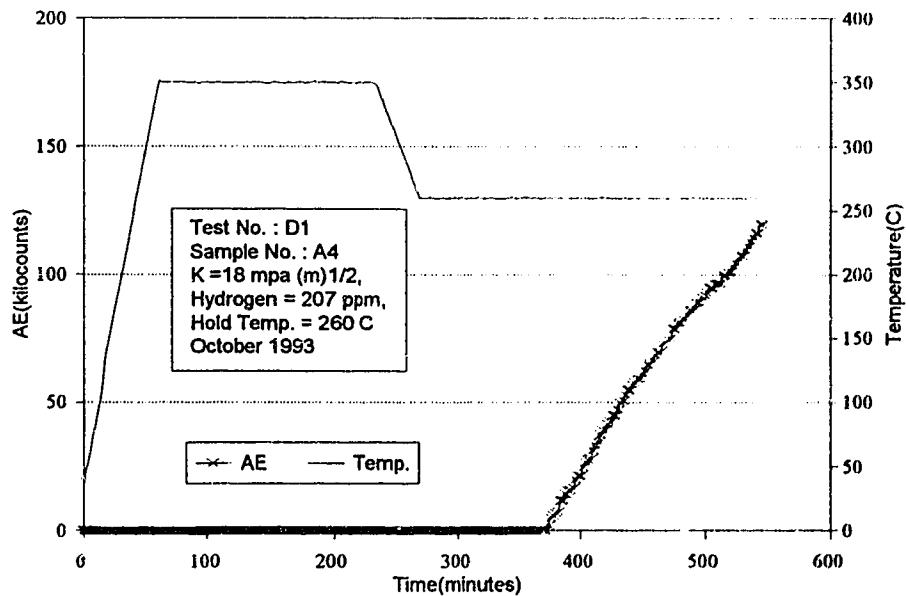
Figure A1.18: "As Manufactured" Material, Acoustic Emission & Temperature vs Time - Sample A4, Test No. D1, Isothermal Hold = 260° C.
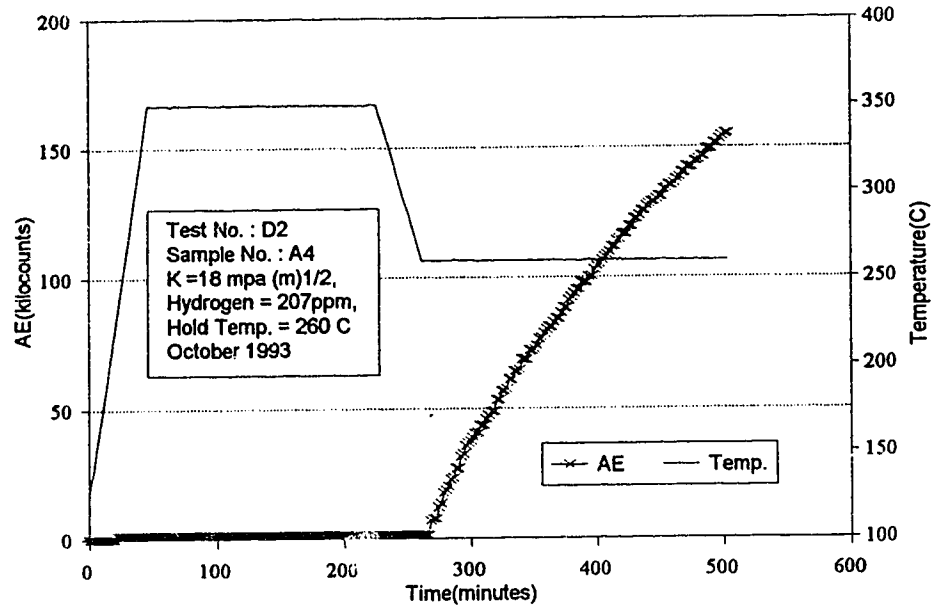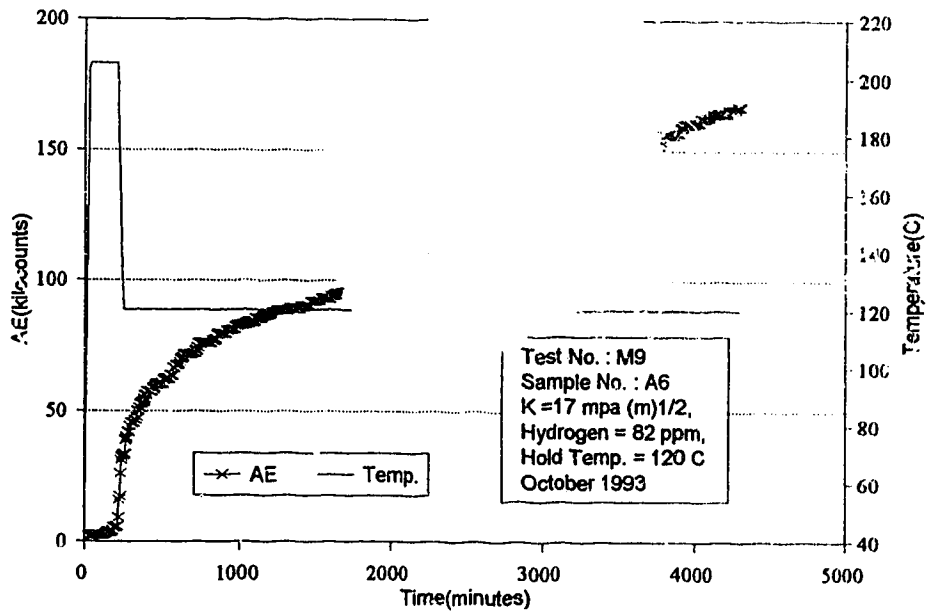
Figure A1.19: **"As Manufactured" Material,** Acoustic Emission & Temperature vs Time - Sample A4, Test No. D2, Isothermal Hold = 260° C.

Figure A1.20: **"As Manufactured" Material,** Acoustic Emission & Temperature vs Time - Sample A4, Test No. D3, Isothermal Hold = 130° C.
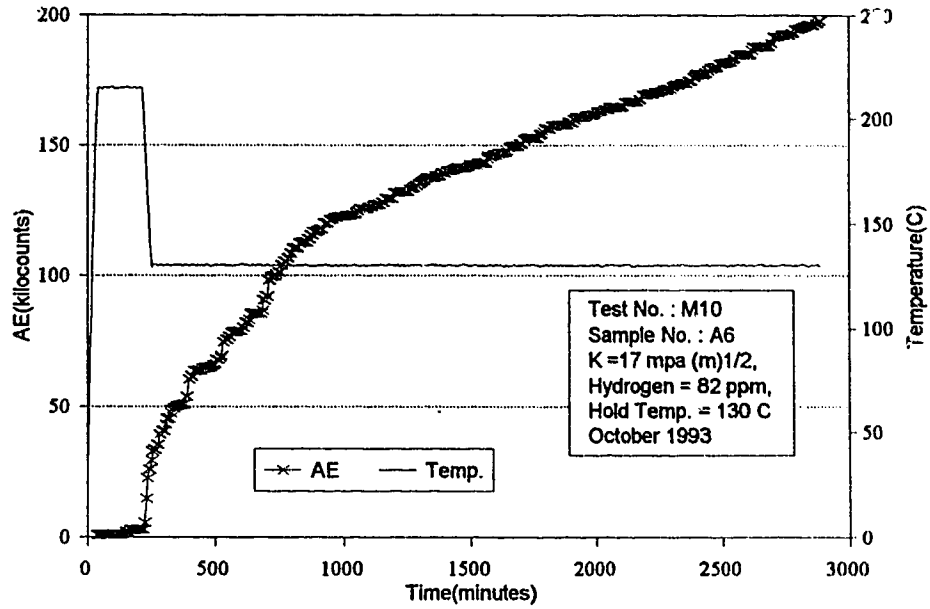
Figure A1.21: "As Manufactured" Material, Acoustic Emission & Temperature vs Time - Sample A4, Test No. D4, Isothermal Hold = 120° C.
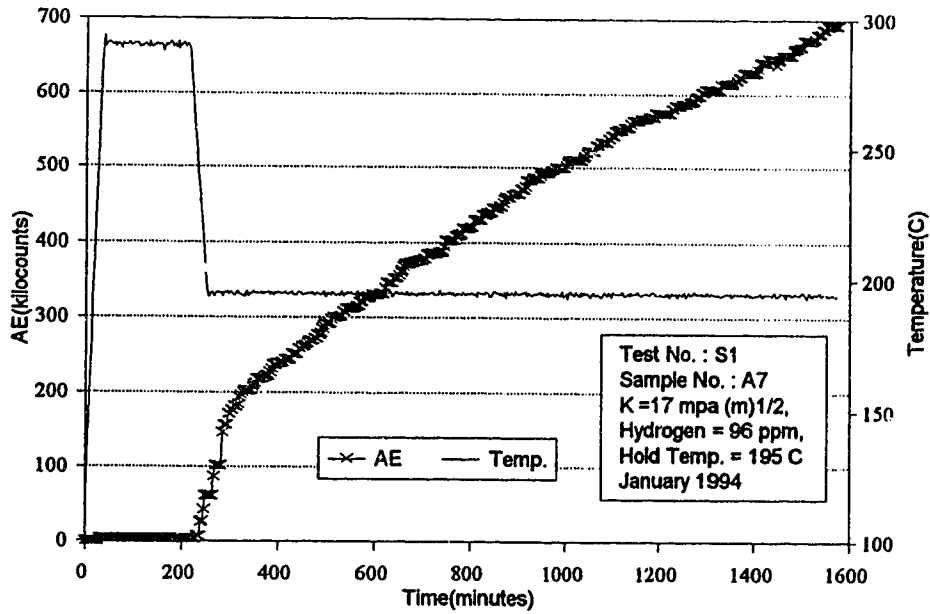

Figure A1.22: "As Manufactured" Material, Acoustic Emission & Temperature vs Time - Sample A4, Test No. D5, Isothermal Hold = 195° C.
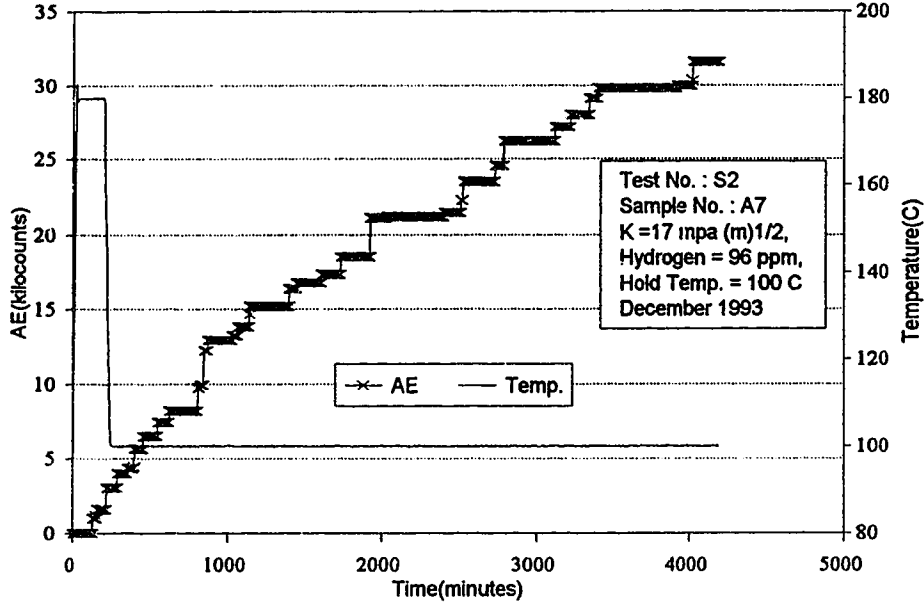
Figure A1.23: "As Manufactured" Material, Acoustic Emission & Temperature vs Time - Sample A5, Test No. M1, Isothermal Hold = 100° C.
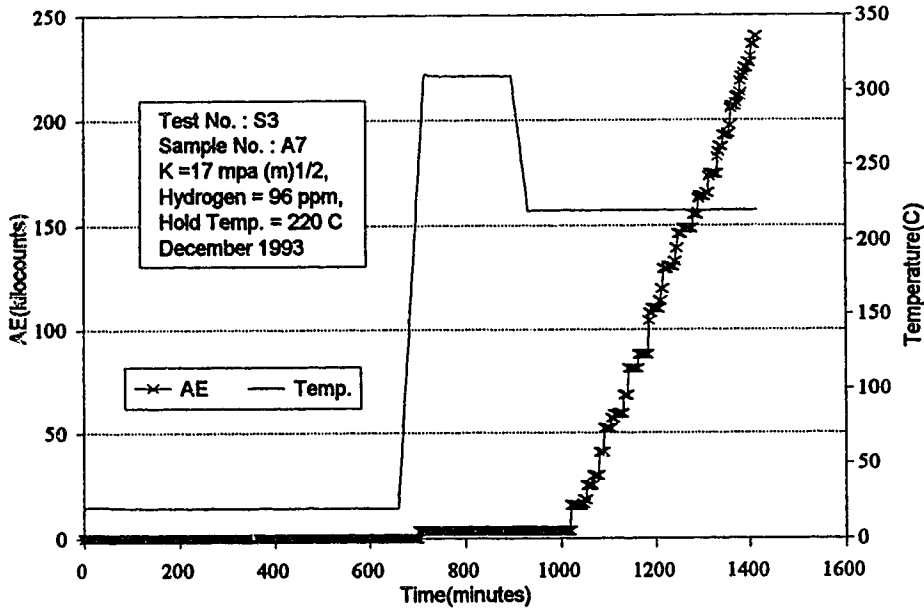

Figure A1.24: "As Manufactured" Material, Acoustic Emission & Temperature vs Time - Sample A5, Test No. M2, Isothermal Hold = 140° C.

Figure A1.25: "As Manufactured" Material, Acoustic Emission & Temperature vs Time - Sample A5, Test No. M3, Isothermal Hold = 200° C.

Figure A1.26: "As Manufactured" Material, Acoustic Emission & Temperature vs Time - Sample A5, Test No. M4, Isothermal Hold = 150° C.

Figure A1.27: "As Manufactured" Material, Acoustic Emission & Temperature vs Time - Sample A5, Test No. M5, Isothermal Hold = 100° C.

Figure A1.28: "As Manufactured" Material, Acoustic Emission & Temperature vs Time - Sample A6, Test No. M6, Isothermal Hold = 100° C.

Figure A1.29: "As Manufactured" Material, Acoustic Emission & Temperature vs Time -- Sample A6, Test No. M7, Isothermal Hold = 120° C.
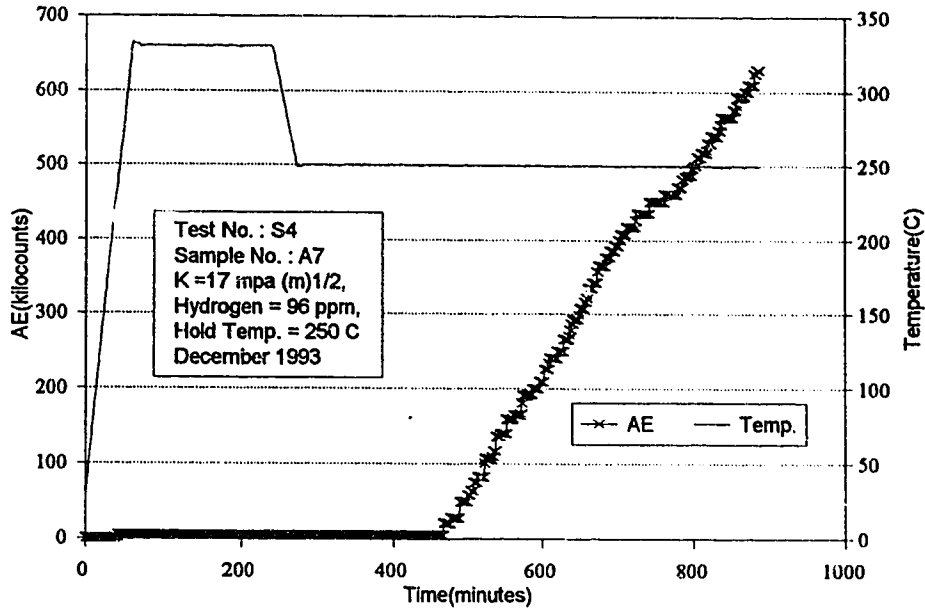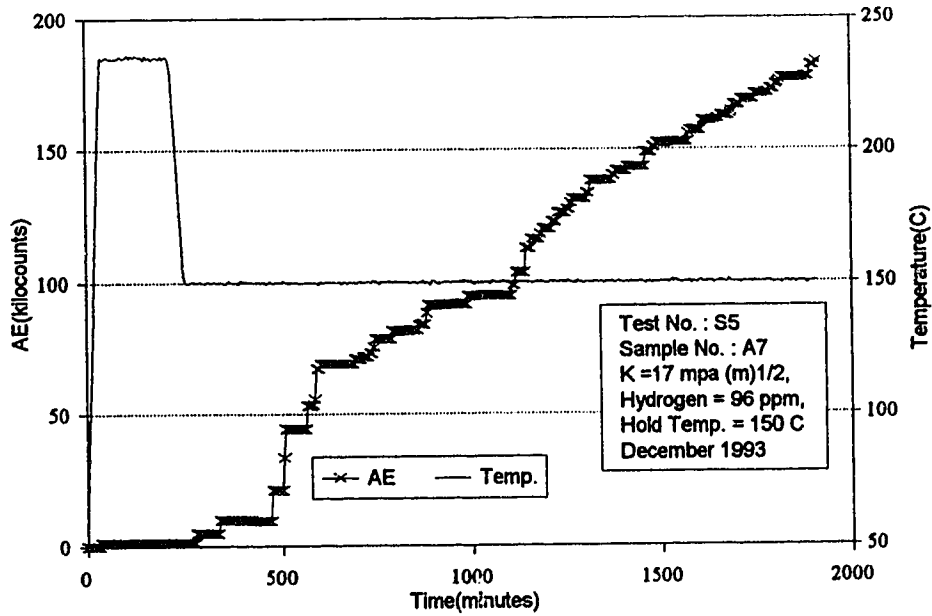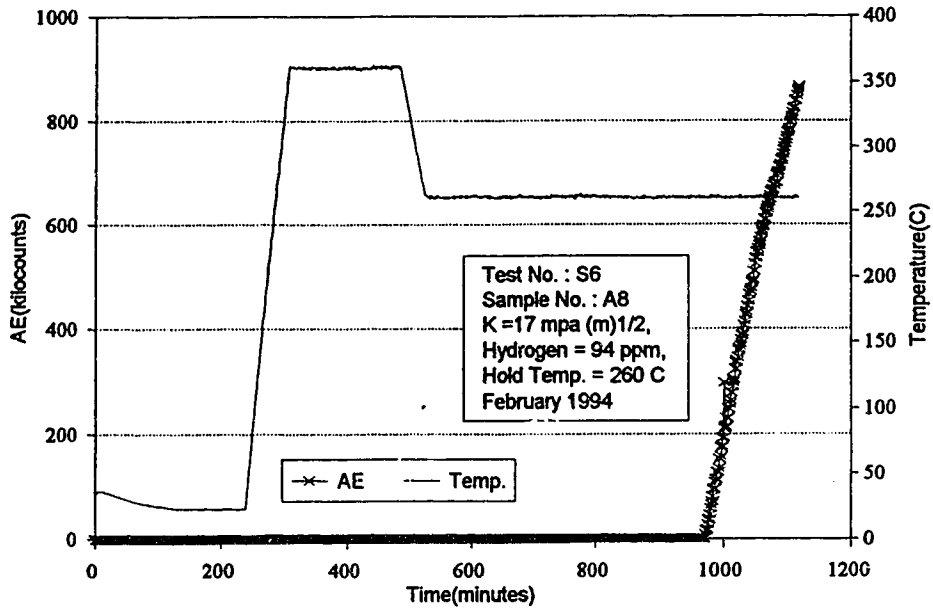

Figure A1.30: "As Manufactured" Material, Acoustic Emission & Temperature vs Time - Sample A6, Test No. M9, Isothermal Hold = 120° C.

Figure A1.31: "As Manufactured" Material, Acoustic Emission & Temperature vs Time - Sample A6, Test No. M10, Isothermal Hold = 130° C.
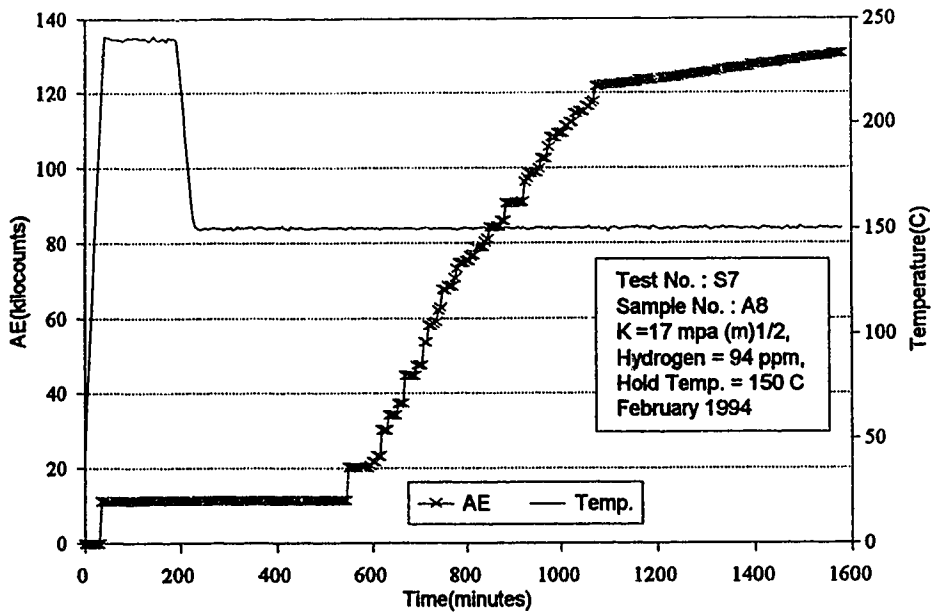

Figure A1.32: "As Manufactured" Material, Acoustic Emission & Temperature vs Time - Sample A7, Test No. S1, Isothermal Hold = 195° C.
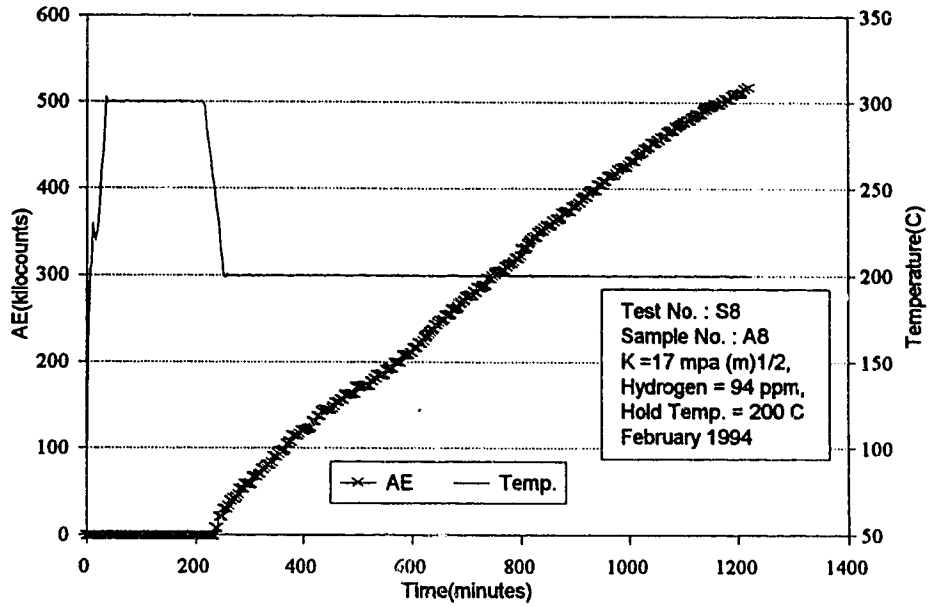
Figure A1.33:   "As Manufactured" Material, Acoustic Emission & Temperature vs Time -
                Sample A7, Test No. S2, Isothermal Hold = 100° C.

Figure A1.34   :"As Manufactured" Material, Acoustic Emission & Temperature vs Time -
                Sample A7, Test No. S3, Isothermal Hold = 220° C.

Figure A1.35: "As Manufactured" Material, Acoustic Emission & Temperature vs Time -
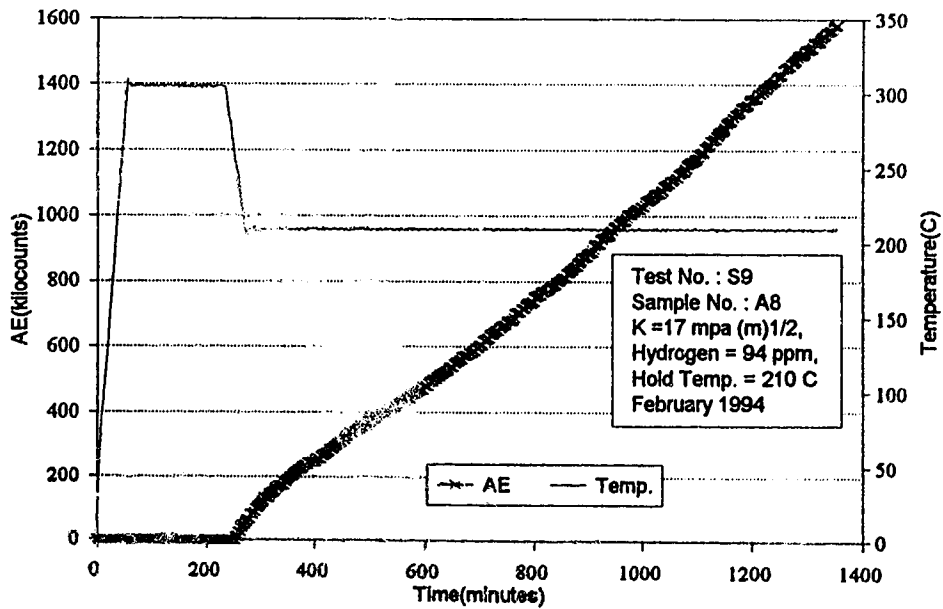Sample A7, Test No. S4, Isothermal Hold = 250° C.

Figure A1.36: "As Manufactured" Material, Acoustic Emission & Temperature vs Time -
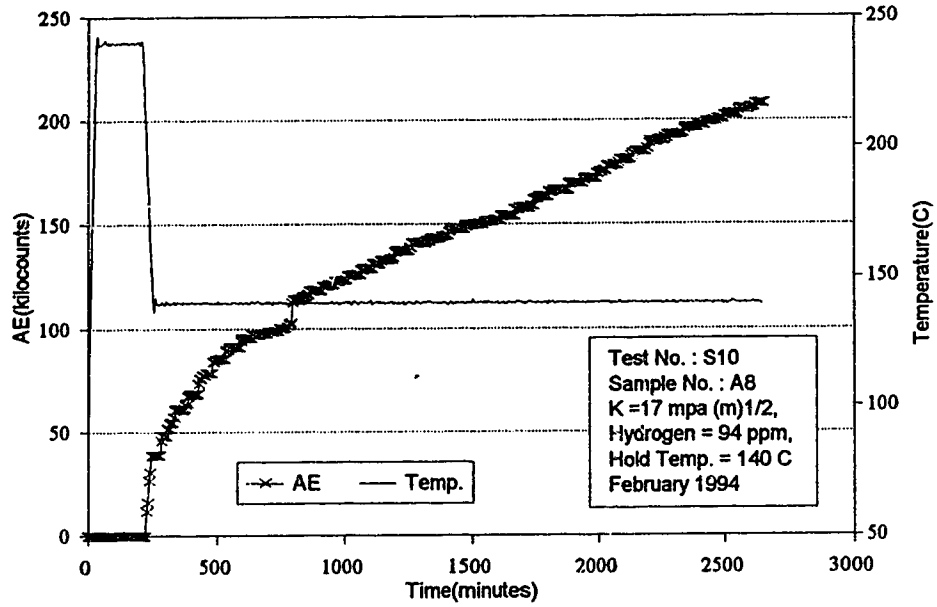Sample A7, Test No. S5, Isothermal Hold = 150° C.

Figure A1.37: "As Manufactured" Material, Acoustic Emission & Temperature vs Time - Sample A8, Test No. S6, Isothermal Hold = 260° C.

Figure A1.38: "As Manufactured" Material, Acoustic Emission & Temperature vs Time - Sample A8, Test No. S7, Isothermal Hold = 150° C.

Figure A1.39: "As Manufactured" Material, Acoustic Emission & Temperature vs Time -
Sample A8, Test No. S8, Isothermal Hold = 200° C.

Figure A1.40: "As Manufactured" Material, Acoustic Emission & Temperature vs Time -
Sample A8, Test No. S9, Isothermal Hold = 210° C.

Figure A1.41: "As Manufactured" Material, Acoustic Emission & Temperature vs Time - Sample A8, Test No. S10, Isothermal Hold = 140° C.
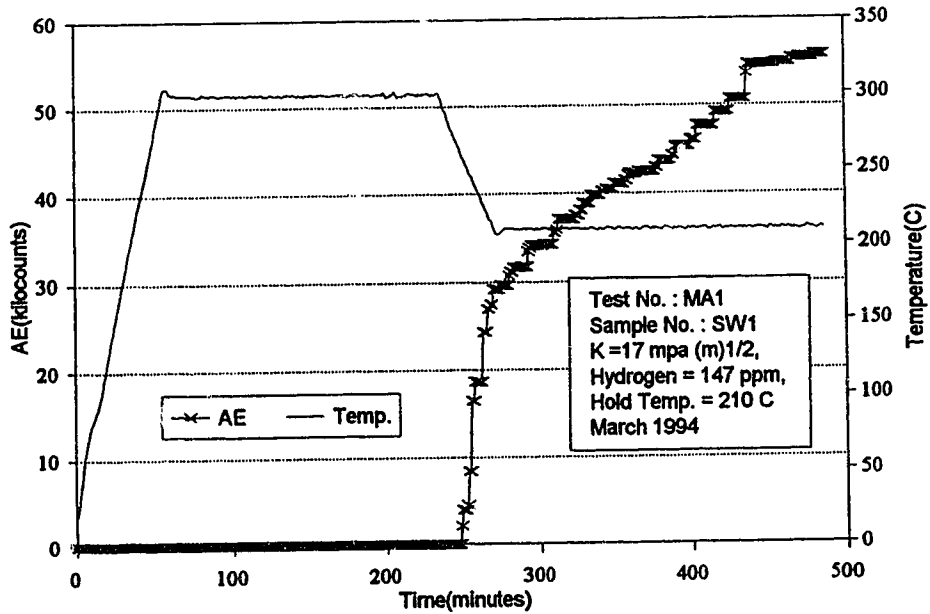

Figure A1.42: "Cold Worked" Material, Acoustic Emission & Temperature vs Time - Sample SW1, Test No. MA1, Isothermal Hold = 210° C.
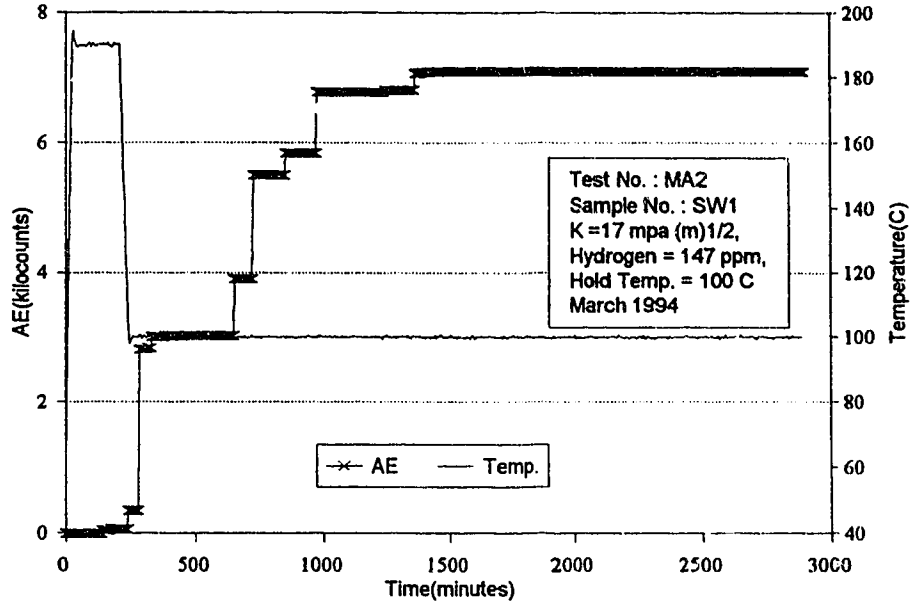
Figure A1.43: "Cold Worked" Material, Acoustic Emission & Temperature vs Time - Sample
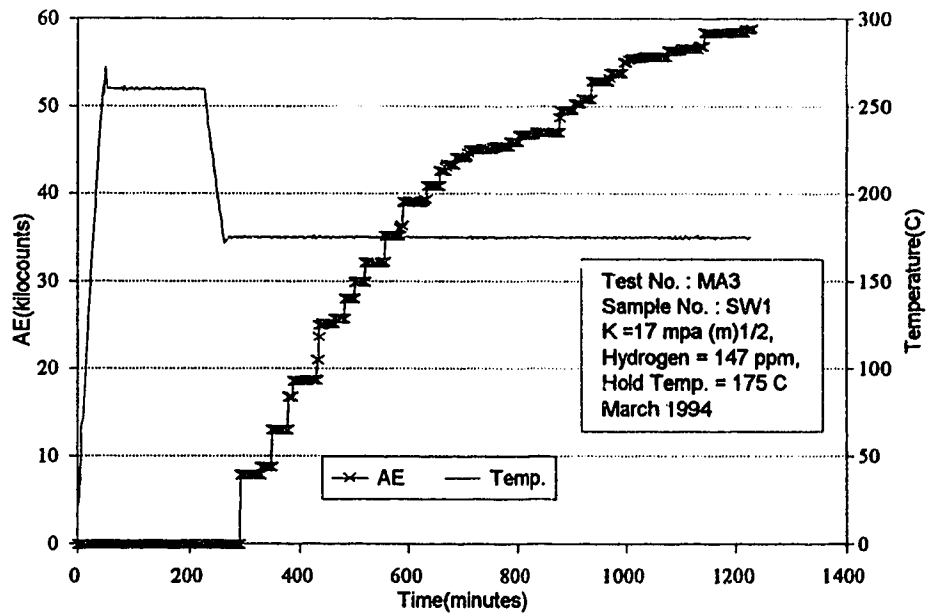SW1, Test No. MA2, Isothermal Hold = 100° C.

Figure A1.44: "Cold Worked" Material, Acoustic Emission & Temperature vs Time - Sample
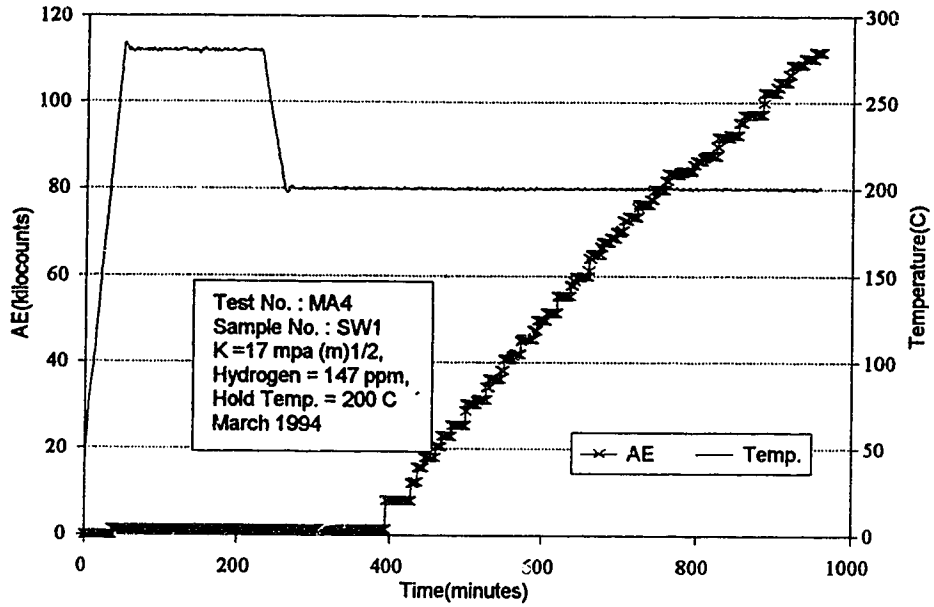SW1, Test No. MA3, Isothermal Hold = 175° C.

Figure A1.45: "Cold Worked" Material, Acoustic Emission & Temperature vs Time - Sample SW1, Test No. MA4, Isothermal Hold = 200° C.
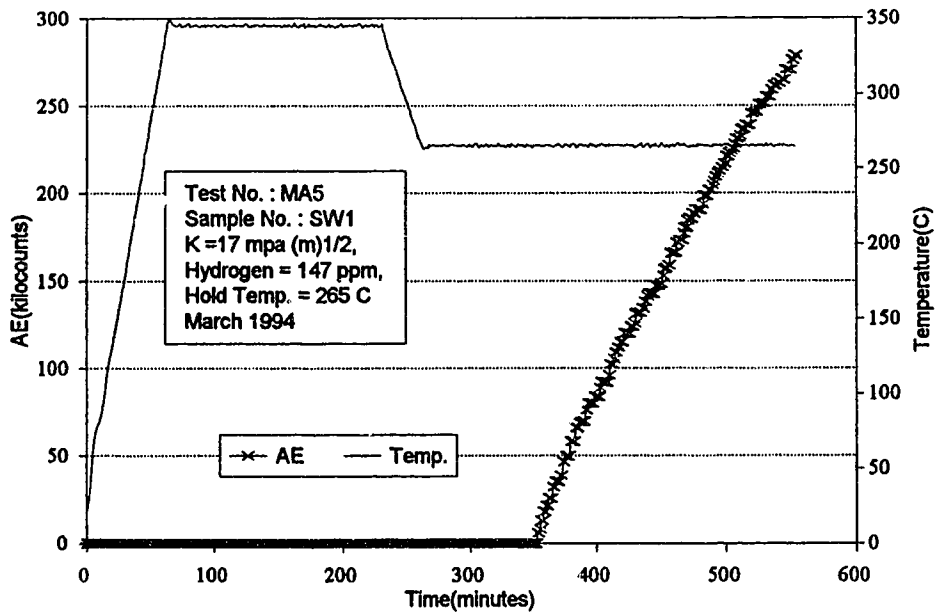

Figure A1.46: "Cold Worked" Material, Acoustic Emission & Temperature vs Time - Sample SW1, Test No. MA5, Isothermal Hold = 265° C.